INFORMATION TO USERS

This reproduction was made from a copy of a document sent to us for microfilming. While the most advanced technology has been used to photograph and reproduce this document, the quality of the reproduction is heavily dependent upon the quality of the material submitted.

The following explanation of techniques is provided to help clarify markings or notations which may appear on this reproduction.

1. The sign or "target" for pages apparently lacking from the document photographed is "Missing Page(s)". If it was possible to obtain the missing page(s) or section, they are spliced into the film along with adjacent pages. This may have necessitated cutting through an image and duplicating adjacent pages to assure complete continuity.

2. When an image on the film is obliterated with a round black mark, it is an indication of either blurred copy because of movement during exposure, duplicate copy, or copyrighted materials that should not have been filmed. For blurred pages, a good image of the page can be found in the adjacent frame. If copyrighted materials were deleted, a target note will appear listing the pages in the adjacent frame.

3. When a map, drawing or chart, etc., is part of the material being photographed, a definite method of "sectioning" the material has been followed. It is customary to begin filming at the upper left hand corner of a large sheet and to continue from left to right in equal sections with small overlaps. If necessary, sectioning is continued again—beginning below the first row and continuing on until complete.

4. For illustrations that cannot be satisfactorily reproduced by xerographic means, photographic prints can be purchased at additional cost and inserted into your xerographic copy. These prints are available upon request from the Dissertations Customer Services Department.

5. Some pages in any document may have indistinct print. In all cases the best available copy has been filmed.

University Microfilms International
300 N. Zeeb Road
Ann Arbor, MI 48106

Brady, Karen S.

IRON PRECIPITATES FROM ACID COAL MINE DRAINAGE IN SOUTHEASTERN OHIO: ORIGIN, OCCURRENCE AND REGIONAL SIGNIFICANCE

The University of Oklahoma PH.D. 1983

University Microfilms International 300 N. Zeeb Road, Ann Arbor, MI 48106

PLEASE NOTE:

In all cases this material has been filmed in the best possible way from the available copy. Problems encountered with this document have been identified here with a check mark ✓.

1. Glossy photographs or pages ✓
2. Colored illustrations, paper or print _____
3. Photographs with dark background ✓
4. Illustrations are poor copy _____
5. Pages with black marks, not original copy _____
6. Print shows through as there is text on both sides of page _____
7. Indistinct, broken or small print on several pages ✓
8. Print exceeds margin requirements _____
9. Tightly bound copy with print lost in spine _____
10. Computer printout pages with indistinct print _____
11. Page(s) _____ lacking when material received, and not available from school or author.
12. Page(s) _____ seem to be missing in numbering only as text follows.
13. Two pages numbered _____. Text follows.
14. Curling and wrinkled pages _____
15. Other: _____

IRON PRECIPITATES FROM ACID COAL MINE DRAINAGE IN SOUTHEASTERN OHIO: ORIGIN, OCCURRENCE AND REGIONAL SIGNIFICANCE

DISSERTATION

Presented in Partial Fulfillment of the Requirements for the Degree Doctor of Philosophy in the Graduate School of The Ohio State University

By

Karen S. Brady, B.A., M.A., M.S.

*****

The Ohio State University

1982

Reading Committee:

Dr. Jerry M. Bigham
Dr. Terry J. Logan
Dr. Neil E. Smeck
Dr. Olli H. Tuovinen

Approved By

Co-advisor
Department of Agronomy

Co-advisor
Department of Agronomy

ACKNOWLEDGEMENTS

Many people have contributed significantly in myriad ways to the successful completion of this investigation and to the degree Doctor of Philosophy. I am deeply grateful to them for their efforts.

Most importantly, I thank my principal advisor, Dr. J. M. Bigham, for his patience, continued encouragement, and counsel throughout this study, and who, I am convinced, would still have a full head of hair, had I not been his first graduate student. From him I have learned to demand of myself a greater precision in thinking and a thoroughness in planning which will be of great benefit. A good team player, he also knows how to speak with courage of conviction. I thank Dr. T. J. Logan, who so kindly served as co-advisor, and made available laboratory facilities, and support for supplies. I am also indebted to him for his suggestions in improving my stride and distance in jogging. I am indebted to Dr. N. E. Smeck for advice and use of laboratory facilities. I also thank Dr. G. F. Hall, and Dr. R. H. Miller for many philosophical discussions on an array of subjects, both sacred and profane. And I thank Dr. W. Dick, of the OARDC, Wooster, for water analyses done in his laboratory.

Many of my fellow graduate students have influenced my thoughts concerning geologic and pedogenic properties, laboratory techniques, and professional deportment (which still hasn't helped my laugh much). I sincerely thank Dr. Darrell Norton, Mickey Ransom, William Jaynes, Jerry Miller, and

Saratchandran Nair for their valuable input. I thank them, and also Lou Lamb, Ron Hartwig, and John Pichtel for the "ragged and funny" comraderie so much a part of the graduate student experience.

Numerous people in the Agronomy Department at Ohio State and OARDC assisted me in both laboratory and field work. They were: Beth Long, Hilde Bumb, Billie Harrison, Joyce Reis, Pam Schechter, Florentina Munoz, Sue Cherry, and Hal Russell. I am grateful to all.

Two professors outside the Department of Agronomy have been instrumental in guiding me in matters related to this investigation: Dr. G. Faure, of the Department of Geology and Mineralogy; and Dr. O. H. Tuovinen, of the Department of Microbiology. Both have shown great patience and effort in endeavoring to abate my ignorance concerning the iron-oxide system.

I am also grateful for the financial support provided by the Department of Agronomy, Ohio State University, and the Ohio Agricultural Research and Development Center, Wooster. I appreciate, also, the use of funds from the Graduate School as a recipient of the Graduate Student Alumni Research Award.

Instruments outside the Department of Agronomy were made available for my use. I thank Dr. A. J. Rubin, Department of Civil Engineering, for use of the BET unit in his lab. Also, I thank John Hanson, Department of Microbiology, for the most hospitable use of the TEM Laboratory facilities.

I am grateful to Neil Ruble and Paul Jenny, of the Soil Conservation Service, USDA, for their initial ideas and suggestions for a field site. This study could not have been as satisfactorily completed as it was without the choosing of a good field site.

I thank Celia and Ernie Brickell, Lou Lamb, and Michael Thompson for their concern and efforts in giving me my first "home away from home". I thank my "wife", Nora Ransom, for feeding me and making sure my clothes were clean. I thank Debbie Miller for preparing this and other manuscripts for publication. Her production of a finished copy from an appalling rough draft is a feat bordering on magic. And I thank the other secretarial staff, particularly Gloria North and Karla Gutheil, for doing the profusion of "little things" that would have us all tearing our hair out if they weren't done.

I thank my parents, Howard and Ann Brady: Mom, for strength and gentleness; Dad, for will and determination. I thank them both for their unwavering moral and financial support.

Lastly, I thank my many personal friends for helping me with the traumas life brings. I particularly thank Carolyn Piper, Carl Brown, and the rest of my "family" at the University Baptist Church. These people have given themselves a bad press by calling themselves a church. A more caring and supportive group of people will be difficult to find, and their friendship has been and is a sustaining lesson in compassion, love, and grace.

In short, we judge our lives by the effort we make to improve the quality of life of those around us both in our private and professional mileau. As anyone can say of a four year span in their life, much has happened. Ohio and the people whom I have met here have been good to me, and good for me. Thank you.

VITA

February 28, 1948	Born - Omaha, Nebraska
1970	B.A., cum laude U.C.L.A.
1971-1972	Graduate Teaching Associate, University of California, Davis
1972	M.A. University of California, Davis
1973-1976	Instructor of Soil Science, California Polytechnic State University, San Luis Obispo, California
1978	M.Sc., California Polytechnic State University, San Luis Obispo, California
1978 -	Graduate Research Associate, Ohio Agricultural Research and Development Center and The Ohio State University

FIELDS OF STUDY

Major Field: Soil Mineralogy and Pedology

Studies in Pedology. Professors J. M. Bigham, K. R. Everett, G. F. Hall and N. E. Smeck

Studies in Geology and Mineralogy. Professors C. Ehlers and Gunter Faure

Studies in Chemistry. Professors L. B. Anderson, L. M. Dorfman, M. H. Klapper, E. P. Schram, and A. A. Wojicicki

LIST OF TABLES

LIST OF TABLES CONTINUED

LIST OF FIGURES

LIST OF FIGURES CONTINUED

LIST OF FIGURES CONTINUED

TABLE OF CONTENTS

TABLE OF CONTENTS CONTINUED Page

TABLE OF CONTENTS CONTINUED Page

TABLE OF CONTENTS CONTINUED Page

APPENDIXES

INTRODUCTION

This study was sponsored jointly by The Ohio State University, The Ohio Agricultural Research and Development Center, and the Office of Water Research and Technology. The study centered on four principal areas of investigation, and was initiated with a water and suspended sediment inventory of the Muskingum River Basin. The primary purpose of this inventory was to identify major sources of water and sediment pollution within the basin. This investigation revealed that Fe-oxide precipitates were often serious pollutants of streams draining areas which had been mined for coal and abandoned prior to legislation requiring reclamation of disturbed lands. Information concerning the nature of these Fe oxides in streams was lacking, as was information on the environment of precipitation. As a result, a study was conducted to determine the impact of acid mine drainage on sediment and water quality in a small watershed within the Muskingum River Basin.

Next, the mineralogical, chemical, and physical characteristics of the stream precipitates were examined in detail, and a laboratory synthesis study was conducted to determine the influence of selected environmental factors on both the nature and rate of Fe-oxide precipitation. Acid mine drainage and the waters of receiving streams were found to contain high concentrations of sulfate; hence, the role of sulfate in the precipitation process was of special interest.

Finally, the presence of low molecular weight iron hydroxide species in polluted waters, and the relation they have to precipitation of iron oxyhydroxides

under natural conditions was examined. A more complete understanding of the spatial distribution of these ionic species and their relationship to sulfur activity was an important goal.

Four chapters follow this introduction. The first chapter reports results from the basin-wide suspended sediment investigation for the Muskingum River. The second chapter addresses the characterization of bottom sediments from both polluted and unpolluted zones in a small watershed tributary to Moxahala Creek, within the Muskingum River Basin. The third chapter examines the nature of a naturally occurring iron oxide precipitate, ferrihydrite, which forms from acid coal mine drainage, and compares its characteristics with similar iron oxides synthesized in the presence of sulfate. The fourth chapter discusses the speciation of dissolved iron in waters affected by acid mine drainage, examines the effect of sulfate on iron solution chemistry, and evaluates possible mechanisms of ferrihydrite formation under natural conditions.

CHAPTER 1

SUSPENDED SEDIMENTS OF THE MUSKINGUM RIVER BASIN

1.1 Introduction

The Muskingum River Basin of southeastern Ohio occupies approximately 1,753,800 ha and encompasses all or part of 27 counties (Figure 1.1, Table 1.1). It is the largest drainage basin in the state, and it is subjected to a variety of land uses. Currently, agriculture and forestry account for 78% of the land use in the basin, but other forms of regional activity are also economically and ecologically important. For example, localized sandstone deposits are used for glass, foundry, and surface sand, and also account for 53% of the dimension stone used in the state. Since 1802, the ceramics industry has been a profitable business in Ohio, and nearly half the state's clay and 69% of the shale deposits are found in the Muskingum Basin. In addition to ceramics, clay and shale are also used in refractories and cement. Small amounts of limestone are mined within the basin and are used in agriculture, ceramics, construction, and steel making. Finally, the Muskingum River Basin is currently the source of 80% of the coal mined in Ohio, and surface mining accounts for 90% of total production.

1.2 Purpose of the Study

Soil and water management problems within the Muskingum Basin have been recognized for several decades. Excess surface runoff and accompanying soil erosion, sedimentation and flooding have resulted in the development of numerous flood-retarding reservoirs throughout the basin. In addition, land treatment measures such as contour and strip farming, terraces, diversions and

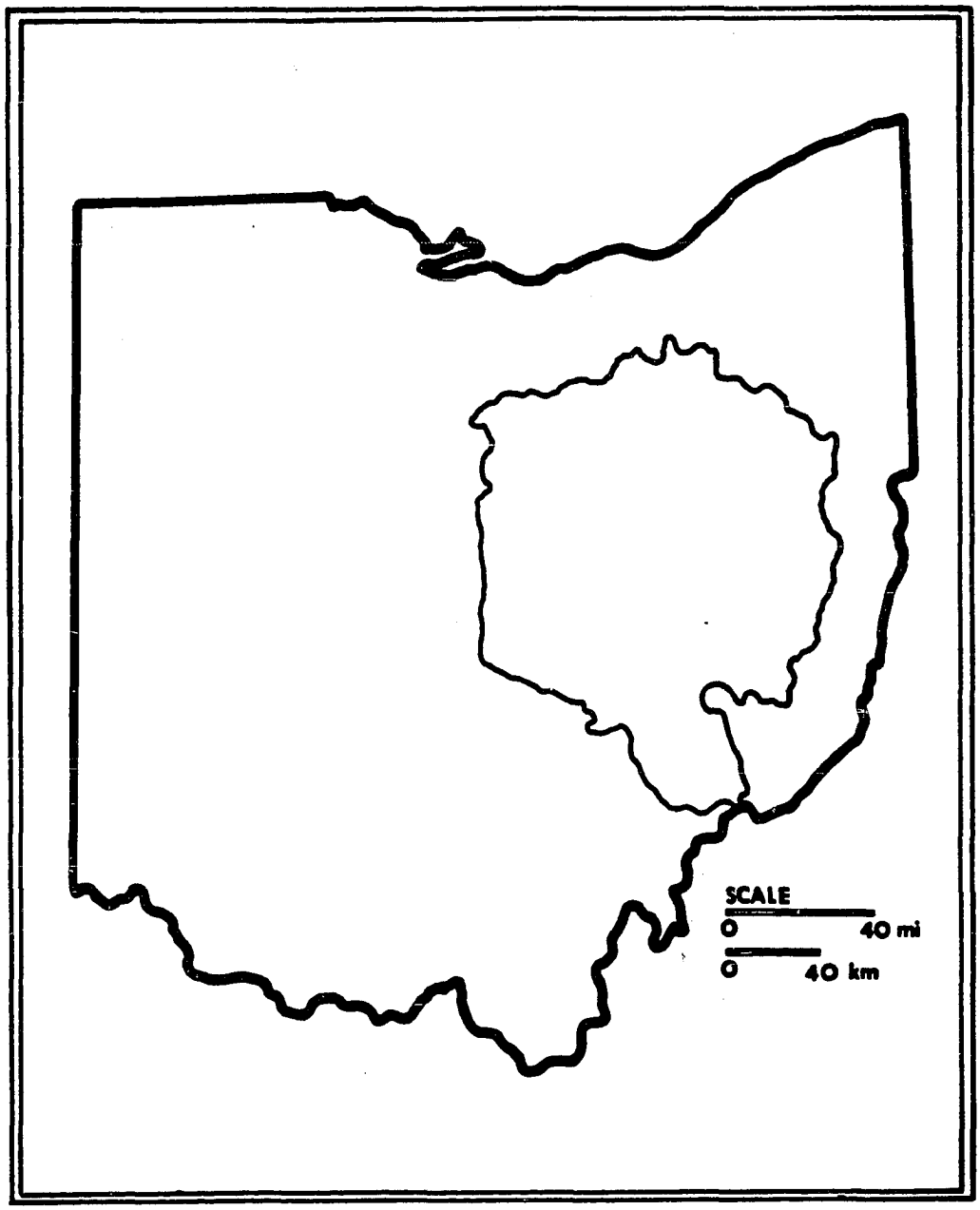

Figure 1.1 Location of the Muskingum River Basin.

Table 1.1 Counties in the Muskingum River Basin
(From Ohio Division of Water, 1968)

County	Square miles in basin	Percent in basin
Ashland	350	82.2
Athens	3	0.6
Belmont	117	21.7
Carroll	314	79.3
Columbiana	52	9.7
Coshocton	563	100.0
Crawford	6	1.5
Fairfield	21	4.1
Guernsey	525	99.2
Harrison	301	73.2
Holmes	424	100.0
Knox	526	98.9
Licking	644	93.7
Medina	144	33.9
Monroe	39	8.6
Morgan	350	83.1
Morrow	140	34.6
Muskingum	670	100.0
Noble	211	52.2
Perry	177	43.2
Portage	2	0.4
Richland	440	88.2
Stark	509	87.6
Summit	156	37.5
Tuscarawas	571	100.0
Washington	222	34.6
Wayne	561	100.0

rotation farming have been actively promoted. Despite these improvements, pollution from municipal, agricultural and industrial sources is still a major problem.

Pollutants originating from municipal and factory wastes are monitored by the Water Control Board of the Ohio Department of Health, and abatement measures are in force. In most cases, time tables for elimination of point-source pollution were established as early as 1970 (Division of Water, 1968).

A more extensive problem in the Muskingum Basin is erosion of agricultural lands. It is estimated that 622,965 tons of sediment reach the mouth of the Muskingum annually; however, this accounts for only 2-3% of the average annual gross erosion in the basin (USDA, 1975). The other 97-98% of the sediment causes damage directly by filling lakes, ponds, and channels. This reduces reservoir capacities and also acts to reduce the water carrying capacities of streams. Sediments removed by soil erosion are usually composed of silt, clay, or organic colloids, which can carry nutrients such as phosphorus and potassium, or organic chemicals such as pesticides, adsorbed to their surfaces. These materials may act as pollutants or as nutrients for algae and aquatic plants. Also, sediment and phosphorus are an important cause of accelerated eutrophication of lakes.

A third and very important source of pollution in the Muskingum Basin results from acid coal mine drainage. The Pennsylvanian coals that are mined throughout the basin are generally high in sulfur impurities, such as pyrite (FeS_2). When tailings from surface or deep mines are exposed to air and water, these sulfur compounds are oxidized to form sulfuric acid (H_2SO_4) and dissolved Fe(II). The sulfuric acid may further react with other minerals in the soil or in adjacent spoil banks to dissolve large quantities of calcium, magnesium,

aluminum and manganese which subsequently enter stream systems or groundwaters along with the sulfate and iron.

The purpose of this study was to produce a single, broad inventory of suspended sediments from sites throughout the Muskingum River Basin to determine if sediment properties could be related to differences in geology, land use, or pollution on a regional basis.

1.3 Literature Review

The amounts of sediment, or chemical pollutants that occur in rivers may vary considerably due to such factors as geology, the geomorphology and slope of the land, soil mineralogy, and agricultural, urban, and industrial activities within a drainage basin.

1.3.1 Terrain, Geology, and Soils of the Muskingum River Basin

The Muskingum River Basin lies entirely within the Appalachian Plateau Province, which is characterized by mature, hilly topography (Williams, 1973). A number of geomorphic cycles of uplift and erosion have resulted in a series of erosional surfaces. During the Cretaceous the entire Appalachian area was supposed to have been eroded to base level; however, no evidence of this surface is now found in the Muskingum Basin. During the Tertiary, there were three such uplift and erosion cycles that are still expressed on the landscape, particularly in the non-glaciated portions of the basin.

Bedrock outcrops occur primarily in the eastern and southern parts of the basin and are dominated by shale and sandstone; however, clay, limestone, coal, and conglomerate are also common. These rocks are from the Mississippian, Pennsylvanian, and Permian systems. Pleistocene glacial drift has obscured much of the bedrock in the northern and western parts (Figure 1.2), and glacial outwash is present in many of the major valleys throughout the basin. Most of

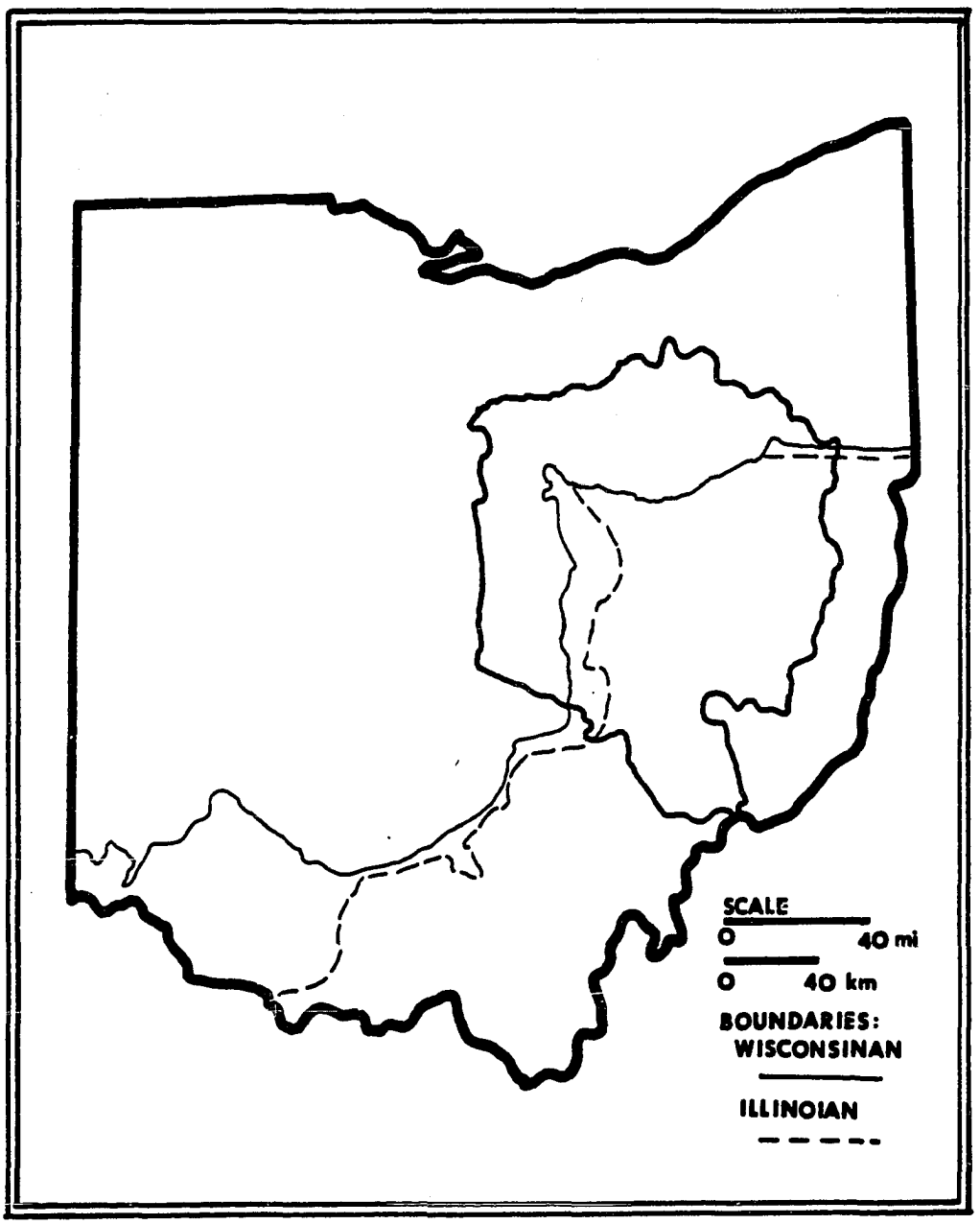

Figure 1.2 Wisconsinan and Illinoian glacial boundaries in Ohio.

the existing glacial till in the Muskingum River Basin was deposited during Wisconsinan glaciation. Two principal till sources are identified; one is found in the northwest, is primarily calcareous, and is part of the Indiana and Ohio Till Plain. The other, north-central in location, is non-calcareous, and is part of the Eastern Ohio Till Plain. The two types of till are characteristic of source areas and the underlying bedrock. Illinoian drift, which lies southeast of the boundary of Wisconsinan drift is characteristically a thin, weathered, discontinuous deposit that only slightly modifies the bedrock topography. Outwash and loess deposits, mostly Wisconsinan in age, occur beyond the drift borders.

The basin has also experienced a number of drainage changes as a result of glaciation. The latest preglacial drainage was the Teays River System, which flowed northwestward across Ohio from the vicinity of Portsmouth and into Indiana south of Fort Wayne. Pre-Illinoian glacial advances blocked this westward flowing stream causing ponding and stream reversals. The Wisconsinan glacier caused additional ponding and further modified the drainage to its present form. Evidence for drainage reversals consists of numerous barbed and underfit streams and narrowing of valleys downstream. The Muskingum River itself shows the most dramatic reversal. At Dresden, the valley is 3.2 km wide, but it is only 0.4 km wide near the Muskingum-Morgan County border (Lamborn, 1956).

The soils of the basin reflect geologic-geomorphic influences, and a noticeable spacial distribution with respect to soil order exists. Soils on the glaciated surfaces are predominantly Alfisols. Soils in the unglaciated portion of the basin are Alfisols, Ultisols, and Inceptisols.

1.3.2 Erosion and Sedimentation within the Muskingum River Basin

Sediment is defined as solid material which originates mostly from soil or disintegrated rock and is transported by, suspended in, or deposited from water. It can, but does not always include chemical and biochemical precipitates and decomposed organic material, such as humus. Suspended sediment is the sediment that at any given time is maintained in suspension by the upward components of turbulent currents or that exists in suspension as a colloid. The quantity, characteristics, and cause of suspended sediment in streams are influenced by environmental factors as well as man's activity. Some major factors are degree of slope, length of slope, soil characteristics, land use, and quantity and intensity of precipitation.

Previous studies in the Maumee River Basin (Jones et al., 1977) have shown that significant sediment losses occur even in nearly level farmland as a result of surface runoff and subsurface tile flow. The range in topographic relief in the Muskingum River Basin is about 280 m. The highest point within the basin, about 457 m above sea level, and the lowest, about 177 m above sea level, provide ample opportunity for erosion. The U. S. Geologic Survey reported the average suspended sediment load of the Muskingum River at McConnelsville to be 134 mg/l for the 12-month period October, 1977-September, 1978 (U. S Geological Survey, 1978). However, suspended sediments can be as high as 700 mg/l or more during periods of storm flow.

A major factor in sediment production is the entrainment and transport of clay minerals by fluvial action. The size, shape, and chemical properties of clay minerals determine not only their resistance to erosion but also their activity in suspension, and eventually the mineral character of sediments in the suspended or the bed load. When specific minerals are identified in determining the

character of sediments, the possibility of using these same minerals as guides to provenance exists.

1.3.3 Sediment Mineralogy and its Relation to Provenance

Provenance is concerned with origin of sediments. Frequently, a mineral or particular suite of minerals occurring in sediment may be characteristic of a certain source area. Knowledge of the bedrock, recent geologic history, and soil weathering products within the source areas can, in turn, aid in determining the origin of a mineral or suite of minerals many kilometers from the point of entrainment.

Ehlman (1968) indicated that clay mineral assemblages which make up the stream load can originate from three possible sources within a watershed: sheet erosion from the land surface, streambank erosion, and resuspension of materials composing the streambed. It is possible for the stream load to mirror these sources, but the relative contribution of any one of them may vary greatly depending upon such factors as topography of the watershed, history of disturbance, and stream flow.

Schneider and Angino (1980) analyzed suspended sediments from selected rivers in eastern Kansas, and observed that vermiculite was a significant component of samples from rivers draining Pleistocene glacial deposits. Walling et al. (1979) reported that measurements of the magnetic properties of suspended sediments in transit can provide a general indication of the relative importance of slope and channel sources to the sediment yield of a drainage basin, and often can yield specific information on the relative contributions of individual sources during a storm event and on contrasts in the pattern of sediment generation between particular events. Klages and Hsieh (1975), in their examination of sediments transported by the Gallatin River of southwestern

Montana, noted that differences in clay mineralogy due to source area variations could be detected only among smaller tributaries. Knebel et al. (1968) noted that clay mineralogy was a function of distance downstream in their study of tributaries of the Columbia River: montmorillonite was observed to increase while the amount of illite decreased. This trend, however, was attributed to differing mineralogies of soils forming in the source areas of the tributaries. Jones et al. (1977) indicated that illite and quartz were the two most abundant minerals leaving watersheds in the Maumee River Basin of Ohio. They reasoned that the preferential removal of these minerals was related to their relatively low plasticities and low surface charge. Imeson and Verstraten (1981) noted a relationship between electrolyte concentration, exchangeable sodium percentage of soils in source areas, and suspended solid concentrations for drainage basins of a small river in Eastern Australia. Changes in the electrolyte concentrations resulted in an alternation between conditions favoring dispersion and flocculation of the suspended load.

Provenance is also a determining factor in the clay mineralogy of bottom sediments. Sartori et al. (1979) related chloritic intergrades occurring in bottom sediments near the estuary of the Arno River of Italy to chloritic intergrades found in suspended samples of the Arno River and one of its tributaries, and, finally, to the soils and underlying rocks in the tributary basin. Stober and Thompson (1979) reported that magnetite concentrated in the sediments of some Finnish lakes could be related to glacial drift, and that the hematite/magnetite ratio was found to decrease in the progression drift-stream bedload-lake sediment.

Knebel et al. (1977) found that differences in the clay mineralogy of bottom sediments were related to source areas by a number of factors, among

them: size segregation of particles due to preferential erosion and settling, and natural particle size. Pinet and Morgan (1979) indicated that amount of freshwater discharge played an important role in determining the composition of bottom sediments in two Georgia estuaries. For one, associated with a large river, bottom sediments of the river and estuary were similar. The other, with low discharge, seemed to derive much of its sediment from erosion of coastal outcrops. Knebel et al. (1977) found that chlorite and kaolinite components were most concentrated in the sediment near the source river and illite predominated at greater distances from the river. This distribution was attributed to particle size differences. In addition, there seems to be a positive correlation between water velocity and expandable clay mineral content (Berry et al., 1970). Three possible causes for this correlation are: resuspension of the expandable clay components from bottom sediments due to increased shear velocities, greater rainfall intensities which detach and entrain the expandable clay minerals from soil surfaces, and the ability of high velocity water to carry aggregates of expandable minerals.

Finally, chemical weathering of iron, manganese, and aluminum containing minerals can result in the widespread appearance of various metal oxides in the secondary environment (Oades, 1963), of which soils and sediment are a part. These oxides may occur as discrete crystalline precipitates, as near-amorphous coatings on other, larger sediment grains, or as complexes with organic matter. Their surfaces are highly reactive, and they are important scavengers of charged species from solution. Chemical fractionation of secondary oxides into mineral phases and chemical forms is possible through the use of selective chemical extractants (Chao and Theobald, 1976). Consequently, the distribution, type and composition of these oxides in stream sediments can be significant indicators of

both origin and environment of deposition. The value of the iron and manganese oxides to geochemical exploration has, in particular, been recognized (Chao and Theobald, 1976).

1.3.4 Phosphorus and Nitrogen in Soils and Sediments

Critical levels of nitrogen and phosphorus are used to indicate the trophic state of natural waters. These levels are 0.3 µg/ml soluble inorganic nitrogen and 0.003-0.015 µg/ml soluble inorganic phosphorus (Stewart and Rohlich, 1967). The literature suggests that despite an overall greater input of nitrogen into most watersheds, phosphorus is frequently the limiting factor for the growth of biomass in a body of water (Hooper, 1969). For this reason, the greatest emphasis in this discussion of nutrient additions is given to phosphorus.

Until recently, the major source of phosphorus entering most streams and lakes was thought to be phosphates from urban sources, especially laundry detergents. Although urban centers still represent important point sources for phosphorus accumulation in sediments, runoff from agricultural land is receiving increasing attention. The US Army Corps of Engineers (1982) has documented that erosion from agricultural lands is the primary source of sediment into Lake Erie, and that land use activities contribute from a third to a half the total phosphorus load in the Great Lakes. Other researchers (Johnson et al., 1976) indicate that phosphorus increases are due primarily to sewage from urban areas and non-functioning single dwelling septic tanks. In any case, the Muskingum River Basin is largely a rural watershed, and the primary concern is the effect phosphorus as a nutrient addition to agricultural soils will have on the sediments entering lakes and streams.

The more important forms of total P in sediments are determined by both organic and inorganic sources. The two forms are controlled by independent

factors. Organic P is a constituent of organic matter, and the decomposition of organic matter is one way that soluble orthophosphates are released into streams and lakes (Black, 1968; Williams, et al., 1976). However, inorganic P frequently constitutes the major portion of the total P, and is usually in the form of the orthophosphate (PO_4^{3-}) ion. While much orthophosphate enters waterways as adsorbed ions on oxides and hydrous oxides of Fe and Al, and $CaCO_3$, P may also be added in subsurface waters. Johnson et al. (1976), for example, showed that 44% of the total phosphate load in a small stream of central New York was derived from percolating water. Factors which determine the entry of orthophosphate into streams from subsurface flow are volume and intensity of precipitation, rate and type of fertilizer additions, permeability of the soil, and phosphate adsorption properties of the soil.

During the process of erosion and transport of sediment across a land surface, the finer clay is selectively transported (Logan, 1977). Since clay contains a higher concentration of total P than the soil as a whole, the sediment in streams will have an enriched P content compared to the soil from which the clay was removed. This is consistent with observations made by Singer and Rust (1975) that a primary loss of agricultural P comes from erosion of tilled lands. In addition, Sharpley and Syers (1979), in a study of an agricultural watershed in New Zealand, report that surface runoff produced a minor portion of the total stream flow, but it contributed a major portion of both soluble and particulate P compared to other sources. For the small agricultural watershed studied, total P load was 1.48 kg/ha/yr in the suspended sediments. Total P values ranging from 900-2000 μg/g in sediments from the Maumee River have been reported by Green et al. (1978).

Total P has also been associated with the mineral character of sediments. Oloya (1981) stated that higher amounts of total P were generally found in non-calcareous versus calcarous sediments, despite the possibility that native apatite could be present locally as a constituent of the total P eroded from a landscape. Thus, differences in total P may arise in tributaries of a large drainage basin based on the calcareous or non-calcareous character of the soils or geologic materials, such as glacial drift, in a watershed.

Nitrogen losses by soil erosion, like phosphorus, is generally related to organic matter removal. Organic nitrogen removal, or the entrainment of organic matter, is usually significant only during higher soil loss periods (Logan and Stiefel, 1979). Total nitrogen in a stream system is a measure of both dissolved and solid-phase organic and inorganic N. Sediment nitrogen, because it is so closely associated with detrital organic matter, is usually equated with organic nitrogen.

The two most common forms of dissolved inorganic nitrogen in stream waters are NO_3 and NH_4. As a pollutant, NH_4-N is generally insignificant in soil and groundwaters (Terry et al., 1981). However, NO_3-N is found in measurable quantities, and has been used as a primary indicator of nitrogen pollution. Nitrate is naturally formed in soils as a product of the nitrogen cycle, and because of its mobility, is found in groundwater. One of the greatest concerns is the ease with which this ion may be reduced to nitrite and cause methemoglobinemia in babies or nitrite poisoning in ruminants. Considerable controversy reigns as to whether the source of nitrate can be directly related to fertilizers applied to fields. Logan and Stiefel (1979) in a study of the Maumee River Basin, indicated that NO_3-N losses from soil were similar to amounts added by precipitation. However, none of their study sites had received

fertilizer nitrogen, soybeans having been grown on all test sites. Nightingale (1972) noted that NO_3-N contents of both soil water and groundwater were a function of crop type and soil depth, and found that orchards and truck crops were major contributors of NO_3-N. Maximum NO_3-N from these sources was found to be in the range of 46 mg/l in the groundwater. This value exceeds the maximum permissible NO_3-N level of 10 mg/l established by the U.S. Public Health Service for public drinking water. Often of greater concern is the NO_3-N losses from feedlot areas which clearly contaminate groundwaters, and which have been monitored at levels as high as 46 mg/l (Terry et al., 1981).

Thus, P and N can vary greatly in their origins within a watershed. Soluble inorganic P (orthophosphates) is usually the greatest constituent of total P, and total P is generally found in greatest amounts in non-calcareous sediments. Nitrate-N, on the other hand, is closely correlated with agricultural fertilization and feedlot activities. While both P and N may be agricultural in origin, total P in sediments is frequently related to areas of major soil erosion while NO_3-N levels may more readily provide evidence of fertilizer and feedlot (farming) differences within a watershed.

1.3.5 Acid Mine Drainage

Abandoned spoil banks from both surface and deep mines can produce serious water quality problems due to erosion and acid mine drainage. As indicated earlier, many eastern U. S. coal deposits are characterized by high-sulfur contents. Sulfide oxidation produces large concentrations of sulfuric acid and dissolved iron. While spoil banks are not homogeneous in character, it is generally considered that a significant portion of spoil within the eastern coal province has a pH of less than 4 (Berg and Vogel, 1969). Further disintegration and decomposition of minerals is accentuated by low pH (acid attack) (Berner,

1971), and adequate rainfall combined with the general good permeability of spoil materials provide optimal conditions for rapid weathering and leaching. Geologic strata associated with coal seams are of sedimentary origin and may consist of shale, siltstone, sandstone, mudstone, and limestone (Chadevich, 1969). Carbonaceous material is abundant in spoils and makes up the bulk of weight loss when spoil is heated to 600° C (loss-on-ignition). Spoil material is generally slow to decompose and supplies few nutrients for plant growth. Usually more than 90% of the inorganic matter in a strip-mine spoil bank is composed of quartz and clay minerals derived from mudstones and shales. Wiram (1976) observed that clay minerals present in spoil near Latta, Indiana consisted of varying proportions of illite and kaolinite. Also commonly present in the spoils are small amounts of iron and aluminum hydroxides, sulfates, and carbonates. The release of ions in weathering is then a function of congruent dissolution of all the above mentioned components. Subsequent leaching of weathering products results in high amounts of Fe, Al, Mn, Mg, K, Na, H, and SO_4 in receiving streams and groundwaters.

Since hydrogen, carbon, iron, aluminum, and manganese are among the most abundant elements released in acid mine drainage, this inventory of suspended sediments in the Muskingum River Basin included direct or indirect measures of all these parameters to determine if they could be related to regional influences of acid mine drainage.

1.4 Materials and Analytical Procedures

1.4.1 Selection of Field Sites

The headwaters of the Muskingum River originate near the city of Akron, within 40 km of Lake Erie. The river flows south to its junction with the Ohio River at Marietta, Ohio. The total basin is 192 km long and 152 km wide at its

widest point and includes 11 major tributaries. In the late fall of 1979 and winter of 1980, extensive field reconnaissance was done in an attempt to establish sample sites for all the major drainage sub-basins. In most cases, sampling sites were selected near the mouth of each major tributary. Larger watersheds such as the Tuscarawas and the Muskingum were assigned two or more sites (Figure 1.3, Table 1.2). As a result, 16 sites in the basin were chosen as points of collection.

1.4.2 Sample Collection and Preservation

All the suspended sediments were collected over a 12-hr period in March of 1980 during a time of high flow resulting from the spring snow melt and widespread precipitation. High flow was preferred because mixing of sediments is optimal, and it was easier to obtain sediment samples that were representative of eroded materials throughout the basin.

Approximately 57 l of suspended sediment were collected at each site using a 9.5 l bucket suspended by rope over the central part of a bridge. The fastest flow free from stream-bank eddy effects and possible problems with channel erosion is in the center of the stream and, since velocity and discharge data were not a goal of the study, more sophisticated sampling devices were not considered necessary. This reasoning may only be applicable to low-gradient streams and rivers where sediment is mostly a mixture of silt and clay. Once entrained, these materials stay in transport with very small energy input, and mixing of the sediment is optimal at high flow periods.

Upon returning to the laboratory, aliquots of the suspended material were immediately removed for determining total sediment, phosphorus, and nitrogen contents. Then, phenol (0.2 g/l) was added to the bulk sample to control microbial activity, and the sediment was placed in a walk-in refrigerator and

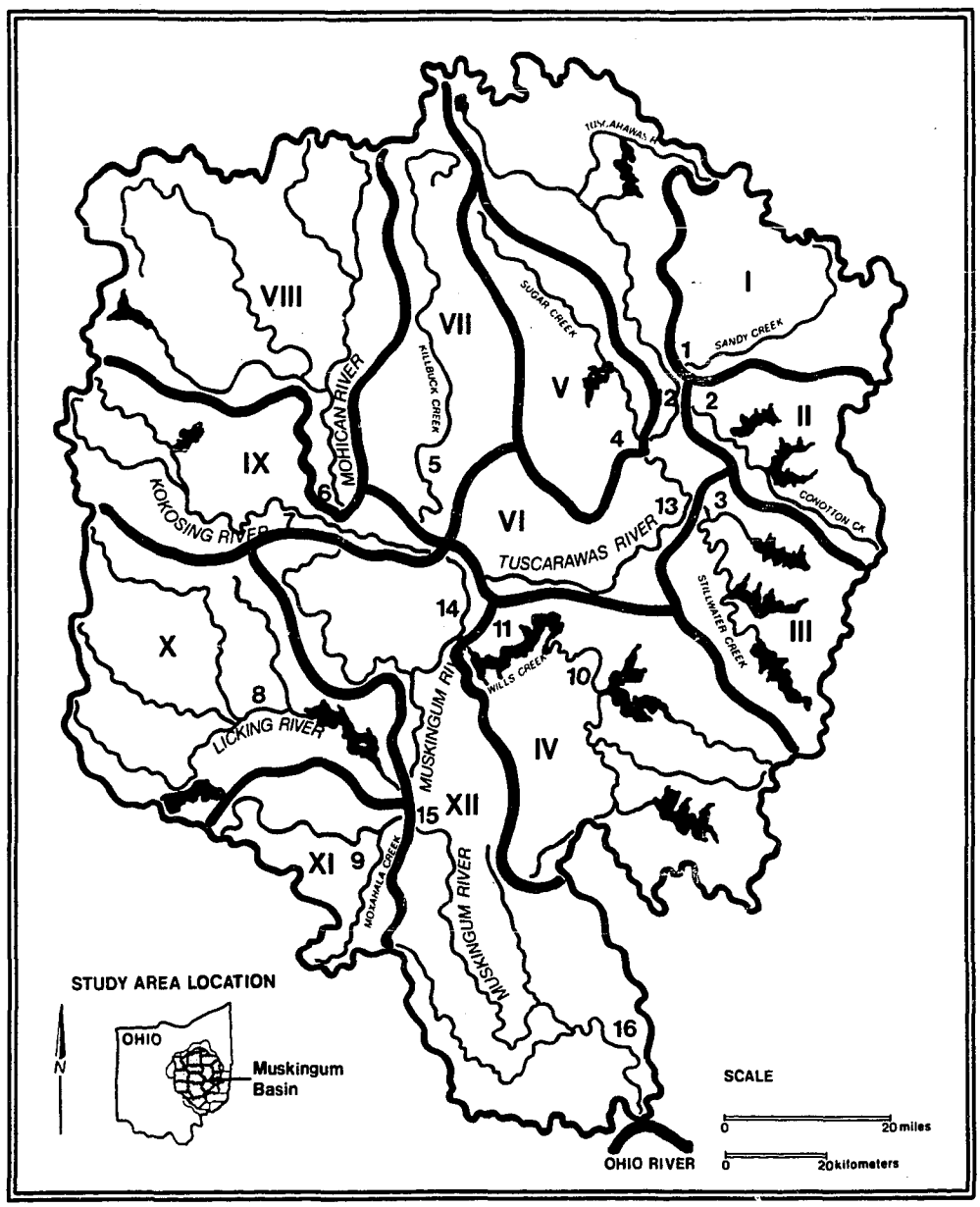

Figure 1.3 Hydrologic sub-basins and sampling locations within the Muskingum River Basin.

Table 1.2 Hydrologic Study Areas of the Muskingum River

Hydrologic Sub-Basin	River or Stream	Approx. Sample Site Town/Location	No.	Drainage Area (sq. ha)
I	Sandy Creek	Sandyville	1	109,800
II	Conotton Creek	Zoarville	2	77,700
III	Stillwater Creek	Midvale	3	122,500
V	Sugar Creek	Strasburg	4	89,400
VII	Killbuck Creek	Killbuck	5	169,400
VIII	Mohican River	Brinkhaven	6	225,800
IX	Kokosing River	Millwood	7	163,200
X	Licking River	Newark	8	196,800
XI	Moxahala Creek	Roseville	9	119,100
VI	Wills Creek	Kimbolton	10	234,100
		Wills Creek	11	
IV	Tuscarawas River	Bolivar	12	246,000
		Gnadenhutten	13	
XII	Muskingum River	Tyndall	14	300,000
		Philo	15	
		Lowell	16	

allowed to settle. Excess water was removed by siphoning, and the sediments were further concentrated by centrifugation at 1500 rpm for 10 min using a Beckman J21B centrifuge and an angle-head rotor. The samples were then frozen in 400-ml polyethylene beakers using a slurry of trichloroethylene and dry ice and freeze-dried in a Virtis lyophilizer. This procedure allowed for estimates of total sediment available for analysis and provided easy storage of dried samples.

1.4.3 Analytical Procedures

The analytical procedures used in this general study of the regional character of suspended sediments in the Muskingum Basin include various physical, chemical, and mineralogical analyses. These procedures are described in detail in the following sections.

1.4.3.1 pH. Measurements of hydrogen ion activity in the stream waters from which the sediments were collected were performed according to EPA standard methods (1980). Measurements were made using a Corning Research Model 12 pH meter with a combination electrode.

1.4.3.2 Total Sediment Contents. Concentrations of suspended sediment were measured by withdrawing a 50-ml aliquot from the dispersed field sample prior to phenol addition. This 50-ml aliquot was then filtered using a pre-weighed Nucleopore membrane with a pore diameter of 1.0 μm. The sediment retained on the filter was dried at 105° C, and the weight of sediment was determined by difference in weight of the filter before and after filtration.

1.4.3.3 Phosphorus Analysis. Dissolved inorganic phosphorus (DIP) and total phosphorus were determined by separate methods. DIP was determined by passing duplicate 25-ml aliquots of suspended sediment through a 0.45 μm Nucleopore filter. Eight ml of a mixture of L-ascorbic acid and Murphy-Riley

solution (John, 1970) were then added to a suitable aliquot of the filtrate and the samples were brought to a 50-ml volume, stoppered, shaken, and set aside for 30 min for color development. The phosphate levels were measured by photon absorption at 730 nm using a Beckman 24 spectrophotometer equipped with a 1 cm cell and a vacuum sipper.

Total phosphorus was determined using the perchloric acid method of Sommers and Nelson (1972). Aliquots (25-ml) of unfiltered sediment were pipetted into 50-ml digestion tubes. Five drops of concentrated H_2SO_4 were added to each suspension and the samples were evaporated in an oven at 105° C overnight. On cooling, 3 ml of 70% perchloric acid were added, and pyrex funnels were placed atop the tubes to ensure complete digestion. The samples were digested at 203° C for 75 minutes, allowed to cool, and then diluted to 50 ml with distilled water. The tubes were then shaken to mix the contents and left to settle overnight or centrifuged to separate solid residues. Ten-ml aliquots from the clear supernatant solutions were then pipetted into 50-ml tubes and neutralized with 5N NaOH using p-nitrophenol as an indicator. Five ml of L-ascorbic acid solution (previously described) were added, and the solution brought to a final volume of 25 ml. Absorbance readings were taken after 1 hr with a Beckman 24 spectrophotometer at 730 nm wavelength.

1.4.3.4 Nitrogen Analysis. Duplicate, 10-ml aliquots of each sample were passed through 0.45 μm Nucleopore filters, and the filtrates were transferred to micro-kjeldahl flasks. For total inorganic N, 1 g MgO + 1 g Devarda's alloy were then added. The flasks were immediately transferred to a distillation apparatus, and the samples were distilled into 50-ml flasks containing 5 ml of 2% boric acid until approximately 30 ml of distillate were collected. The distillates were then titrated with 0.01N HCl solution to a blue-green end point. Ammonia-nitrogen

was determined using the same method but without Devarda's alloy. Nitrate-N was determined by subtraction of the NH_4-N from the total inorganic N. Results were reported as NO_3-N and NH_4-N in µg/ml.

1.4.3.5 Organic Carbon. Total organic carbon was determined on the whole, freeze-dried sediment prior to any treatment with H_2O_2 for removal of organic matter. The method used was modified from those given by the Soil Survey Staff (1972) and Post (1956). Duplicate 0.5 g samples were placed in small, heat resistant ceramic boats containing powdered MnO_2 as a catalyst. The boats were transferred to a Lindberg oven and heated at 1000° C for 10-12 min. Dry combustion resulted in the volatilization of CO_2 which was trapped in ascarite treated with NaOH. Carbon dioxide was then determined gravimetrically, and organic carbon was calculated from a standard curve prepared by combustion of known amounts of oven dried (110° C) $CaCO_3$.

1.4.3.6 Fractionation and Particle Size Analysis. The freeze-dried whole sediment was fractionated after total organic carbon analysis had been completed (see section 1.4.3.5). In most cases, the total sediment yield was limited, so the entire sample was fractionated. This was accomplished by transferring the sediment to a 250-ml centrifuge bottle after which approximately 60 ml of distilled water were added. The sample was then washed once with 100 ml of 1N NaCl and twice with 100 ml of 60% methanol, using centrifugation after each washing. The washings were discarded, and the sample was transferred to a 400-ml plastic beaker. Thirty ml of 0.5N Na_2CO_3 were added, and distilled water was used to adjust the final volume to 200 ml. An ultrasonic probe (Branson Sonifier Cell Disruptor Model W 185) was immersed into the suspension and the sample was dispersed for 5 min at 100 watts. The suspension was allowed to stand 4 sec for each cm of suspension depth. The

supernatant suspension was then decanted onto a 300-mesh sieve, and the fines were washed through the sieve with distilled water directly into the sample holder of an automatic clay separator (Rutledge et al., 1967). Wet sieving was continued until the material on the 300-mesh sieve was washed free of silt and clay. Retained sands were transferred to a beaker, dried at 60° C, and weighed. The clay (<2 μm) was separated from the silt by repeated siphoning (up to seven cycles) at a convenient depth and time interval calculated according to Stoke's Law (Jackson, 1969). Volume of the siphoned, suspended clay was controlled by flocculation with 1N $MgCl_2$ and subsequent decantation of the supernatant liquid. The sedimented silts were transferred to a beaker, dried at 60° C, and weighed; the clay content was then determined by difference from the original sample weight.

The flocculated clays were washed free of excess salts using sequential, 100 ml distilled water washes. Occasionally, dispersion occurred before salts were completely removed. Dispersion was then controlled by washing with 60% methanol and/or acidification with 1 or 2 drops of 0.1N HCl. The washed clays were quick-frozen and freeze-dried as stated above. It should be noted that care was taken to treat all sediments in as gentle a manner as possible. Clay minerals, especially the iron oxides, can be altered by harsh treatments involving elevated temperatures. For this reason, most of the original whole sediment samples were not exposed to the usual H_2O_2 treatment for removal of organic matter, and the temperature was not elevated above 60° C during freeze-drying. The freeze-dried clays were used for nearly all the chemical and mineralogical analyses in this study. The moisture content of each freeze-dried clay was determined gravimetrically and sample weights were adjusted when necessary to their oven-dry (110° C) equivalents.

1.4.3.7 Sodium Pyrophosphate Extractions. A 0.1 M solution of sodium pyrophosphate ($Na_4P_2O_7$) was prepared as directed by Bascomb (1968). Fifty ml of the solution were then added to 0.25 g of clay material in a 100-ml polypropylene test tube. The tube was stoppered and placed on an oscillating shaker, and shaken overnight. After shaking, 1 drop of 0.4% superfloc solution was added to the sample, and the suspension was centrifuged at 1500 rpm for 6 min. The resulting supernatant liquid was decanted into a 50-ml Erlenmeyer flask and analyzed for Fe and Al using a Varian AA-6 atomic absorption spectrophotometer.

Samples were analyzed directly for Al using the original extracts but Fe was determined after dilution by a factor of 10. Concentrations of Fe in the sample extracts were compared to standard solutions ranging from 0 to 20 μg/ml; Al standards ranged from 0-100 μg/ml. All standards were prepared from Fisher certified atomic absorption reference materials and appropriate quantities of blank solution. The samples were extracted and analyzed in duplicate.

1.4.3.8. Acid Ammonium Oxalate Extractions. Tamm's Reagent, a buffered solution of ammonium oxalate and oxalic acid was prepared as directed by McKeague et al. (1971). The pH was adjusted to 3.0 with concentrated NH_4OH, and the solution was stored in the dark. A 0.25 g sample of clay material was placed into a 100-ml polypropylene test tube, and, in near darkness, 50 ml of the ammonium oxalate buffer was added. The test tubes were stoppered and shaken in an oscillating shaker for 4 hr in complete darkness. Following extraction, superfloc was added, the samples were centrifuged, and the extract was transferred to a 50-ml Erlenmeyer flask. The extracts were then stored in the dark until ready for analysis.

Samples were analyzed for Al and Mn with no further dilution of the original extracts. Concentrations of Al and Mn were compared to standard solutions ranging from 0-100 μg/ml and 0-2 μg/ml for Al and Mn, respectively. Iron was determined from a 1 to 10 dilution of the original extract by comparison with standard solutions containing 0-20 μg/ ml Fe. Duplicate analyses for all three elements were made with a Varian AA-6 spectrophotometer.

1.4.3.9 Sodium Citrate-Bicarbonate-Dithionite Extractions. Sodium citrate-bicarbonate-dithionite (CBD) extractions were done on 0.5 g of clay using a procedure adapted from that of Mehra and Jackson (1960). The clay was placed in a 100-ml polypropylene test tube, and 40 ml of sodium citrate-bicarbonate buffer were added. The sample was placed in a water bath and the temperature elevated to 75-80° C. One g of $Na_2S_2O_4$ was then added and the sample was stirred occasionally for 5 min. Then a second 1 g portion of $Na_2S_2O_4$ was added. After an additional 5 min, the sample was removed from the water bath and centrifuged for 5 min at 1500 rpm. The supernatant liquid was then decanted into a 250-ml volumetric flask and brought to volume with distilled water. A 1 to 20 dilution of this solution was used for analysis of Fe; Al and Mn were determined with no further dilution.

All samples were analysed using a Varian AA-6 atomic absorption spectrophotometer with standards made from 1000 μg/ml stock solutions of Fisher atomic absorption standards and CBD reagent. Standard solutions ranged from 0-20 μg/ml for Fe, 0-100 μg/ml for Al, and 0-2 μg/ml for Mn.

1.4.3.10 Total Chemical Analysis. Total dissolution of clay materials was achieved using a Parr acid digestion bomb and the method of Bernas (1968). All samples were prepared in duplicate and stored in polyethylene bottles after digestion. Fe and K were determined by a Varian AA-6 atomic absorption

spectrophotometer. Iron was analyzed using a 1 to 10 dilution and K was determined directly from the original 100-ml digests. Again, standard solutions of these elements were prepared using Fisher certified reference materials and appropriate quantities of blank solution. The standard range employed was 0-20 μg/ml for both Fe and K.

1.4.3.11 X-ray Diffraction Analysis. Clay samples from the sediments were K- and Mg-saturated and prepared for analysis using the oriented slide procedure described by Brindley (1972). Potassium saturation was achieved by placing approximately 0.5 g of air-dried clay into a 50-ml centrifuge tube. Twenty ml of 1N KCl were added, the tube was stoppered, and the sample was dispersed by shaking. The tubes were then centrifuged at 1500 rpm for 5 min and the clear liquid decanted. This salt wash was repeated twice, after which the clay was washed free of excess salts using one 20-ml distilled water wash and subsequent 20-ml, 60% methanol washes as needed. When washing was completed, 30 ml of distilled water plus 1 or 2 drops of 0.5N KOH were added, and the sample was dispersed for one minute using a Branson Sonifier Cell Disruptor (Model W 185). Two ml of the resulting suspension were pipetted onto a 27 x 46 mm petrographic microscope slide and allowed to air dry. The K-saturated clays were subsequently analyzed at room temperature, after heating to 350° C, and after heating to 550° C.

All clays were Mg-saturated prior to freeze-drying; therefore, 0.5 g of clay was placed in a 50-ml plastic beaker, 30 ml of water plus 1-2 drops of 0.5N KOH were added and the sample was dispersed with an ultrasonic probe without additional washing. Duplicate two-ml aliquots of suspension were transferred to glass slides and allowed to air dry. When dry, one was analyzed directly and the

other was placed in a covered vessel over ethylene glycol and held at 60° C for 12 hr prior to analysis.

X-ray diffraction analyses were conducted using a Philips PW 1316/90 wide range goniometer equipped with a theta compensating slit, a curved crystal monochrometer, and a scintillation detector. The diffraction tube was operated at 35 kV with a current of 15 mA, and provided CuKα radiation. A one-sec time constant and a 1000-count per sec range factor were used for most analyses. Diffractograms were normally obtained over an angular range of 2-30° 2θ with a scanning speed of 2° 2θ per min and a recorder speed of 1 in per min.

1.5 Results and Discussion

1.5.1 pH, Nitrogen, and Phosphorus Analyses

Analytical results for pH, nitrogen and phosphorus are given in Table 1.3. The pH's of the water samples from most of the Muskingum Basin are very uniform and are at or slightly below neutrality. A noticeable difference is seen only in water taken from Moxahala Creek which has a pH of 4.2 and which is probably indicative of high levels of acid coal mine drainage within the small Moxahala watershed (BUSML, 1976).

Total nitrogen contents are generally low, and NH_4-N levels are likewise low to non-detectable (detection limit was 0.001 μg/ml) in a majority of the waters. In addition to being in greater concentrations compared to NH_4-N, NO_3-N appears to reflect regional differences within the watershed. Undetectable to low concentrations of NO_3-N are found in samples from Conotton, Stillwater, Moxahala, and Wills Creeks, all watersheds left unglaciated during the Pleistocene. There is as much as a seven-fold increase in NO_3-N in samples from sub-basins affected by glaciation and, presumably, greater agricultural activity.

Table 1.3 Nitrogen and Phosphorus Contents and pH of Waters in the Muskingum River Basin

River or Stream	Site	pH	Nitrogen		Phosphorus	
			NH_4-N	NO_3-N	DIP**	Total P
			µg/ml			
Sandy Creek	1	6.3	0.24	1.75	--	0.37
Conotton Creek	2	6.5	--	--	0.01	0.16
Stillwater Creek	3	6.7	--	0.46	0.01	0.11
Sugar Creek	4	7.2	--	3.15	0.01	0.37
Killbuck Creek	5	6.4	--	1.56	0.02	0.36
Mohican River	6	6.6	--	1.40	0.02	0.58
Kokosing River	7	6.8	--	1.33	0.07	0.26
Licking River	8	6.8	--	--	0.02	0.21
Moxahala Creek	9	4.2	0.11	--	0.01	0.16
Wills Creek						
Kimbolten	10	6.8	0.24	0.46	0.01	0.16
Wills Creek	11	6.7	0.25	0.46	0.01	0.16
Tuscarawas River						
Bolivar	12	6.5	0.24	2.87	0.08	0.42
Gnadenhutten	13	6.6	--	2.67	0.01	0.32
Muskingum River						
Tyndall	14	6.5	0.53	2.38	0.15	0.42
Philo	15	6.5	*	*	*	*
Lowell	16	6.4	--	1.54	0.01	0.26

* Sample missing
** DIP = dissolved inorganic phosphorus
— Not detectable at 0.001 µg/ml

Dissolved inorganic phosphorus (DIP) is much lower than total P, and is uniform throughout the basin. The highest values come from two glaciated areas, the Kokosing and the upper Tuscarawas, but the sources of glacial drift for these two sub-basins are different. Glacial drift in the area drained by the Kokosing is predominantly calcareous, while that drained by the Tuscarawas is not. Variation in dissolved P, therefore, does not seem to be attributable to geologic provenance. This observation does not prohibit the possibility of an agricultural origin for the DIP. Under usual conditions, fertilizer phosphorus is readily immobilized by soil (Tisdale and Nelson, 1975). Increased quantities of dissolved P in runoff may indicate direct loss of this fraction as might occur if manure or other fertilizers were applied to frozen soil. Both the Tuscarawas and Kokosing sub-basins have high agricultural activity. However, samples from the other sub-basins draining glacial areas are low in DIP, despite similar agricultural activity.

Total P concentrations generally increase with increases in suspended sediment within the basin (Tables 1.3 and 1.4), which indicates that most P lost in surface runoff occurs as sediment-P. This observation is supported by Sharpley and Syers (1979) in their study of sources of P from agricultural soils in New Zealand. As with NO_3-N, geologic or land use differences seem to influence total P. Values for total P from unglaciated areas average 0.15 µg/ml; whereas, total P contents average 0.36 µg/ml in the sediments from glaciated areas.

1.5.2 Whole Sediment Analyses

The results of analyses performed on the bulk sediment (<2 mm) are given in Table 1.4, and indicate that most of the sediment is a combination of silt and clay. This size distribution reflects the geology of the basin and the low gradient

Table 1.4 Particle Size Distribution, Organic Carbon Content, and Concentration of Suspended Sediments in the Muskingum River Basin

River or Stream	Site	Sand	Silt	Clay	O.C.	Suspended Sediment Load
		%				mg/l
Sandy Creek	1	1.3	50.5	48.2	4.5	280
Conotton Creek	2	1.4	53.2	45.4	3.6	128
Stillwater Creek	3	1.4	43.1	55.5	4.9	120
Sugar Creek	4	1.8	36.3	61.9	4.6	228
Killbuck Creek	5	5.1	47.9	47.0	2.5	264
Mohican River	6	4.4	57.3	38.3	3.2	428
Kokosing River	7	2.7	48.7	48.6	3.9	224
Licking River	8	3.9	51.5	44.6	3.9	908
Moxahala	9	6.0	52.4	41.6	4.2	188
Wills Creek						
Kimbolton	10	1.1	37.9	61.0	4.4	132
Wills Creek	11	--	--	--	8.7	64
Tuscarawas						
Bolivar	12	1.6	52.2	46.2	4.1	256
Gnadenhutten	13	1.4	54.1	44.5	3.6	212
Muskingum						
Tyndall	14	2.6	57.2	40.2	3.6	356
Philo	15	1.9	49.8	48.3	3.7	166
Lowell	16	2.3	52.7	45.0	3.1	328

of the Muskingum River. Much of the till in the glaciated portions of the basin has a high silt + clay content in the <2 mm portion, and the surface geology of the unglaciated portion of the basin is predominantly represented by siltstone and shale members. Size fractionation data from Wills Creek at Wills Creek hamlet are missing. This is because the total sediment yield was too small for analysis. Only suspended sediment concentration and organic carbon data are available for this site.

Suspended sediment concentrations (Table 1.4) are highly variable throughout the basin. As described in section 1.4.2, an effort was made to collect all samples during high flow. However, it was not possible to know if the samples were taken at the time of maximum flow in each watershed. Effective drainage area of the sub-basins (Table 1.2) also does not seem to provide a consistent explanation for the variation in suspended sediment concentrations. Sub-basins with reservoirs above sampling sites are Sugar, Conotton, Stillwater, and Wills Creeks, and the South Fork of the Licking River (Figure 1.3). The suspended sediment concentrations of Conotton, Stillwater, and Wills Creeks are among the lowest reported (128, 120, and 64 mg/l, respectively). However, Sugar Creek, and especially the Licking River, have much greater sediment concentrations (228 and 908 mg/l, respectively).

A better explanation of load variability is permitted when sub-basins are again grouped according to surface geology and land use. In this case, all of the sub-basins yielding <200 mg/l suspended sediment can be identified with the unglaciated portion of the basin. This portion accounts not only for Wills, Conotton, and Stillwater Creeks, but the Moxahala watershed as well. All those watersheds with concentrations >200 mg/l, including the Tuscarawas above Bolivar, drain glaciated areas of the basin. However, amongst these watersheds,

there is still great variability in sediment concentrations. The lowest concentration is from the Kokosing River, while the highest is found in the Licking River (224 and 908 mg/l, respectively). This difference may reflect greater farming activity, especially in the Licking watershed, where row and field cropping practices may increase soil losses and, hence, suspended sediment loads in the streams and rivers. With respect to this observation, it may also be that an apparent division of the watersheds along a glaciated and an unglaciated line of demarcation actually reflects the importance of farming as an economic activity associated with the more fertile soils found in glaciated areas.

A comparison of the organic carbon values does not reveal any significant trends within the Muskingum Basin, and comparisons with sediment size data do not permit association with any one sediment size fraction. The highest value for organic carbon was yielded by sediment from Wills Creek just below the Wills Creek Reservoir (site 11). This value is 2-3 times greater than those from all other sites sampled and may reflect the flushing of detrital matter accumulated in the reservoir during the winter months.

Limited organic carbon data is available for the Muskingum River. The yearly average organic carbon concentrations at McConnelsville (a city along the Muskingum River between Philo and Lowell) was reported by the U.S.G.S. (1974 and 1978) as 5.8 and 8.2 mg/l during 1974 and 1978, respectively. Multiplication of per cent organic carbon by sediment concentration measured at the Philo and Lowell sites in this study gives 6.1 mg/l and 7.7 mg/l organic carbon, respectively.

1.5.3 Clay Mineralogy by X-ray Diffraction.

The clay fraction was considered to be of primary importance for analysis as several studies (e.g., Klages and Hsieh, 1975; Jones et al., 1977) have

indicated that clay mineralogy of suspended sediments may indicate differences in source areas. Table 1.5 gives relative quantities of clay minerals detected in the Muskingum River Basin by X-ray diffraction techniques. Total K (Table 1.6) was also used to estimate the relative amounts of clay mica present in the suspended sediments. This analysis is based on the work of Jackson (1975), who estimated clay mica using the relationship 1% K_2O = 10% clay mica.

The results are considerably different from observations made by Jones et al. (1977) in a study of sediments in tributaries to the Maumee River. The Maumee drains an area where the surface geology is exclusively glacial in origin, and illite and quartz were the two most abundant minerals leaving the watersheds. Illite, or clay mica as shown here, is abundant, but it is not the dominant clay mineral in any of the sediments. However, note that in three of the four cases in which it is estimated to range in the 35-50 percentile, the watersheds (Mohican, Licking, and Killbuck) drain Wiscinsinan glacial materials. Note also, that the two lowest estimates for kaolinite are from watersheds (Kokosing and Killbuck) which drain glacial areas. All the watersheds have small amounts of clay-sized quartz (<5%) and traces of clay-sized feldspar moving downstream, and 60% of the samples showed traces of (<5%) goethite. Only one watershed, the Licking, gave evidence of chlorite, and then only a trace. Chloritized (Al-interlayered) vermiculite, on the other hand, is abundant in all the clays, especially those derived from glaciated watersheds.

Despite the above mentioned differences, and despite great differences in terrain, geology, and parent material within the Muskingum River Basin, the suspended sediments from the different watersheds seem to be relatively uniform. The typical clay fraction of the average suspended sediment would contain 20-35% kaolinite; 20-35% clay mica; 5-20% interstratified smectite-clay

Table 1.5 Estimated Clay Mineralogy[+] of Suspended Sediments in the Muskingum River Basin

River or Stream	Site	[ξ]K	M	I	AV	Q	C	G	F
Sandy Creek	1	XXX	XXX	XX	XXXX	X	--	--	t
Conotton Creek	2	XXX	XXX	XXX	XX	X	--	t*	t
Stillwater	3	XXXX	XXXX	X	XXX	X	--	--	t
Sugar Creek	4	XXX	XXX	XX	XXXX	X	--	t	t
Killbuck	5	XX	XXXX	XX	XXX	X	--	t	t
Mohican	6	XXX	XXXX	XX	XXX	X	--	--	t
Kokosing	7	XX	XXX	XX	XXXXX	X	--	t	t
Moxahala Creek	9	XXXX	XXX	XX	XXX	X	--	t	t
Wills Creek									
Kimbolten	10	XXXX	XXX	XXX	XX	X	--	--	t
Tuscarawas River									
Bolivar	12	XXX	XXX	XX	XXXX	X	--	t	t
Gnadenhutten	13	XXXX	XXX	XX	XXX	X	--	--	t
Muskingum River									
Tyndall	14	XXX	XXX	XX	XXXX	X	--	t	t
Philo	15	XXXX	XXX	XX	XXX	X	--	t	t
Lowell	16	XXX	XXX	XXX	XX	X	--	--	t

[+] Relative quantities XXXXX = >50%, XXXX = 35-50%, XXX = 20-35%, XX = 5-20%, X = <5%.

[ξ] K = Kaolinite, M = Clay Mica, I = Interstratified Smectite-Clay Mica, AV = Al-interlayered Vermiculite, Q = Quartz, C = Chlorite, G = Goethite, F = Feldspar.

* t = trace.

Table 1.6 Extractable Manganese* and Total Potassium Contents of the <2 μm Fractions from the Muskingum River Sediments

Stream or River	Site	Mn_o	Mn_d	K	K_2O
		%			
Sandy Creek	1	0.004	0.030	2.20	2.65
Conotton Creek	2	--	0.020	2.54	3.06
Stillwater Creek	3	--	0.020	2.34	2.82
Sugar Creek	4	0.004	0.035	2.02	2.43
Killbuck Creek	5	0.004	0.035	2.54	3.06
Mohican River	6	0.004	0.020	2.54	3.06
Kokosing River	7	0.008	0.030	2.64	3.18
Licking River	8	0.004	0.020	2.70	3.25
Moxahala Creek	9	0.006	0.020	2.04	2.46
Wills Creek					
Kimbolton	10	--	0.020	2.28	2.75
Tuscarawas River					
Bolivar	12	--	0.025	2.28	2.75
Gnadenhutten	13	0.004	0.025	2.60	3.13
Muskingum River					
Tyndall	14	0.004	0.035	2.12	2.55
Philo	15	0.004	0.040	2.46	2.96
Lowell	16	0.004	0.040	2.42	2.92

* Mn_o and Mn_d are ammonium oxalate and CBD extractable Mn, respectively.
— Not detectable

mica; 20-35% Al-interlayered vermiculite, less than 5% quartz, and traces of feldspar and possibly some goethite. In general, the unglaciated watersheds of Conotton, Stillwater, Wills, and Moxahala Creeks seem to have higher kaolinite, lower mica, and lower Al-vermiculite contents than the glaciated watersheds.

1.5.4 Chemical Dissolution Data

The chemical dissolution data described in this discussion are from the selective extraction of secondary Mn, Al, and Fe compounds using pyrophosphate, oxalate, and CBD reagents. Total Fe content was also measured.

Manganese, as indicated by Cummins et al. (1965), is one of the more important elemental products of acid mine drainage. The partitioning of Mn into "amorphous" and crystalline oxide fractions can be achieved through acid ammonium oxalate and CBD extraction, respectively. The results of analysis for Mn are given in Table 1.6, and indicate remarkably little oxalate extractable Mn throughout the Muskingum Basin; the range is from non-detectable to 0.008% Mn. Oxalate-Mn to CBD-Mn ratios (Mn_o)/Mn_d) range from 0.1 to 0.3 and indicate that crystalline oxides of Mn are the dominant forms of Mn in the suspended sediments. However, there does not seem to be any noticeable trend within the basin concerning the distribution of either amorphous or crystalline manganese oxides with respect to glacial history; nor does manganese seem to be a useful indicator of the effects of acid mine drainage on a regional basis.

Except for the Moxahala Creek site, (Table 1.7), lower amounts of all forms of extractable aluminum occur in watersheds draining unglaciated areas of the basin compared to sediments in waterways draining glaciated portions of the basin. Likewise, the ratios of oxalate extractable to CBD extractable Al (Al_o/Al_d) are generally lower in the sediments of watersheds draining

Table 1.7 Extractable Aluminum Data (<2 μm) in the Muskingum River Basin

River or Stream	Site	Al_p	Al_o	Al_d	Al_p/Al_o	Al_o/Al_d
		%				
Sandy Creek	1	0.28	0.39	0.44	0.64	0.89
Conotton Creek	2	0.10	0.21	0.35	0.29	0.60
Stillwater Creek	3	0.08	0.22	0.35	0.23	0.63
Sugar Creek	4	0.12	0.23	0.30	0.40	0.77
Killbuck Creek	5	0.18	0.32	0.48	0.38	0.67
Mohican River	6	0.12	0.35	0.42	0.28	0.83
Kokosing River	7	0.14	0.33	0.38	0.37	0.87
Licking River	8	0.25	0.29	0.38	0.66	0.76
Moxahala Creek	9	0.43	0.54	0.63	0.68	0.86
Wills Creek						
Kimbolton	10	0.08	0.19	0.25	0.32	0.76
Tuscarawas River						
Bolivar	12	0.18	0.29	0.44	0.41	0.66
Gnadenhutten	13	0.14	0.27	0.38	0.37	0.71
Muskingum River						
Tyndall	14	0.16	0.30	0.36	0.44	0.83
Philo	15	0.14	0.29	0.38	0.37	0.76
Lowell	16	0.24	0.29	0.30	0.80	0.97

* Al_p, Al_o, and Al_d are sodium pyrophosphate, ammonium oxalate and CBD extractable aluminum, respectively.

unglaciated areas and suggest that the Al oxides are more crystalline in those clays.

The highest values for all forms of extractable Al are from the Moxahala Creek watershed with the pyrophosphate, oxalate and CBD extractions accounting for 0.43, 0.54, and 0.63%, respectively, of the total clay. These values, though low, represent 1.5-3 fold increases over other sites in the Muskingum River Basin. Overall increases, especially of poorly crystallized aluminum oxide materials can be expected in areas affected by acid mine drainage, and it is possible that the increases in Al detected in the suspended sediments are a result of mining disturbance.

Extractable Fe data are given in Table 1.8 and show many of the same trends as described for extractable Al. Excluding the Moxahala creek sites, data for all forms of extractable Fe are lowest in clays derived from unglaciated portions of the basin. The Fe data from the Moxahala sediments stand out by comparison. Pyrophosphate, oxalate, and CBD Fe are between 2-6; 2-7; and 1-3 times greater than respective values for the same type of extractable Fe in other areas of the Muskingum Basin. Also, Fe_o/Fe_d ratios indicate that amorphous and organically-held Fe account for 97% of the extractable Fe in the Moxahala sediment. This is the highest value for the entire Muskingum Basin, and is consistent with the work of Cummins et al. (1965), who indicate that Fe concentrations will be greatly increased in waters draining spoil materials which contain pyrite as an impurity. Observations concerning Fe in the Moxahala sediment are also supported by Nordstrom (1980) in his review of pyrite oxidation and "amorphous" iron oxide precipitation in acid mine drainage water.

Table 1.8 Extractable and Total Iron Contents* of the <2 μm Fractions from the River Sediments

River or Stream	Site	Fe_p	Fe_o	Fe_d	Fe_t	Fe_p/Fe_d	Fe_o/Fe_d
		%					
Sandy Creek	1	1.00	2.17	3.00	6.20	0.33	0.72
Conotton Creek	2	0.50	1.15	2.20	5.60	0.23	0.52
Stillwater Creek	3	0.45	1.03	2.00	4.50	0.22	0.51
Sugar Creek	4	0.63	1.20	2.50	4.25	0.25	0.48
Killbuck Creek	5	0.78	2.22	3.40	6.50	0.23	0.65
Mohican River	6	0.63	2.05	3.15	6.10	0.20	0.65
Kokosing River	7	0.74	2.18	3.10	6.60	0.24	0.70
Licking River	8	0.78	1.61	2.90	6.20	0.27	0.56
Moxahala Creek	9	2.46	5.89	6.10	9.90	0.40	0.97
Wills Creek							
Kimbolton	10	0.39	0.85	2.20	4.45	0.18	0.39
Tuscarawas River							
Bolivar	12	0.66	1.47	2.60	5.40	0.25	0.57
Gnadenhutten	13	0.54	1.45	2.60	6.00	0.21	0.56
Muskingum River							
Tyndall	14	0.68	1.36	2.70	5.80	0.25	0.50
Philo	15	0.58	1.38	2.35	5.50	0.24	0.59
Lowell	16	0.99	1.86	4.85	5.30	0.21	0.38

* Fe_p, Fe_o, and Fe_d are sodium pyrophosphate, ammonium oxalate, and CBD extractable iron, respectively. Fe_t = total iron content.

Total Fe, which includes Fe held in alumino-silicate structures, ranges between 1.1 and 2.5 times greater than CBD-extractable Fe at all sites. For the Moxahala watershed, total Fe is 1.6 times that obtained by CBD extraction.

1.6 Summary and Conclusisons

With little exception, DIP, NH_4-N, sediment size fractions, organic carbon and clay mineralogy did not yield definitive information concerning source areas for suspended sediments within the Muskingum River Basin. On the other hand, extractable oxides, especially those of Al and Fe, do seem to be related to geologic source areas, and are generally higher in sediments from areas affected by glaciation. Also, total P, which generally reflects sediment P, and NO_3-N show some correlation with geology and/or land use.

The most convincing evidence of regional differences within the Muskingum Basin came from Moxahala Creek. The low pH of its water and the high extractable Al and Fe contents of its sediment all reflect problems with acid coal mine drainage. As a result, the Moxahala Creek watershed was chosen for further study.

CHAPTER 2

WATER AND BOTTOM SEDIMENT QUALITY IN STREAMS AFFECTED BY ACID COAL MINE DRAINAGE - A STUDY OF THE BLACK FORK CREEK WATERSHED, OHIO

2.1 Introduction

The coal beds in Ohio comprise one of the four largest coal deposits in the continental United States. This deposit, known as the Main Bituminous Coal Basin, is associated with the Appalachian Plateau, and occurs in a northeast - southwest trending band which extends from north-central Pennsylvania through eastern Ohio, West Virginia, Western Maryland and Virginia, and southward into Kentucky, Tennessee and Alabama. The coal-bearing rocks in the basin were formed from alternating sea and swamp deposits of detrital inorganic and organic constituents of Pennsylvanian Age (280 to 320 million years B.P.). The sedimentary units within the Ohio coal field gradually slope to the southeast, toward the center of the basin in northern West Virginia. As a result, coal-bearing seams are nearer the surface in the western part of the field, and are more deeply buried near the Ohio River.

Pennsylvanian coal seams average 1 to 2 feet in thickness and occur interbedded with common sedimentary rocks. In Ohio, there are over 40 coal seams, only 13 of which have been mined commercially. The cyclical character of the Pennsylvanian system resulted from the recurrence of a geologic environmental sequence involving swamps associated with the shoreline of an ancient sea. The prevailing view of coal formation is one of accumulation and compaction of organic matter in freshwater swamps according to the following

sequence of events: primary formation of a swamp; rise in sea level and flooding of the swamp; accumulation of inorganic sediments on top of the swamp; and finally a drop in sea level and formation of a new swamp.

Portions of thirty counties in the bituminous basin in Ohio have been mined for coal since the early 1800's. Early operations involved primarily deep mines, but now more than 70% of the state's coal production is from surface mining. The recent expansion of surface mining activity has resulted in comprehensive state legislation which requires the complete reclamation of areas currently being mined. However, it does not provide for reclamation of land mined prior to 1972. As a result, the utility of at least 72,800 ha of land has been lost due primarily to toxic spoils from abandoned surface and deep mines (BUSML, 1974). While loss of productive land is a major concern, a more serious and pervasive problem is the environmental damage caused by pollution of streams, rivers and groundwaters with acid mine drainage. According to the Board on Unreclaimed Strip Mine Lands (BUSML, 1974), over 454,000 kg of acid are discharged into Ohio streams every day.

Acid mine drainage arises from the microbially catalyzed oxidation of iron sulfides, principally pyrite and marcasite, which occur as impurities in coal and associated rocks, particularly roof shales. These iron sulfides not only create phytotoxic conditions in spoils and polluted waterways, but also lower the coking quality of coal, accelerate the corrosion of boilers firing the coal, and contribute to air pollution. In southeastern Ohio, mine effluents release copious amounts of both acid and iron to surface and ground waters where they cause severe stress to aquatic organisms and a general deterioration of the regional water supply. Much of the iron is ultimately transformed to gelatinous precipitates that increase the sediment load in receiving streams. In addition, these precipitates

may have a significant impact on chemical reactions which occur at the sediment/water interface. The primary objectives of this study were to evaluate the impact of acid mine drainage on water quality in a representative stream system, and to evaluate the mineralogy and surface chemistry of bottom sediments in waterways affected by acid mine drainage.

2.2 Literature Review

2.2.1 Pyrite Oxidation

Pyrite (FeS_2) is one of the most abundant and ubiquitous impurities in coal and associated rocks, and its oxidation has been the subject of a great deal of research. In spite of this research, exact oxidation mechanisms are still in doubt.

Pyrite is stable under reducing conditions and will oxidize abiotically in the presence of oxygen. A number of pathways have been proposed for this inorganic oxidation. These nearly always require water as both product and reactant, and usually involve the action of dissolved oxygen on pyrite to produce ferrous iron and elemental sulfur according to the reaction:

(2.1) $FeS_2 + 1/2O_2 + 2H^+ \longrightarrow Fe^{+2} + 2S^\circ + H_2O$

Then, elemental sulfur is oxidized:

(2.2) $2S^\circ + 3O_2 + 2H_2O \longrightarrow 2SO_4^= + 4H^+$

Next, ferrous iron is oxidized:

(2.3) $4Fe^{+2} + O_2 + 4H^+ \longrightarrow 4Fe^{+3} + 2H_2O$

The fate of the Fe^{+3} produced in reaction 2.3 is considered to be 3-fold: The ferric iron can oxidize more sulfur (2.4); it can oxidize more pyrite (2.5); or it can precipitate as ferric hydroxide (2.6).

(2.4) $S^\circ + 6Fe^{+3} + 4H_2O \longrightarrow 6Fe^{+2} + SO_4^= + 8H^+$

or:

(2.5) $FeS_2 + 2Fe^{+3} \longrightarrow 3Fe^{+2} + 2S^\circ$

or:

(2.6) $Fe^{+3} + 3H_2O \longrightarrow Fe(OH)3 + 3H^+$

A much more succinct description emphasizing the role of iron in the above reactions is given by Singer and Stumm (1970) in which two phases are proposed:

A. Initiator reaction:

(2.7) $FeS_2 + 1/2O_2 + 2H^+ \longrightarrow Fe^{+2} + 2S^\circ + H_2O$

B. Propagating cycle:

(2.8) $4Fe^{+2} + O_2 + 4H^+ \longrightarrow 4Fe^{+3} + 2H_2O$

(2.9) $Fe^{+3} + FeS_2 \longrightarrow 2S^\circ + 3Fe^{+2}$

The rate of abiotic oxidation of pyrite seems to be closely associated with degree of crystallinity, and FeS_2 may also be more easily attacked in other mineral forms such as marcasite (Harmesen et al., 1954). However, Singer and Stumm (1970) feel that oxidation rates are primarily a function of Fe(III) concentration. Their study indicated that continuous removal of Fe(III) by flowing water decreased the rate of pyrite oxidation by a factor of 10^6. They refer to the oxidation of Fe(II) to Fe(III) as the rate determining step. Further, these researchers showed that inorganic oxidation of Fe(II) is pH dependent, and is rapid above pH 5. At lower pH's inorganic oxidation is slow and bacterial catalysis is required.

Bacterially catalyzed pyrite oxidation has been well documented, and at least two types of microbes appear to be capable of accelerating the oxidation process (Kelley, 1967; Dugan and Randles, 1968). The first are autotrophic microoganisms that rely on the oxidation of minerals for their energy while utilizing carbon dioxide and a few other nutrients in small quantities for life

support. The second are heterotrophic microorganisms which depend upon the oxidation of organic compounds for both their energy and cellular carbon requirements. The autotrophic microorganisms include several species of Thiobacillus and are of primary interest in this discussion. Thiobacilli achieve maximum growth between pH 2 and 3.5, and are classified as acidophilic. Thiobacillus ferrooxidans has been widely implicated as a catalyst in the production of acid mine waters because: it is associated with acid mine drainage waters in significant quantities; it actively increases pyrite oxidation in laboratory experiments; and it can speed up the oxidation of dissolved Fe(II) by 5 to 6 orders of magnitude over inorganic rates (Dugan, 1975). Another Thiobacillus, T. thiooxidans, has been observed in contact with pyrite surfaces (Tuovinen and Kelly, 1972) and is thought to oxidize elemental sulfur by a direct contact mechanism. A "direct contact" mechanism has also been suggested for the oxidation of pyrite by T. ferrooxidans (Arkesteyn, 1979). Thus, iron and sulfur oxidation by autotrophic bacteria can be given as:

(2.10) $Fe^{+2} \xrightarrow{T.\ ferrooxidans} Fe^{+3} + e^-$

and

(2.11) $2S^\circ + 3O_2 + 2H_2O \xrightarrow{T.\ thiooxidans} 2SO_4^{-2} + 4H^+$

Microbial oxidation may be much more important in oxidation of pyrites than abiotic chemical mechanisms, as microbial activity can be attained under extremely low levels of dissolved oxygen. Brock and Gustafson (1976) report that Fe(III) is used as an energy source by T. ferrooxidans during sulfur oxidation under anaerobic conditions.

Microbially catalyzed pyrite oxidation is only beginning to be understood, and evidence given by Kelly et al. (1979) show that bacteria other than the two Thiobacilli are also active in pyrite oxidation, and that mixed cultures are often

more efficient in oxidizing pyrite than are monocultures. Almost all evidence indicates that microbial catalysis of pyrite oxidation can greatly increase the rate of oxidation above that possible by inorganic mechanisms.

2.2.2 Water Quality Resulting from Acid Mine Drainage

The products of pyrite oxidation, sulfuric acid and dissolved iron, are recognized as the primary pollutants in acid mine drainage (Dugan, 1975). They affect water quality of streams and rivers when surface waters flow across spoil banks or percolate through disturbed land and enter the groundwater. The BUSML (1974) indicates that three quarters of all the acid mine drainage produced in the Appalachian Province originates in underground mines. The underground mines expose the sulfide impurities to atmospheric oxidation and cause alterations in subsurface water patterns which allow for greater water contact with oxidized pyrite. The oxidation products are flushed from the mines after rains or are continually discharged under hydrostatic pressure.

Although spoils in the eastern coal mining province can range in pH from 2.5 to 8 (Berg and Vogel, 1969), depending on differences in local mineralogy, the pH of streams heavily affected by acid mine drainage can be as low as 2.1, as reported for Campbell's Run in southwest Pennsylvania (EPA, 1976). More frequently, however, the pH's of streams affected by acid mine drainage range between 3.7 and 4.2 (EPA, 1977). A number of factors contribute to this variation. The pH is primarily a function of rate of oxidation of the pyrite, rate of flow and discharge from the pyrite source, and amount of dilution after entering a stream system. The acidity levels in acid mine drainage are in sharp contrast to the near neutral pH of other natural groundwaters that are also high in dissolved iron and manganese (Mustoe, 1980; Carlson et al., 1980). Acidity introduced to groundwater, streams, and lakes by coal mine drainage often limits

the use of water for recreation and drinking purposes, and frequently destroys normal biological activity. However, abatement through chemical neutralization might well be possible if acidity were the only pollutant.

Iron concentrations can also be extremely high. Minear and Tschantz (1976), in their water quality study of drainage basins affected by acid mine drainage in eastern Tennessee, report an average of 20 µg/ml total dissolved Fe with highs of up to 80 µg/ml near drainage sources. The EPA (1976) reported total Fe concentrations in a small catchment in Pennsylvania as high as 55 µg/ml. Other reports indicate lower quantities of iron (Cronse et al., 1980) but, regardless of the level reported, the effect of acid mine drainage is usually the same: concentrations of iron are above the 0.3 µg/ml U.S.drinking water standard, and there is considerable visual pollution as a result of iron oxide or oxyhydroxide precipitation.

Sulfate levels are often high as well. Sulfate concentrations ranging up to 2400 µg/ml have been reported for the Campbell Run area of Pennsylvania (EPA, 1976). Studies throughout eastern Tennessee and Pennsylvania indicate that yearly averages in streams receiving acid drainage range between 100-200 µg/ml SO_4 (Minear and Tschantz, 1976; Cronse et al., 1980). Concentrations of SO_4 are dependent on water discharge, and can locally be much higher. Rose (1975), for example, reports an average SO_4 concentration of 700 µg/ml in a small stream tributary to one of those studied by Minear and Tschantz (1976).

In addition to SO_4, Al and Mn can also be significant components of acid mine drainage. Usually, Al is found in higher concentrations than Mn. Various studies of streams in Pennsylvania report average dissolved Al contents of 8-9 µg/ml (EPA, 1977; Cronse et al., 1980) and high concentrations near 80 µg/ml (EPA, 1976). In nearly all cases, manganese is present in much

lower quantities, and levels are usually no more than 3-6 μg/ml in areas affected by acid mine drainage.

Considerable differences in solute levels are reported by researchers working with acid mine drainage within the eastern coal province. These differences are related to type of mining activity, extent of precipitation, runoff, and discharge of receiving streams. Two studies (Curtis, 1975; Minear and Tschantz, 1976) report annual cycles in the quality of water, with increasing concentrations through the summer months, and decreasing concentrations during the winter. Curtis (1975) found that the highest concentrations of dissolved materials were generally associated with late summer rains which he attributed to the role of alternate wetting and drying periods in concentrating salts near spoil surfaces. However, summer increases in temperature may also play a significant role, especially with respect to microbial oxidation.

2.2.3 Sediment Quality in Streams Affected by Acid Mine Drainage

Water quality is usually judged by the types and concentrations of materials found in solution; whereas, sediment quality is related to the physical and chemical characteristics of the solid phase. However, a study of sediment quality in waters influenced by acid mine drainage demands that sediments be examined in light of the quality of the water. During low flow periods, concentrations of iron and sulfate increase in the water. Corollary with this occurrence, great quantities of yellowish, gelatinous precipitates called "yellow boy" are produced. Although most of these precipitates are removed during subsequent storm cycles, it is very likely that these precipitates also influence the character of the more permanent bottom sediments.

Erosion and siltation have long been considered a problem associated with mining activity and affect both suspended and bottom sediments. Dramatic

differences in concentrations of suspended solids between unmined watersheds and those disturbed by surface mining exist. Minear and Tschantz (1976) have reported sediment concentrations of 25 μg/ml in undisturbed watersheds as compared to 100-400 μg/ml in watersheds disturbed by mining activity. Values in the mined watersheds often exceeded 1000 μg/ml following heavy rainfalls. These same researchers also reported increases in bottom sediment loads, especially during the early stages of mining.

Bottom sediment usually occurs when stream energy cannot support the entrainment, suspension and transport of sediment, and the particles subsequently settle out. These particles are deposited along with associated inorganic and organic constituents adsorbed by the sediment. In a study of rock formations containing anakeesta pyrite in the Great Smoky Mountains of Tennessee and North Carolina, Bacon and Maas (1979) reported increases in lead, zinc, sulfate and in some cases, manganese in bottom sediments of streams draining the formation. Although no attempt was made to identify the way these constituents were associated with the bottom sediments in that study, Jenne (1977) has reported that clay-size materials, especially oxides of iron and manganese, carbonates, sulfides, and organic matter, may serve as major sinks for heavy metals in fluvial systems.

The survey reported in Chapter One of this dissertation established an increase in iron and aluminum oxides in sediments from areas influenced by acid mine drainage. Yellowish precipitates were visibly apparent, and these precipitates may greatly influence both the nature and reactivity of stream sediments.

2.3 Materials and Analytical Procedures

2.3.1 Site Selection

During the winter of 1981, field reconnaissance led to the selection of the Black Fork Creek watershed as a detailed study site. This 74 km^2 basin is located in northwest Morgan and adjacent Perry counties, and consists of Black Fork Creek, Ogg Creek, and Bennett Run (Figure 2.1). The watershed has experienced both surface and, especially, deep mine activity. The deep mines are now abandoned and large quantities of acid drainage are released from both mine tunnels and tailings adjacent to the receiving streams. Tailings from the Jones or Misco Mine are a primary source of pollution along Bennett Run. Former entrances to the Tropic Mine and an air vent for the Number 52 Mine affect Black Fork Creek. Groundwater pollution is extensive in the watershed, as nearly 80% of the study area has been undermined; however, unpolluted reference areas exist at the headwaters of all three tributaries.

Coal has been mined in the area since the early 1800's (Norling, 1957), but the greatest activity occurred from the 1930's through the late 1950's. The major source of coal for the mines in the watershed was the Middle Kittanning Number 6 coal seam. The sedimentary sequence associated with the Middle Kittanning Coal is shown in Figure 2.2. This seam is approximately 1.6 meters thick, and is the middle member of the Allegheny Formation which includes acid shales and sandstones of Pennsylvanian Age.

2.3.2 Sample Collection

During March of 1981, water and bottom sediments were collected at periods of low discharge from nine sites indicated in Figure 2.3. Additional water samples were collected at these same sites again in August, 1981, during another period of low flow. Sites 1-3 represent unpolluted reference areas

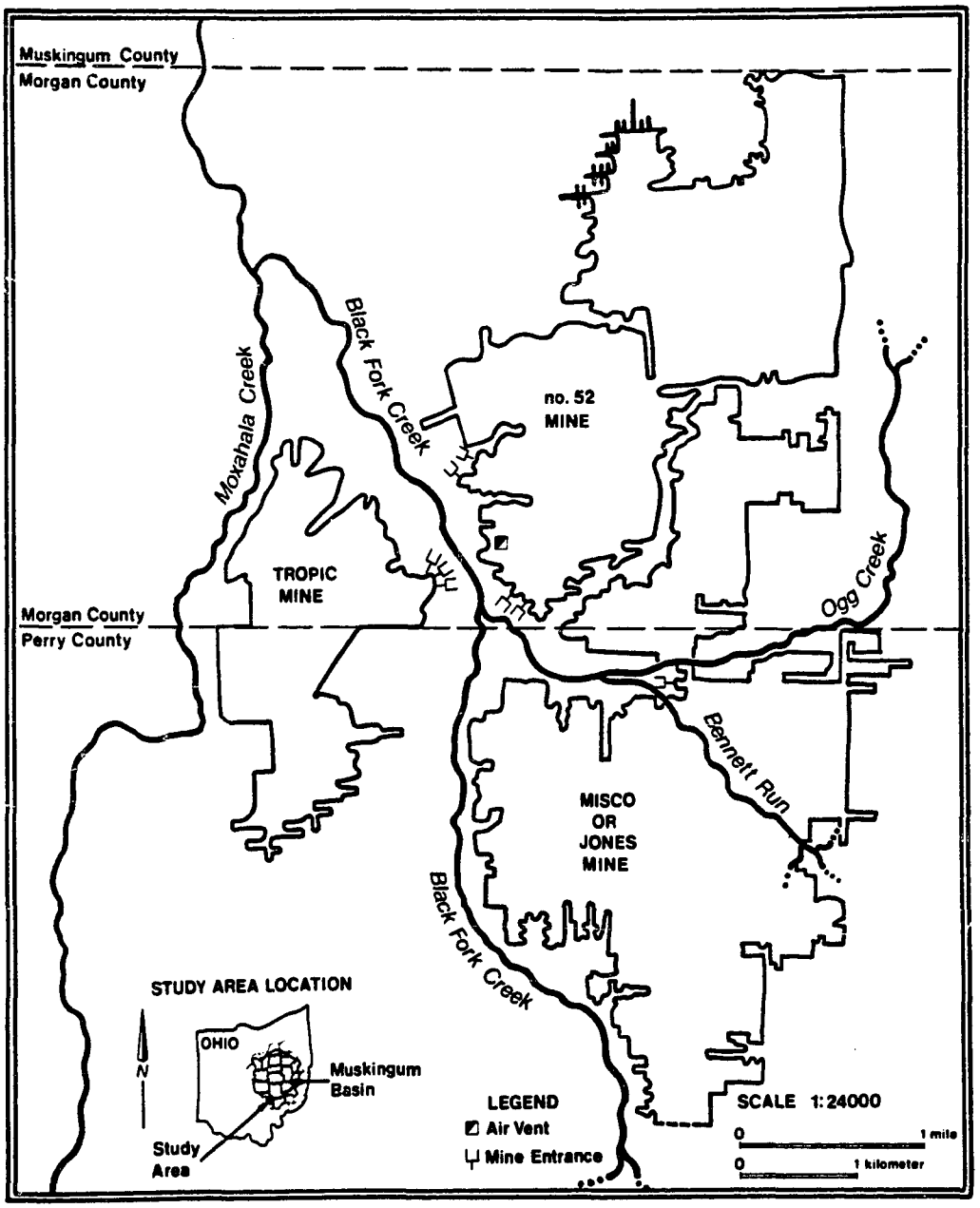

Figure 2.1 Study area location with respect to abandoned underground mines.

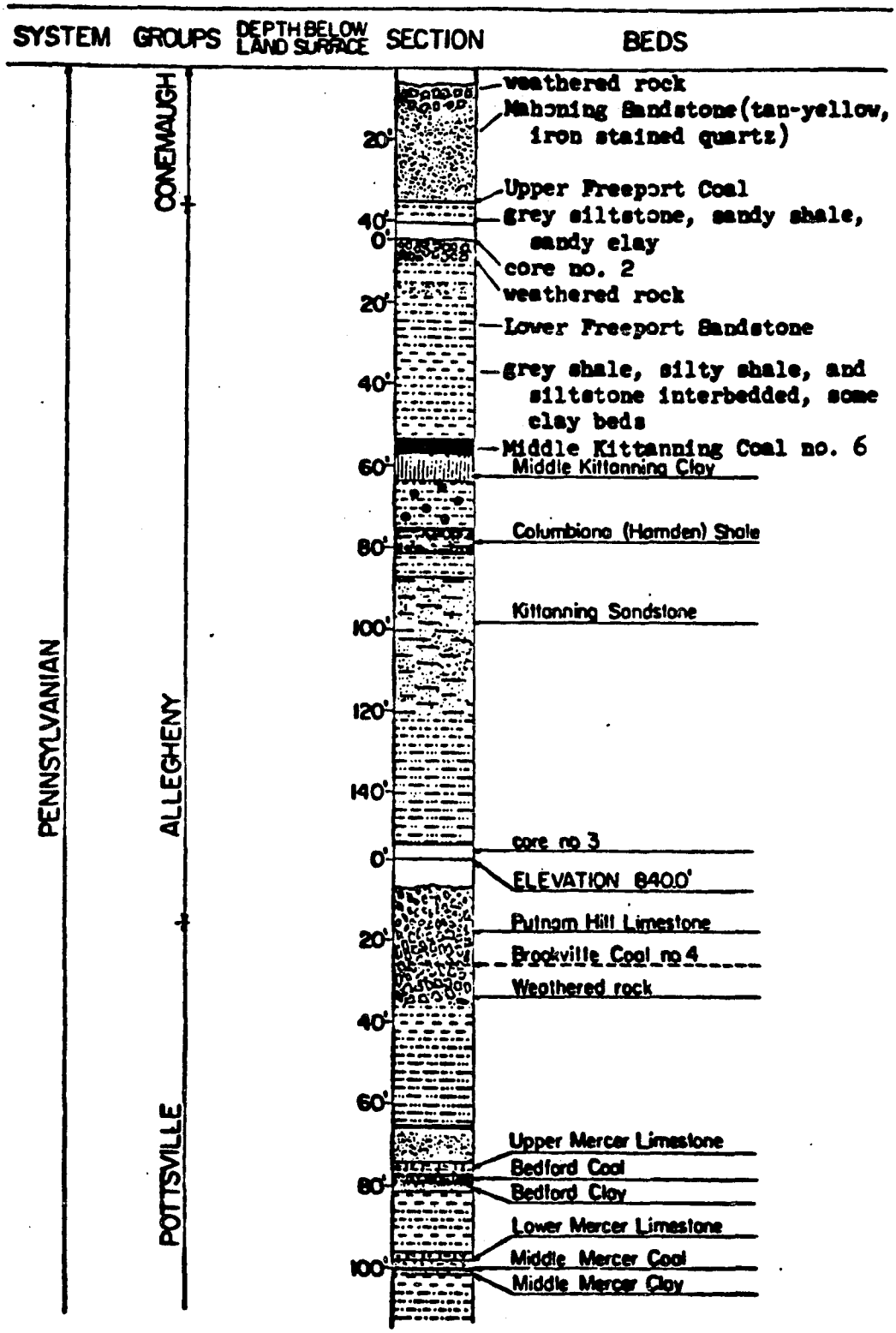

Figure 2.2 Strata associated with Middle Kittanning Coal No. 6. (Bureau of Mines, 1977).

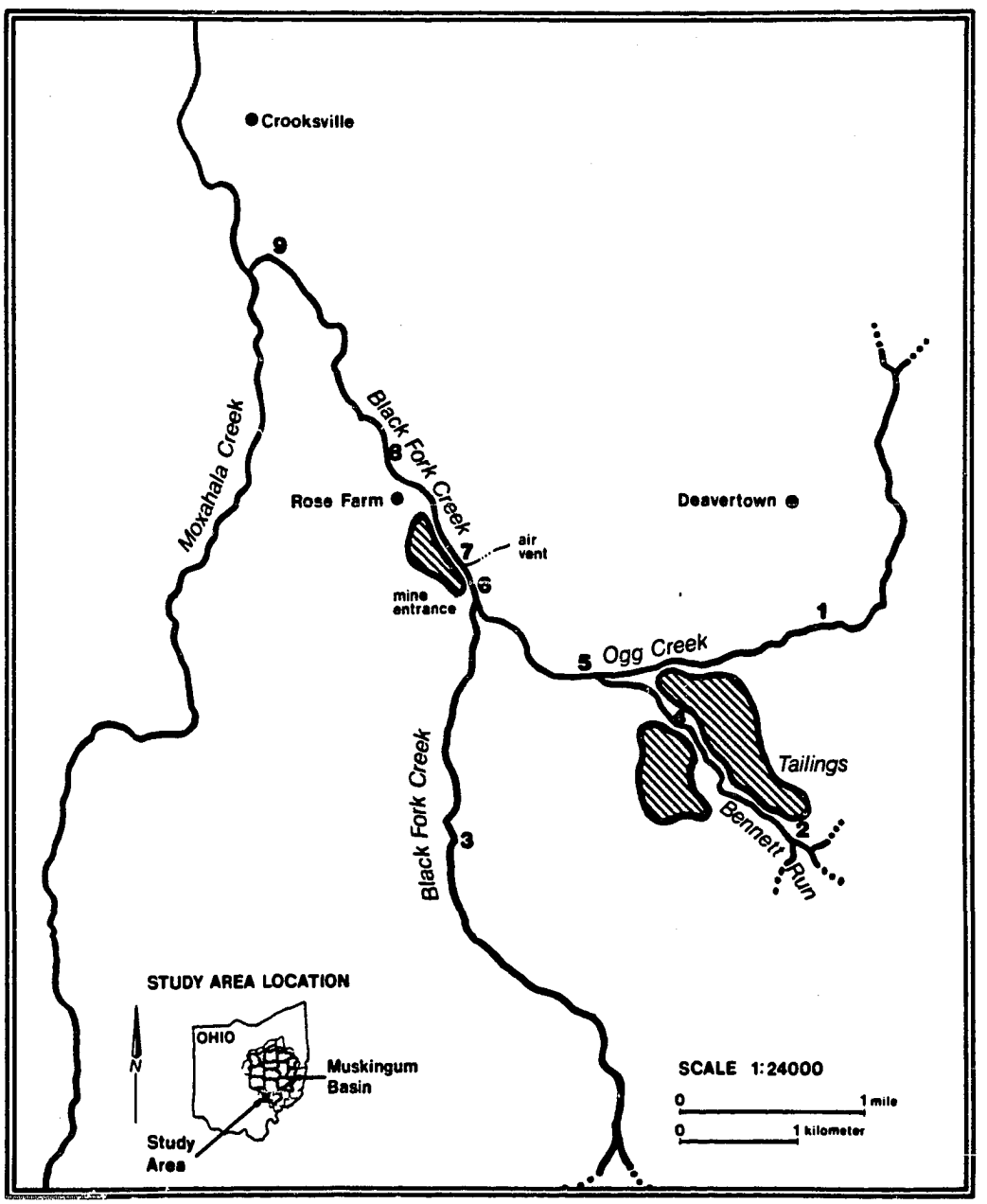

Figure 2.3 Location of collection sites (1-9).

upstream from the zone of pollution along Ogg Creek, Bennett Run, and Black Fork Creek, respectively. Near site 4, approximately 16 ha of mine tailings are exposed. Site 5 is just below the confluence of Ogg Creek and Bennett Run. Site 6 was selected so that the samples would reflect mixing between Ogg Creek and Black Fork Creek and is located just below the confluence of those two streams. Site 7 was chosen to reflect influences in water and sediment quality caused by water flow from the breached air vent. Site 8 was chosen so that changes in water and sediment quality downstream from all known sources of pollution could be monitored. Site 9, located near the mouth of Black Fork Creek, was chosen to provide a final measure of water and sediment quality prior to the merger of Black Fork and Moxahala Creeks.

For each site, three equally spaced samples of water and sediment were collected in transect across the channel of the stream. Water samples were collected in 250-ml polyurethane bottles which had been washed in 5N HCl. The upper 4-5 cm of bottom sediments were collected using a 4-l, flat-bottomed plastic scoop, and were placed in gallon polyurethane containers which had also been washed with 5N HCl. Water samples were transported from the field in an ice chest, and both water and sediment samples were immediately refrigerated at 4° C upon arrival at the laboratory.

2.3.3 Analytical Procedures

The methods of analysis described in this section involve the characterization of both water and sediment. Five of these procedures have been discussed in appropriate sections of Chapter 1 and will not be described again at length. All new or modified procedures will be discussed in detail.

2.3.3.1 pH. The hydrogen ion activity of all water samples was measured in the same manner as that described in Chapter 1, section 1.4.3.1.

2.3.3.2 Sulfate Determination Measurements. Sulfate was measured by a turbidimetric technique (EPA, 1980) after filtration of the stream waters through a 0.4 μm filter.

2.3.3.3 Dissolved Metals. Dissolved metal ions were determined by plasma emission spectroscopy (ICAP) after filtration of the stream waters through a 0.4 μm filter. Metals (Ca, Mg, Na, Al, Mn, Sr, Cd, Cu, Pb, Ni, and Zn) were measured with a Jarrell-Ash Model 975 Plasma Automcomp Spectrometer.

2.3.3.4 Fractionation and Particle Size Determinations. During the March, 1981 sampling, triplicate samples of bottom sediment (∿ 5 kg each) were collected across the stream channel at each of the nine sites. Gravel and cobbles (all material >2 mm) were removed from the sediments by sieving, placed in beakers, and then oven dried at 105° C. All materials less than 2 mm were then concentrated by centrifugation at 1500 rpm for 10 min using a Beckman J21B centrifuge and an angle-head rotor. The samples were subsequently frozen in 400-ml polyurethane beakers using trichloroetheylene and dry ice, and freeze-dried in a Virtis lyophilizer. This procedure allowed for estimates of total sediment (<2 mm) available for analysis, and also provided for easy storage of dried samples. In all cases, the freeze-dried whole sediment (except for 0.5 g withheld for organic carbon) was fractionated, and a particle size analysis was performed in the manner described in Chapter 1, section 1.4.3.6.

2.3.3.5 Organic Carbon. Measurements of organic carbon were obtained in the same manner as described in Chapter 1, section 1.4.3.5.

2.3.3.6 Total Sulfur. Duplicate 0.1 g samples of clay (<2 μm) were placed in a crucible containing iron and tin oxide catalysts and then heated to approximately 1650° C in a Leco 521 high frequency induction furnace according

to a procedure recommended by McKibbon (1975). Sulfur evolved as SO_2 was collected in a starch solution and quantified using a semi-automatic titrator with KIO_3 as the titrant. In this manner the percent total sulfur released by each sample was determined. The completeness of combustion and the accuracy of the titration were determined using known samples provided by the Leco Corporation.

2.3.3.7 Selective Dissolution Analyses. Due to extremely limited net quantities of clay materials, Na-pyrophosphate, acid NH_4-oxalate, and CBD extractions were performed in a sequential fashion on duplicate, 0.25 g samples of clay. Analyses were otherwise conducted in the same manner as described in Chapter 1, sections 1.4.3.7-9. In order to express the results in a meaningful way, metal ion concentrations in the Na-pyrophosphate extracts were reported as measured. These values were then summed with those obtained by acid ammonium oxalate extraction to yield a final data set for oxalate-extractable metals. Likewise, results from the Na-pyrophosphate, ammonium oxalate, and citrate-bicarbonate-dithionite extractions were summed to yield a final data set for CBD-extractable metals.

2.3.3.8 Total Chemical Analysis. Clays from the bottom sediments were analyzed for total contents of K, Fe, Mn, and Al. Digestion and analysis procedures were the same as those given in Chapter 1, section 1.4.3.10.

2.3.3.9 X-ray Diffraction Analysis. Portions of clay from the bottom sediments were prepared and analyzed in the same manner as that described in Chapter 1, section 1.4.1.1.

2.3.3.10 Phosphate Adsorption. Standard phosphate adsorption isotherms were determined for clays from sites 3, 5, and 6.

Air dried equivalents of 0.25 g of oven-dried clay were weighed into 50-ml polyethelyne centrifuge tubes which had been acid washed. Appropriate amounts of 0.01M $CaCl_2$ and KH_2PO_4 solutions were added to duplicate clay samples to make suspensions that contained 0.0, 0.2, 0.5, 1.0, 5.0, 10.0, 15.0, and 20.0 μg/ml phosphate while maintaining a solid-solution ratio of 1/100. The tubes were sealed with plastic caps and placed in a rotary shaker for 24 hr.

After shaking, the soil suspensions were centrifuged for 15 min at 5,000 rpm. Appropriate aliquots of the supernatant liquids were analyzed colorimetrically for P by the heteropoly blue method of Watanabe and Olsen (1965). Absorbance values were obtained using a 1 cm quartz cell in a Beckman Model 24 spectrophotometer at a wavelength of 730 nm. Equilibrium P concentrations were calculated from a standard curve prepared from 0, 0.1, 0.2, 0.4, 0.6, 0.8 and 1.0 μg/ml P solutions. Sample 6 proved so adsorptive that it was necessary to use initial P concentrations as high as 400 μg/ml to achieve an adequate isotherm. The difference between the P contents of the solutions before and after equilibration with the clay materials was considered to represent the quantity of P adsorbed by the clay.

After sampling for P analysis, the pH of the remaining equilibrium solution was determined using a Corning Research Model 12 pH meter with a combination electrode.

2.3.3.11 Surface Area. Non-expanded (external) surface areas of clay materials from sites 3, 5, and 6 were determined by nitrogen gas (N_2) adsorption after the procedure of Brunauer, Emmett, and Teller (1938).

A sample of clay was dried for 2 weeks over concentrated H_2SO_4, and then for 48 hours over P_2O_5. It was then placed into an adsorption cell and "outgassed" at ambient temperature for 12 hr before analysis. This procedure

was necessary to assure replacement of H_2O by the N_2 gas and also to protect against possible alterations in the iron oxides which can result from treatment at elevated temperatures (above 60° C). Post adsorption sample weights were determined by weighing the filled adsorption cell and then subtracting the weight of the washed and dried glass cell.

Nitrogen adsorption on the clay was achieved by immersing the adsorption cell in liquid nitrogen while passing a mixture of N_2 and He gases through the cell and sample. After the adsorption process was finished, the cell was removed from the liquid nitrogen bath and the sample was allowed to warm. As the sample warmed, desorption of N_2 was followed using a thermal conductivity detector. The desorption signal was calibrated by manually injecting a known quantity of pure N_2 into the sample stream with a syringe.

A triple point adsorption isotherm was calculated for each sample using N_2 -He gas mixtures of 10.14, 20.45, and 30.48 percent N_2. The size of the sample used ranged between 0.03 and 0.15 g, and the attenuator settings were varied between 28 and 256 to optimize the intensity of the desorption signal. The bridge current was held at 130 mA. The instrument used was a Quantachrome Quantasorb Surface Area Analyzer.

2.4 Results and Discussion

2.4.1 Water Quality Analysis

Water quality data from samples collected during March and August, 1981 under low flow conditions (Table 2.1) show a marked change in stream environment as a result of acid mine drainage. Waters from the reference areas have neutral pH's and low background levels of all other measured parameters. Data from the reference areas are, in fact, so similar that they are presented as averaged values. No difference in pH was detected at the reference sites for the

Table 2.1 Water Quality of Black Fork Creek Watershed

Site	Basic* Cations	Metals**	SO_4	Mn	Al	Fe	pH
	µg/ml						
	March, 1981						
1-3	48.8	0.04	41	0.0	0.1	0.1	6.8
4	70.6	0.35	589	1.2	37.4	94.6	3.3
5	62.5	0.26	254	0.8	13.7	18.0	4.6
6	59.1	0.07	163	0.5	2.0	15.2	4.8
7	65.3	0.07	193	0.6	2.9	19.7	4.9
8	67.8	0.08	199	0.6	3.4	19.0	4.8
9	84.4	0.09	207	0.8	3.3	18.0	4.8
Air Vent	381.5	0.44	1750	6.6	9.0	301.0	4.8
	August, 1981						
1-3	74.6	0.02	39	0.1	0.1	0.5	6.8
4	116.9	0.57	1630	4.4	94.3	329.0	2.7
5	105.2	0.20	570	2.4	33.3	52.6	2.8
6	143.4	0.32	777	3.7	40.8	61.1	2.8
7	222.9	0.39	1007	5.0	34.3	132.0	2.9
8	251.5	0.39	1080	5.2	30.3	123.0	2.9
9	308.2	0.42	963	5.0	27.7	69.3	2.9
Air Vent	495.0	0.66	2360	9.9	12.9	466.0	4.4

*Calcium, magnesium and sodium (See Appendix A for individual analyses).
**Cadmium, copper, lead, nickel, and zinc (See Appendix A for individual analyses).

two different sampling dates. All other values indicate that lower concentrations of pollutants were present in waters sampled in March due, most likely, to higher total discharge at that time. Discharge measurements for the watershed were taken only at site 9 and only during the August collection; the calculated discharge at that time was 62 l/sec. The August data represent the most extreme example of poor water quality observed in the Black Fork Creek watershed.

Data from site 4 reflect the immediate impact that runoff waters from exposed tailings have on streams in the watersheds. While the levels of dissolved pollutants at this site are substantial, they are a fraction of those contained in waters exiting the former air vent between sites 6 and 7 (Table 2.1).

Basic cations (calcium, magnesium, and sodium) increase at all points downsteam from the initial source of acid drainage. Heavy metals also increase, with zinc accounting for about 95% of the total metal load at all sites. Manganese shows a more dramatic rise in the zone of pollution, especially in the samples collected in August. However, the most significant increases are in concentrations of sulfate, aluminum, and iron, with an accompanying decrease in pH. Sulfate is clearly the most concentrated and Fe the next most concentrated pollutant. The pH is lowest at site 4 for both sampling dates and increases somewhat downstream from the tailings, but levels off near site 6.

Levels of all pollutants in the receiving streams fluctuate, as expected, with inflow of low or high quality water. Trends in data from the March sampling show that pollutants, except for pH, uniformly decrease with distance from the tailings site, and then show increases at site 7 due to discharge from the abandoned air vent on the east side of Black Fork Creek. By contrast, an increase in pollutants is also noticeable at site 6 in the August samples. Site 6 is

just below the confluence of Black Fork Creek and Ogg Creek, and seepage from shafts of the Tropic Mine (see Figure 2.1) are probably the cause of this increase. At slightly higher flow periods, as exemplified by the March sampling, the influence of acid drainage from the west side of Black Fork Creek is not readily detected at site 6. At the August sampling, no major quantities of acid drainage or fresh water entered Black Fork Creek below site 8. Consequently, the concentrations of heavy metals, aluminum, manganese, and sulfate, as well as the pH at site 8, are very similar to the measurements taken at site 9. However, concentrations of dissolved iron decrease by almost one half from site 8 to site 9. This decrease over a linear distance of 2.5 km is possibly indicative of the rapidity with which iron is removed by precipitation.

2.4.2 Bottom Sediment Analyses

Coarse fragments comprised 47.4 to 88.0% by weight of all bottom sediments collected in the Black Fork Creek watershed; the average over all sites was 58.2%. Most of the fragments consisted of shale and sandstone, but an increase in coal fragments was noted at sites 4 and 5. Gravel and cobbles removed from sites within the polluted zone were generally coated with reddish-yellow, CBD-soluble material considered to be iron oxide. While coarse fragments comprise a significant portion of the total mass of bottom sediment, they are not the mobile, reactive fraction of the sediment load. Consequently, most attention is focused on the <2 mm fractions.

Particle size data for the <2 mm fractions of the sediment are given in Table 2.2. They are variable, but also show a distinct trend toward higher silt and especially clay contents in sections of the stream influenced by mining activities. For the same sites, increases in organic carbon are also noted. These increases are most likely due to coal fragments observed to be concentrated in

Table 2.2 Particle Size Distribution and Organic Carbon Content of Bottom Sediments from Black Fork Creek Watershed

Site	Sand	Silt	Clay	Organic Carbon
	%			
1-3	81.7	13.4	4.9	0.8
4	82.0	12.1	5.9	2.5
5	66.3	16.6	17.1	2.2
6	44.9	48.2	6.9	2.3
7	70.9	17.3	11.8	1.5
8	83.1	5.1	11.8	2.3
9	75.3	17.0	7.7	2.3

the sand fractions. After the sediments were fractionated, the yellowish coloration characteristic of polluted sections of the stream was exhibited primarily by the clay-sized materials. As a result of this observation, the clay fractions were studied in more detail.

The mineralogy of the bottom sediment clays (<2 μm) as estimated from X-ray diffraction analyses are presented in Table 2.3 and representative X-ray patterns from three sites in the watershed (sites 3, 6, and 9) are given in Figures 2.4 and 2.5. Results indicate that several crystalline clay minerals are uniformly present in the bottom clays at all nine locations. All samples contain high amounts of kaolinite, illite, and aluminum interlayered vermiculite with lesser amounts of smectite and quartz. Table 2.4 presents total K values for these clays, and permits estimation of the amount of illite (clay mica) in the samples by employing the relationship 1% K_2O = 10% mica (Jackson, 1975). A slight decrease in total K in the zone of pollution is associated with increases in smectite. In addition, expansion of the smectite peak with ethylene glycol is evident in the CBD-treated clays (Figure 2.4), but is not apparent in the natural clays (Figure 2.5). This behavior suggests that poorly crystallized hydroxides of Fe or Al may fill the interlayers and prevent expansion of the smectites under natural conditions. Samples untreated by CBD, (Figure 2.5) are remarkably similar and reveal low background levels of crystalline goethite and lepidocrocite in both the reference and polluted samples. Hence, no crystalline iron oxides can be directly related to the gelatinous precipitates resulting from acid mine drainage.

Total sulfur contents of the bottom sediment clays are given in Table 2.4. The contents are considerably higher in clays from polluted sections of the stream, but are much lower than levels which would be expected if bottom

Table 2.3 Estimated Clay (<2 μm) Mineralogy[+] of Bottom Sediments from Black Fork Creek Watershed

Site	[ξ]K	M	AV	S	Q	G	L
1-3	XXXX	XXX	XXX	X	X	X	X
4	XXX	XX	XXX	XX	X	X	X
5	XXXX	XXX	XX	XX	X	X	X
6	XXXX	XXX	XX	XX	X	X	X
7	XXXX	XXX	XX	XX	X	X	X
8	XXXX	XXX	XX	XX	X	X	X
9	XXXX	XXX	XX	XX	X	X	X

[+] Relative quantities: XXXX = 35-50%, XXX = 20-35%, XX = 5-20%, X = <5%

[ξ] K = Kaolinite, M = Clay Mica, AV = Al/Fe interlayered vermiculite, S = Expanding component (smectite), Q = Quartz, G = Goethite, L = Lepidocrocite

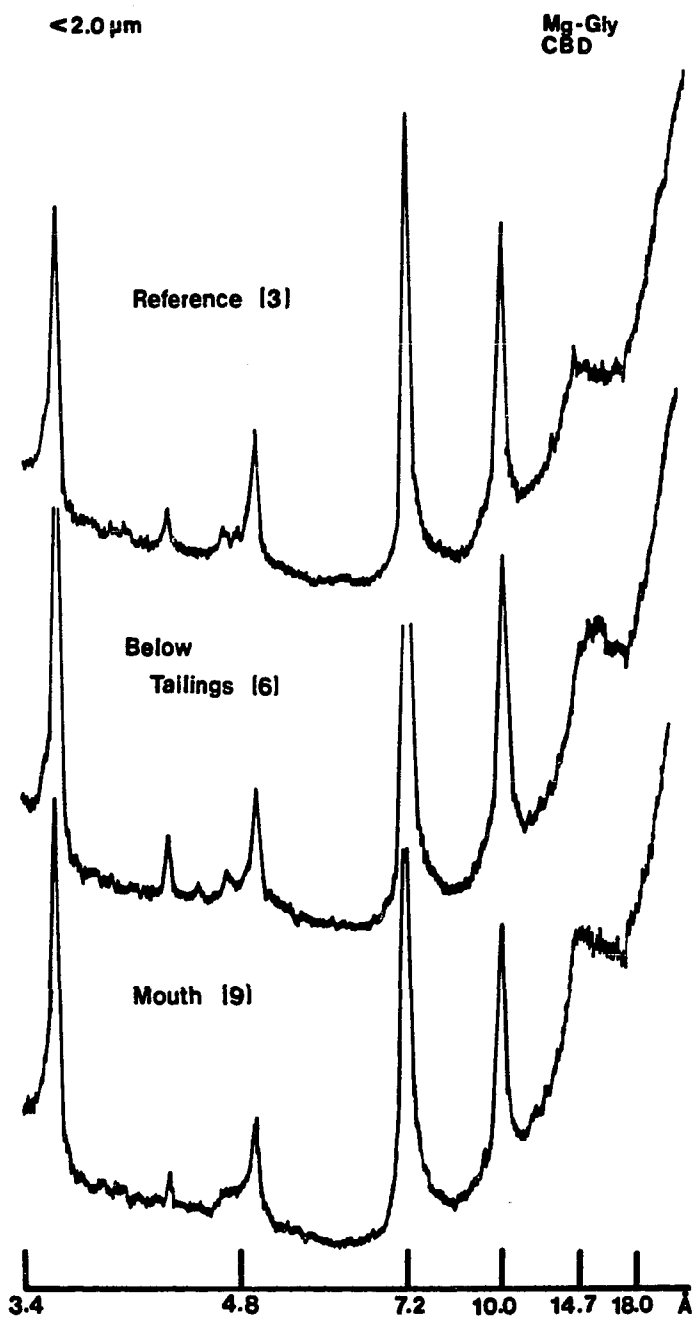

Figure 2.4 XRD spectra for selected sites in the Black Fork Creek watershed; CBD treated clay.

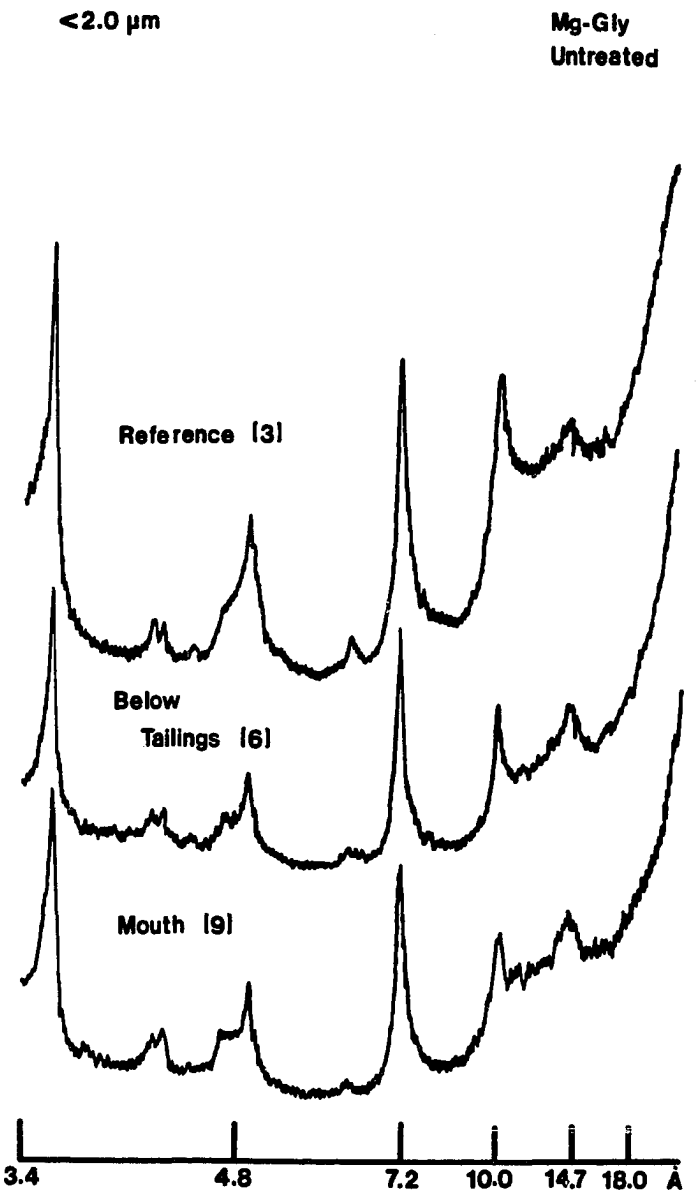

Figure 2.5 XRD spectra for selected sites in the Black Fork Creek watershed; total clay.

Table 2.4 Total Potassium and Total Sulfur Contents of Bottom Sediment Clays (<2 μm) in the Black Fork Creek Watershed

Site	K	K_2O	S
		%	
1-3	2.11	2.54	0.06
4	1.79	2.16	0.38
5	1.85	2.23	0.21
6	1.69	2.04	0.44
7	1.65	1.99	0.29
8	1.55	1.87	0.36
9	1.83	2.20	0.16

sediments in the zone of pollution contained sulfate minerals precipitating as a direct result of acid mine drainage. For example, if all the extractable iron (Fe_d ~ 10%; See Table 2.5) in the contaminated clays were due to the mineral jarosite, then at least 3.8% total sulfur should also be present. The sulfur contents of these clays are less than one tenth the stoichiometric requirement for jarosite and could easily be due to surface adsorbed sulfate. In addition, no sulfate minerals were identified by X-ray diffraction.

Selective dissolution and total chemical analyses for iron, aluminum, and manganese (Tables 2.5, 2.6, and 2.7, respectively) provide evidence that oxides and/or oxyhydroxides of these metals are important components of the bottom sediments. Secondary iron compounds provide the most significant contribution of materials followed by aluminum and manganese.

All forms of extractable iron in the reference areas are relatively low (Table 2.5), but increase markedly at and below sources of pollution. Increases in iron held by organic matter (Fe_p) are notable, and are most likely due to the breakdown and release of organics from coal. Ratios of CBD extractable to total iron (Fe_d/Fe_t) indicate that a majority of the iron in the reference areas is held within the structures of silicate clay minerals, but in the zone of pollution, iron held by the silicate minerals is greatly diminished in importance. Between 70-90% of the iron is CBD extractable in this zone. In addition, ratios of oxalate to dithionite extractable iron (Fe_o/Fe_d) suggest that 75-90% of the secondary iron extracted from the clays is in the form of a very poorly crystallized iron oxide.

Selective dissolution and total chemical data for aluminum (Table 2.6) suggest a pattern similar to that observed for iron. All forms of extractable aluminum in the reference areas are low and increase in the zone of pollution;

Table 2.5 Extractable and Total Iron Contents* of Bottom Sediment Clays (<2 μm) in the Black Fork Creek Watershed

Site	Fe_p	Fe_o	Fe_d	Fe_t	Fe_d/Fe_t	Fe_o/Fe_d
	%					
1-3	0.19	2.24	3.65	8.43	0.43	0.61
4	0.45	10.27	11.64	14.27	0.81	0.88
5	0.77	9.37	10.50	11.80	0.88	0.89
6	0.28	11.40	13.63	16.80	0.81	0.84
7	0.18	10.36	12.35	14.30	0.86	0.84
8	0.51	8.46	10.88	15.03	0.72	0.78
9	0.86	8.40	10.35	13.03	0.79	0.81

* Fe_p, Fe_o and Fe_d are pyrophosphate, ammonium oxalate, and CBD extractable Fe, respectively. Fe_t is total iron.

Table 2.6 Extractable and Total Aluminum Contents* of Bottom Sediment Clays (<2 μm) in the Black Fork Creek Watershed

Site	Al_p	Al_o	Al_d	Al_t	Al_d/Al_t	Al_o/Al_d
	%					
1-3	0.03	0.40	0.58	11.02	0.05	0.68
4	0.19	1.01	1.10	10.50	0.10	0.92
5	0.07	0.47	0.60	9.23	0.06	0.78
6	0.06	0.93	1.21	9.10	0.13	0.77
7	0.04	0.80	1.04	9.40	0.11	0.77
8	0.14	1.45	1.69	9.33	0.18	0.86
9	0.20	0.83	1.19	10.00	0.12	0.70

*Al_p, Al_o and Al_d are pyrophosphate, ammonium oxalate, and CBD extractable Al, respectively. Al_t is total aluminum.

Table 2.7 Extractable Manganese Contents* and Surface Area of Bottom Sediment Clays (<2 μm) in the Black Fork Creek Watershed

Site	Mn_o	Mn_d	Mn_o/Mn_d	Surface Area	
				Natural Clay	CBD Clay
	μg/g			m^2/g	
1-3	722	712	0.89	28	22
4	237	267	0.89	--	--
5	207	227	0.91	52	21
6	200	263	0.76	77	32
7	265	365	0.73	--	--
8	303	393	0.77	--	--
9	277	283	0.98	--	--

*Mn_o and Mn_d are oxalate and CBD extractable Mn, respectively.

however, values are always a fraction of those obtained for iron. Total aluminum levels are similar in magnitude to total iron values but are more uniform throughout the watershed. CBD extractable aluminum accounts for only about 10% of the aluminum in the bottom sediments, and 70-90% of this amount is also oxalate-extractable. These results suggest that some aluminum is probably co-precipitated with iron as acid drainage waters are introduced to the receiving streams.

Secondary manganese components are present in the bottom sediments in much smaller amounts (Table 2.7), and the distribution is opposite to that observed for aluminum and iron. Total manganese is not reported, as it is within the range obtained by dithionite extraction. Contents of manganese oxides appear to be higher in the bottom sediments of the reference areas, and to decrease in the zone of pollution. Although oxalate extractable manganese accounts for between 75-98% of the CBD extractable manganese, the distribution is puzzling, especially when water quality data (Table 2.1) are considered. These data show low concentrations of manganese in the reference areas, and high concentrations in the zone of pollution, exactly the opposite trend from that observed for the bottom sediments. The data suggest that the solubility of secondary manganese minerals is increased in the zone of pollution, perhaps due to the effect of reduced pH. This may have implications for the preferential dispersal of Mn from a source of pollution and warrants further study.

In any case, selective dissolution analyses indicate that poorly crystallized iron oxide is a major product of acid mine drainage in the Black Fork Creek watershed. This poorly crystallized iron oxide, besides enlarging the sediment

load of the receiving streams, also increases the surface area and chemical reactivity of the bottom sediments.

A comparison of surface areas for clays from one reference (site 3) and two sampling points in the zone of pollution (sites 5 and 6) reveals almost a three-fold increase in the downstream samples (Table 2.7). Since all three clays have similar surface areas after secondary iron compounds are removed with CBD, the increases must be due to the accumulation of iron precipitate in the receiving stream. Note also that there is little difference in the measured surface area of the reference clay before and after extraction with CBD.

Increases in surface area generally produce greater chemical reactivity. This is especially true when the increase is due to additions of poorly crystallized iron oxide, which is widely recognized as a scavenger of heavy metals and certain anions, such as phosphate, in fluvial environments (Chao and Theobald, 1976). An example of its effect on the sorptive capacity of bottom sediment clays from Black Fork Creek is given in Figure 2.6. Phosphate adsorption isotherms from a reference site (3) and from two polluted sites (5 and 6) show that clays from the polluted sections of Black Fork Creek are at least 2 to 4 times more adsorptive of added phosphate than are clays from the reference sites. The clay from site 6, constituted primarily of colloidal iron precipitate, probably represents an extreme case. The general reactivity of clays from sediment within the polluted portion of the basin is considered to be best represented by data for site 5.

2.5 Summary and Conclusions

Although water quality of streams affected by acid mine drainage varies with the season and with rainfall, the greatest contributors to pollution are increases in sulfate, iron, and aluminum with an associated decrease in pH.

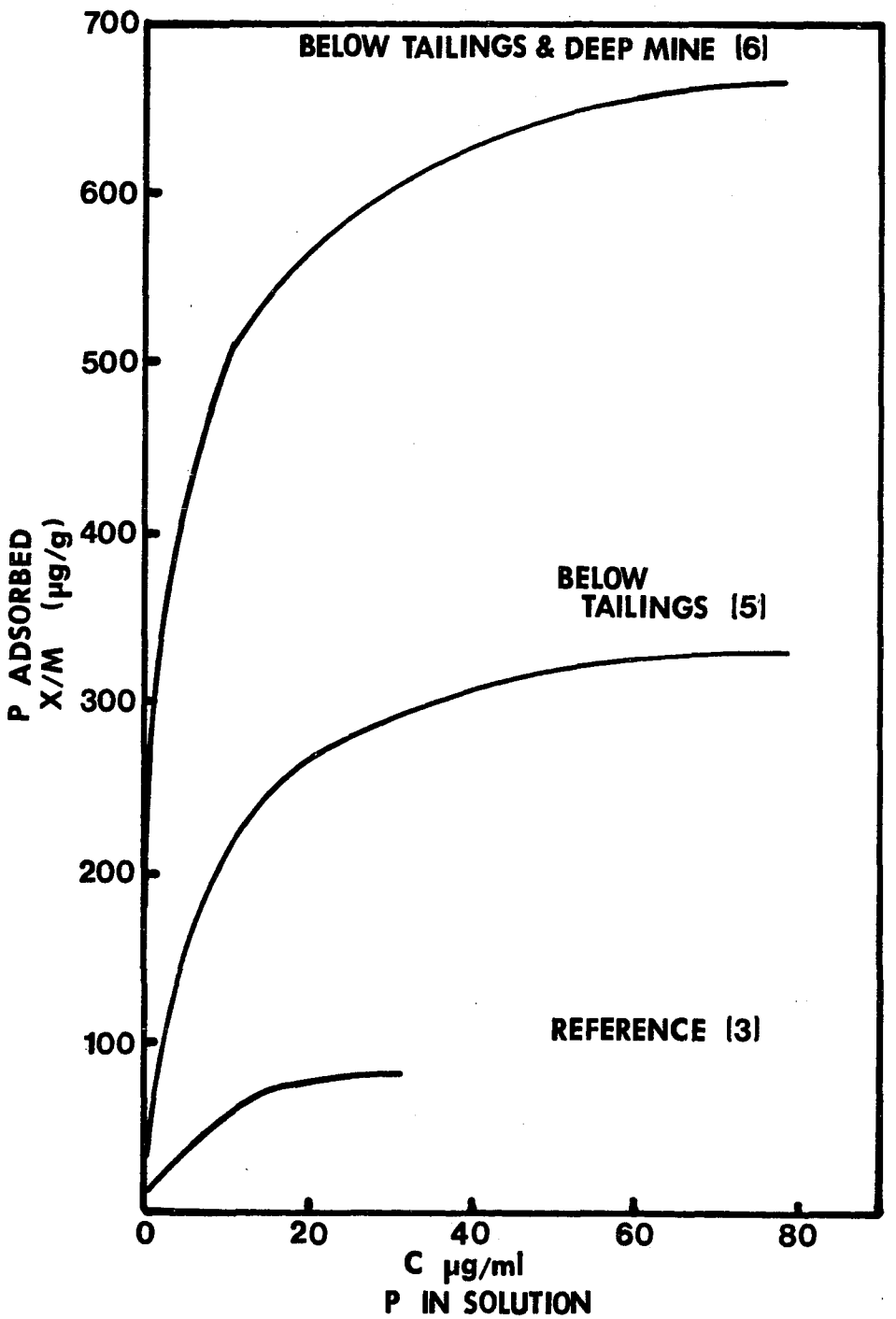

Figure 2.6 Phosphate adsorption isotherms of selected bottom sediments (<2 µm) from the Black Fork Creek watershed.

Crystalline clays contained in the bottom sediments of the Black Fork Creek watershed are remarkably similar throughout all portions of the drainage catchment. However, poorly crystallized minerals, particularly of iron, are significantly represented in the bottom sediments below sources of pollution. These iron oxide or oxy-hydroxide minerals greatly increase the surface area and reactivity of the bottom sediments, and are directly linked to the gelatinous precipitates resulting from acid mine drainage.

CHAPTER 3

PROPERTIES OF A NATURALLY OCCURRING STREAM PRECIPITATE RESULTING FROM ACID MINE DRAINAGE AND A COMPARISON TO LABORATORY SYNTHATES

3.1 Introduction

In Chapter 2, a poorly crystallized iron oxide or oxyhydroxide precipitate was shown to affect the physical and chemical properties of bottom sediments in streams receiving acid coal mine drainage. However, the precipitate was not sufficiently concentrated to allow for further identification and characterization. Consequently, the purpose of this investigation was to isolate, identify, and characterize the natural precipitate which is voluminous during low stream flow, and to compare its characteristics with those of laboratory synthates.

3.2 Literature Review

3.2.1 Mineral Precipitates Associated with Coal Spoils and Acid Mine Drainage

A large number of weathering products have been reported to be associated with both coal spoils and acid mine drainage. These minerals have a wide range in properties, and their distribution can vary regionally or even seasonally depending on rainfall or other environmental factors.

Hydrated ferrous sulfate minerals commonly appear as efflorescences on oxidizing coal and mine spoils. When conditions are sufficiently dry, Fe(II) and sulfate will combine to form melanterite, ($FeSO_4 \cdot 7H_2O$), and with further desiccation, the white, frost-like mineral rozenite ($FeSO_4 \cdot 4H_2O$), or even the monohydrate, szomolnokite ($FeSO_4 \cdot H_2O$). Other hydrated species have also been

identified, but the most common is the mixed-valence iron sulfate, copiapite ($Fe^{+2}Fe_4^{+3}(SO_4)\bullet 20H_2O$). This mineral is reported to be abundant and stable in coal and sulfide mine tailings in Virginia provided it is protected from rainfall or flowing water (Nordstrom, 1980). Apparently, other trivalent metals can substitute for Fe(III) within the structure, as alumino-copiapate has been reported by Zodrow et al. (1979) in a study of pyrite alteration products from a coalfield in Nova Scotia. Nuhfer (1967) also reports that melanterite, rozenite, szomolnokite, and copiapate were abundant in his study of oxidizing coal deposits in West Virginia. All of these iron sulfates are highly soluble in water and are considered by Nordstrom and Dagenhart (1978) to contribute heavily to the acidity and the dissolved metal load of receiving streams during rainstorm events. This conclusion is supported by Curtis (1972) in his study of chemical changes in streams influenced by surface mining in eastern Kentucky.

With further oxidation and hydrolysis of iron, the yellow, hydroxy-sulfate mineral jarosite may be formed. Jarosite [K, Na, $Fe(SO_4)_2(OH)_6$] is stable at pH <3 and moderate to high oxidizing conditions (Brown, 1971). It is commonly associated with coal tailings and acid sulfate soils but is probably unstable in most stream environments. However, Nordstrom (1980) suggests that the voluminous "yellow boy" precipitate that forms almost immediately upon mixing of acid mine drainage with fresh waters may be jarosite. Most other sources, including mining trade journals and the EPA (1971), refer to this material simply as "ferric hydroxide" precipitate.

The positive identification of jarosite or "ferric hydroxide" compounds in streams affected by acid mine drainage has been hindered by the poor crystallinity of the precipitate and its short residence time between storm cycles. In an earlier study of bottom sediments in Black Fork Creek, Ohio

(Chapter 2), X-ray diffraction analyses of the sediment clays gave no indication of jarosite. In addition, as reported in Chapter 2, section 2.4.2, sulfur was not present in the clays in quantities great enough to indicate the presence of jarosite. All indications were that the reddish-yellow precipitate from acid mine drainage was a poorly crystallized iron oxide.

3.2.2 Origin and Properties of Ferrihydrite

In recent years, considerable attention has been focused on the mineral precipitate(s) formed by rapid hydrolysis of Fe(III) in water. Under aerated conditions the major product of this reaction appears to be a poorly-crystallized compound that has been assigned the mineral name "ferrihydrite" (Chukrov et al., 1973). Ferrihydrite is a poorly ordered Fe-oxide with a layer structure and average composition of $5Fe_2O_3 \cdot 9H_2O$. It is most often described as being a rusty or ocherous precipitate with a high surface reactivity (Carlson & Schwertmann, 1981). Ferrihydrite is associated with soils in a number of environments such as drainage ditches, low discharge water sources, seeps, and groundwater flows (Schwertmann and Fischer, 1973; and Carlson and Schwertmann, 1981). It is also known to be associated with lichen weathering crusts of basalt (Jackson and Keller, 1970) and occurs with goethite in bog ores. Ferrihydrite probably also constitutes the Fe(III) oxide of Bir horizons in true podzols (Schwertmann and Taylor, 1977). However, it has not previously been directly linked to acid mine drainage.

Ferrihydrite, in contrast to other iron oxides, is very soluble in acid ammonium oxalate, and varies in its crystallinity. Chukhrov et al. (1971) reported five broad X-ray diffraction lines for ferrihydrite at 2.50-2.54, 2.21-2.28, 1.96-1.98, 1.70-1.725, and 1.47-1.48 Å. Other researchers have reported more disordered structures which yield only two reflections at 2.5 and 1.5 Å

(Carlson and Schwertmann, 1981); these less ordered versions have in some cases been referred to as "protoferrihydrite". Towe and Bradley (1967) developed a structural model for ferrihydrite that is related to hematite and that is based on a hexagonal cell with $a = 5.08$ and $b = 9.4$ Å.

Attempts to characterize the mineral by DTA and infrared analyses have also been made. Towe and Bradley (1967) reported a DTA curve which showed a broad endotherm at 100° C due to adsorbed water followed by an exotherm at 400-450° C due to the formation of hematite under a static nitrogen atmosphere. In an O_2 atmosphere, Carlson and Schwertmann (1981) observed a very sharp exothermic peak between 300 and 350° C that marked the hematite transformation and that was a distinctive feature of pure, synthetic ferrihydrite. For natural ferrihydrites, Schwertmann and Fischer (1973) reported an endotherm near 100° C due to adsorption of water followed by an exothermic peak between 200 and 300° C due to the presence of organic matter. Infrared analysis of ferrihydrite has shown resonance features arising primarily from OH groups. Russell (1979) reported that an absorption band at 3430 cm^{-1} was related to OH stretching in the ferrihydrite structure, and that a 3615 cm^{-1} band was most likely due to free surface OH groups. Towe and Bradley (1967) observed an additional absorption feature at 1620 cm^{-1} which they related to hydrogen-bonded water.

Electron microscopy has been used to characterize both naturally-occurring and synthetic ferrihydrites, and has typically shown spherical particles 2-10 nm in diameter, which commonly associate to form larger aggregates of 100-300 nm diameter (Schwertmann and Taylor, 1977, and Carlson and Schwertmann, 1981). Surface areas have been reported by the same researchers to range between 200-560 m^2/g.

3.2.3 Laboratory Synthesis of Ferrihydrite

Materials taken from the natural environment are seldom pure substances. For this reason, laboratory synthates produced under more controlled conditions are frequently used for comparison. In addition, laboratory synthates are also used to study the processes of nucleation and crystal growth.

Preparation of synthetic ferrihydrite usually involves the dissolution and hydrolysis of soluble Fe(III) salts such as ferric nitrate or ferric chloride. Towe and Bradley (1967) synthesized ferrihydrite by hydrolyzing a 0.06M solution of $Fe(NO_3)_3 \cdot 9H_2O$ at 85° C. It was then dialyzed against distilled water. Russell (1979) also reported preparing ferrihydrite by boiling a 0.01M aqueous solution of $Fe(NO_3)_3 \cdot 9H_2O$ followed by dialysis of the precipitate against distilled water. Other researchers have described the preparation of "hydrous Fe(III) oxides" in the presence of ions and elements found in the natural environment in an effort to determine bond placement and surface adsorption characteristics. For example, Carlson and Schwertmann (1981) synthesized Si-containing ferrihydrites which they prepared by hydrolyzing a 0.1M $Fe(NO_3)_3$ solution to which a solution with 2 mM Si/l was added to give Si/Si + Fe mole ratios in the precipitate between 0 and 0.15. The infrared characteristics of the synthates were then compared to those of natural, Si-bearing ferrihydrites isolated from spring precipitates in Finland.

Harrison and Berkheiser (1982) prepared hydrous Fe(III) oxides by the dropwise addition of 1N $FeCl_3$ to a 1N NH_4OH solution until the OH/Fe(III) ratio equaled 3.0 at pH 6.5. The resulting precipitate was dialyzed and concentrated by freeze-drying. Anion interactions were then studied by equilibrating specific concentrations of $NaNO_3$, Na_2SO_4, and other salts with the freeze-dried Fe(III) oxide over a 24 hr period. Investigations of these anion interactions were

conducted using infrared spectroscopy with AgCl windows as the supporting medium.

Additional studies of nucleation and crystal growth have used other iron salts for the production of Fe(III) gels and sols. A more comprehensive review of these studies is given in Chapter 4, where processes of precipitate formation are considered in greater detail.

3.3 Methods and Analytical Procedures

3.3.1 Collection and Concentration of a Naturally-Occurring Stream Precipitate

In September, 1981, during a period of extreme low flow, approximately 60 l of a yellowish, voluminous stream precipitate was collected in suspension from an eddy pool along Ogg Creek (near Site 5, Chapter 2). A 4-l plastic container which had been acid washed was used for the removal of the precipitate from the stream. This material was poured directly into a larger, 20-l bucket (also acid washed) and allowed to settle for a few minutes. The water was then decanted, and more precipitate was placed in the bucket. Upon arrival at the lab, the samples were refrigerated at 4° C and allowed to settle further before concentration by additonal decantation. The bulk sample was then quick frozen and freeze-dried at 60° C.

3.3.2 Preparation of Laboratory Synthates

A standard ferrihydrite sample was prepared by hydrolyzing a 0.02M $Fe(NO_3)_3 \cdot 9H_2O$ solution (U. Schwertmann, personal communication) at 60° C for 12 min. This was accomplished by heating distilled water to 60° C in a water bath and then adding the water to the appropriate amount of $Fe(NO_3)_3 \cdot 9H_2O$ in a 500-ml volumetric flask. This flask was then placed in the water bath for 12 min. The resulting wine-colored suspension was dialyzed against distilled water for one month, quick frozen, and freeze-dried.

In an effort to determine the effect of sulfate on the properties of ferrihydrite, Na_2SO_4 was added to the $Fe(NO_3)_3 \cdot 9H_2O$ prior to hydrolysis in quantities which resulted in solutions that were 0.0, 0.025, 0.05, 0.1, 0.15, and 0.20% SO_4. These concentrations bracket the range of SO_4 (0-2000 μg/ml) found in Black Fork Creek and its tributaries. Two dialysis procedures were used in synthate production. One set of sulfate treatments was dialyzed against distilled water. In an effort to further approximate conditions of natural precipitation, another set was dialyzed against solutions which contained the same percent sulfate as was added before hydrolysis (an exception was the 0.0% sulfate treatment which was dialyzed against a 0.1% sulfate solution). All synthates were washed for one month. Dialysis solutions were changed daily following adjustment of the pH to 6.0 using 1N HCl. The synthates were then concentrated by freeze-drying at 60° C. Care was taken to ensure that the temperature was no higher than this, as it was found that the natural ferrihydrite could be altered by heating at 105° C. After drying, both the natural precipitate and the synthates were stored in new, acid-washed plastic beakers with snap-on lids.

Prior to some analyses, subsamples were placed in a vacuum desiccator over concentrated sulfuric acid, evacuated for 30 min with a vacuum pump, and placed in a dark cabinet for 2 weeks in a drying procedure modified from that of Orchiston (1953). After drying over H_2SO_4, the samples were stored in a desiccator over P_2O_5 as suggested by Kolthoff et al. (1971). This drying process was necessary because conventional oven drying to estimate dry weights for numerical adjustments produced misleading phase changes in the samples.

3.3.3 Analytical Procedures

The methods of analysis described in this section generally pertain to the characterization of both the natural and synthetic precipitates. Some procedures have been used previously, and will not be described again at length; however, all new or modified procedures will be discussed in detail.

3.3.3.1 Total Chemical Analyses. The chemical composition of the natural precipitate was analyzed using two methods. The first method involved total dissolution with HF in a digestion bomb as described in Chapter 1, section 1.4.11. The second method employed was that of Carlson and Schwertmann (1981) and involved HCl dissolution of the poorly crystallized iron oxide. This procedure was performed at room temperature and required the addition of 40 ml of 5N HCl to 200 mg of sample in a 100-ml polypropylene test tubes. The test tube was stoppered, allowed to set for 1 min, and the extract was decanted. From this extract a 1 to 10 dilution was made.

Solutions from both types of digests were assayed for Fe, Al, K, Na, Ca, Mg, Si, and Mn using a Varian AA6 atomic absorption spectrophotometer. All elements except Fe were analyzed with no further dilution. The total dilution factors for HF digestable and HCl extractable Fe were 250 and 200, respectively. The samples were compared to standards made from Fisher certified atomic absorption reference materials and the appropriate blank solution. Standard solutions ranged from 0-2 μg/ml for Mg and Mn; 0-10 μg/ml for Ca; 0-20 μg/ml for Na and Fe; 0-25 μg/ml for K; and 0-100 μg/ml for Si and Al. All analyses were performed in duplicate.

The residue left after HCl extraction was dried and measured gravimetrically. Also, weight loss on ignition (LOI) at 600° C was measured gravimetrically. The residue and LOI determinations, when combined with

results from the HCl extractions, enabled an analysis of the natural precipitate without contamination from silicate impurities in the sample (Schwertmann and Fischer, 1973).

3.3.3.2 Phosphate Adsorption. Phosphate adsorption characteristics of the natural precipitate were examined by the method described in Chapter 2, section 2.3.3.9. Minimum initial phosphate concentrations of 400 μg/ml were required to achieve measurable P in solution following equilibration with the precipitate.

3.3.3.3 Total Sulfur Measurements. Duplicate 0.1 g samples of the natural precipitate and the synthates were analyzed for total sulfur content as described in Chapter 2, section 2.3.3.6.

3.3.3.4 Organic Carbon. Duplicate 0.25 g samples of the natural precipitate were analyzed for organic carbon content by the method described in Chapter 1, section 1.4.3.5.

3.3.3.5 Color. Dry colors of the natural and laboratory precipitates were described with a Munsell soil color chart. All measurements were made under sunlight.

3.3.3.6 Selective Dissolution Analyses. Both the natural precipitate and the synthates were subjected to acid ammonium oxalate and sodium citrate-bicarbonate-dithionite extractions. In addition, the natural precipitate was extracted with sodium pyrophosphate to determine the amount of organically-complexed iron. All procedures were the same as described in Chapter 1, sections 1.4.3.7-9.

3.3.3.7 X-ray Diffraction Analysis. The samples were analyzed by X-ray diffraction using random powder mounts of material that had been held in a desiccator over P_2O_5 for at least 36 hr prior to analysis. These analyses were conducted on the same instrument as described in Chapter 1, section 1.4.3.11.

The diffraction tube was operated at 35 kV with a current of 20 mA. A one-sec time constant and a 500 count per sec range factor were used for these samples. Diffractograms were normally recorded over an angular range of 2°-72° 2θ using a scanning speed of 2° 2θ per min and a recorder speed of 1 in per min.

3.3.3.8 Infrared Analysis. Twenty-five mg of freeze-dried sample were placed in 25 ml of distilled water and dispersed with an ultrasonic probe (Branson Sonifier Cell Disruptor Model W185) for 1.5 min. The resulting aqueous suspension (1.0 mg/ml) was plated onto an AgCl window to give a uniform deposit with a weight of 0.5 mg/cm^2 (Russel, 1979). The suspension was allowed to air dry overnight, and was then dried over P_2O_5 in a desiccator for at least 24 hr prior to analysis.

The samples were scanned with a Beckman Model 4250 infra-red spectrophotometer at a rate of 600 cm^{-1} per min, utilizing speed supression, and a blank AgCl window as reference.

3.3.3.9 Differential Scanning Calorimetry (DSC). All samples were heated to 59° C for 12 hr and were then stored over P_2O_5. Immediately before analysis, 4.0 mg of precipitate were weighed into an aluminum sample pan. The pan was then covered and placed over a Chromel-Constantan thermocouple in the sample chamber of a DSC cell. An empty pan was also covered and placed on the reference platform in the sample cell. All thermal scans were made from room temperature to 600° C using a DuPont 990 Thermal Analyzer with a heating rate of 50° C/min and a range factor of 2 and 5 in most cases. Each sample was analyzed in three different atmospheres: air, N_2 and O_2.

3.3.3.10 Surface Area. Surface area measurements were conducted using N_2 gas adsorption in the manner described in Chapter 2, section 2.3.3.11, except that the chemically desiccated samples were not subjected to additional oven drying prior to analysis.

3.3.3.11 Transmission Electron Microscopy. Morphological and diffraction characteristics of both the natural and synthetic precipitates were studied by transmission electron microscopy (TEM). In all cases, a dilute aqueous suspension was prepared by dispersing 1 mg of precipitate in 50 ml of water with an ultrasonic probe for 1.5 min. Then, using a micro pipet, one drop of suspension was transferred to a 200 mesh, 3.05 mm diameter copper TEM grid which had been coated with a formvar support film (0.2% formvar in chloroform). One half the sample grid was shadow coated with gold using a Denton vacuum evaporator. Electron micrographs and selected area diffraction patterns were subsequently obtained using a Zeiss 9-S electron microscope.

3.4 Results and Discussion

3.4.1 Total Chemical Analyses of the Natural Precipitate

Total dissolution of the natural precipitate with HF and extraction with HCl produced similar quantities of Fe (Table 3.1) which indicates that almost all the Fe is in oxide (non-silicate) form. X-ray diffraction analysis of the material left as residue from the HCl extract revealed the presence of quartz and small amounts of kaolinite and clay mica impurities. These materials are responsible for the increases in Si, Al, K, Na, Mg and Mn in the HF digest as compared to the HCl extract. The HCl data further indicate that iron, structural and adsorbed water (LOI), and insoluble residue account for 98% of the composition of the natural precipitate. Schwertmann and Fischer (1973) reported that loss on ignition, Fe, Ca, Mn, and HCl-insoluble products accounted for 98 to 100% of the

Table 3.1 Composition of the Natural Precipitate

Element (Oxide)	HCl		HF	
	Element	Oxide	Element	Oxide
	%			
Fe (Fe_2O_3)	31.20	44.60	31.62	45.24
Al (Al_2O_3)	0.08	0.15	0.99	1.87
K (K_2O)	0.02	0.03	0.49	0.59
Na (Na_2O)	0.01	0.01	0.20	0.28
Ca (CaO)	0.05	0.07	0.08	0.12
Mg (MgO)	0.01	0.01	0.21	0.36
Si (SiO_2)	0.14	0.33	2.91	6.93
Mn (Mn_3O_4)	0.00	0.00	0.01	0.01
LOI*	43.00	43.00	43.00	43.00
Residue**	10.00	10.00	----	----
	84.51	98.20	79.51	98.40

*LOI = weight loss on ignition to 600° C
**Residue = HCl insoluble residue

composition of rusty iron oxide precipitates deposited from soil-borne waters, drainage ditches, and springs from various sites in northern Europe.

3.4.2 X-ray Diffraction Analyses

XRD spectra from the natural precipitate and selected samples of the laboratory synthates are found in Figures 3.1 and 3.2. The spectrum from the natural precipitate (Figure 3.1) shows a sharp reflection at 3.34 Å, due to quartz, and two broad reflections at 2.5 and 1.5 Å that are apparently produced by the iron oxide component. Feitknecht et al. (1973) have reported the same two-line spectrum for poorly crystallized, synthetic, "hydrous Fe(III) oxide" with a structure consisting of disordered $Fe(O, OH, OH_2)_6$-octahedral units. The two XRD lines at 2.52 and 1.5 Å were thought to correspond to diffraction by the (110) and (300) structural planes within these units. Chukhrov et al., (1972) have assigned the name protoferrihydrite to natural compounds with these structural characteristics, and protoferrihydrite is, in turn, considered to be a disordered form of the mineral ferrihydrite. A continuum of crystallinity exists between protoferrihydrite and ferrihydrite, and Carlson and Schwertmann (1981) have argued that the distinction is arbitrary. As a result, the term ferrihydrite is utilized throughout this discussion.

The crystallinity of synthetic ferrihydrites produced in this study clearly depends upon the amount of sulfate added at the time of hydrolysis but is influenced to a lesser extent by the ensuing dialysis procedure. With 0% sulfate and water dialysis (Figure 3.2) a "crystalline" ferrihydrite is formed with five distinct diffraction lines at 2.5, 2.24, 1.97, 1.7, and 1.5 Å. The 1.5 Å line is, in fact, a doublet with maxima at 1.53 and 1.48 Å. At the lowest levels of added sulfate (e.g., 0.025% sulfate in Figure 3.1), co-formation of ferrihydrite and poorly crystallized goethite is indicated by an additonal weak reflection at 4.18

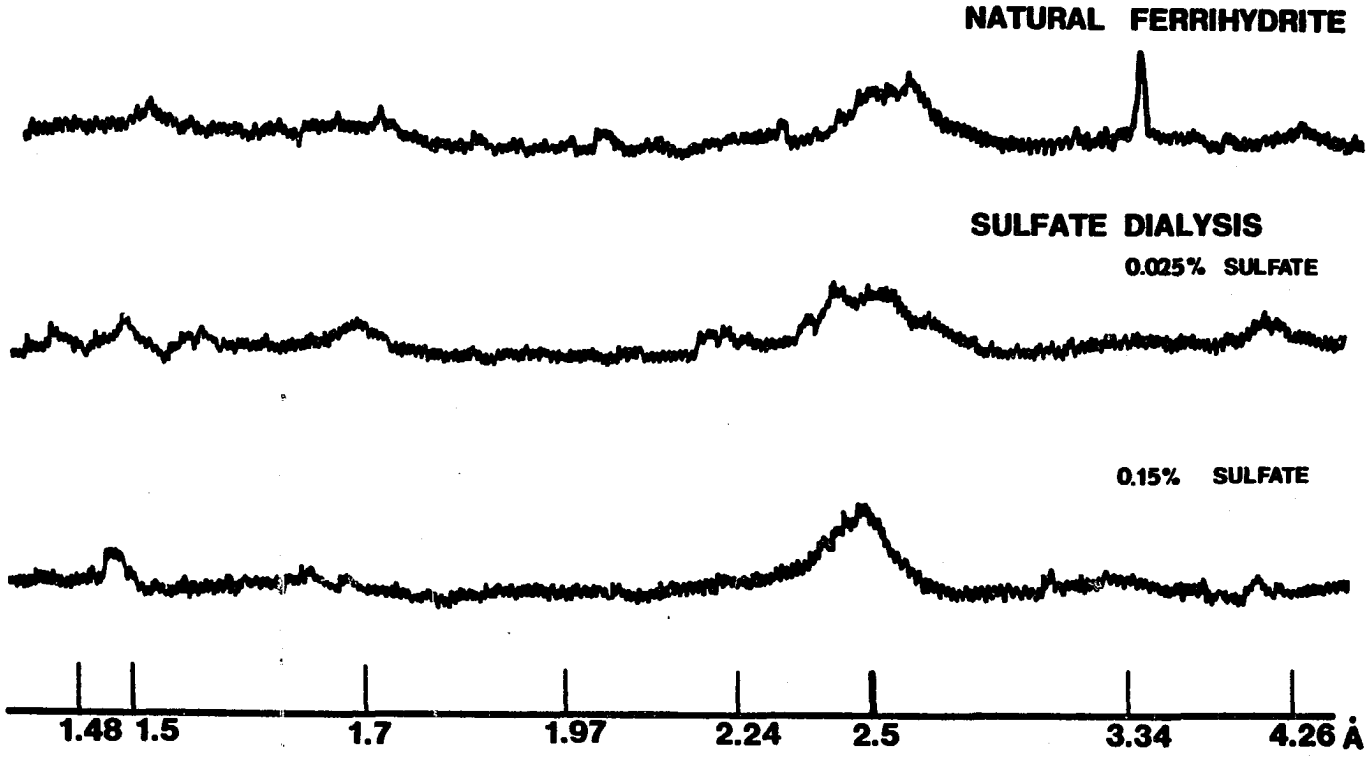

Figure 3.1 XRD spectra of naturally occurring ferrihydrite from acid mine drainage and selected sulfate dialyzed laboratory synthates.

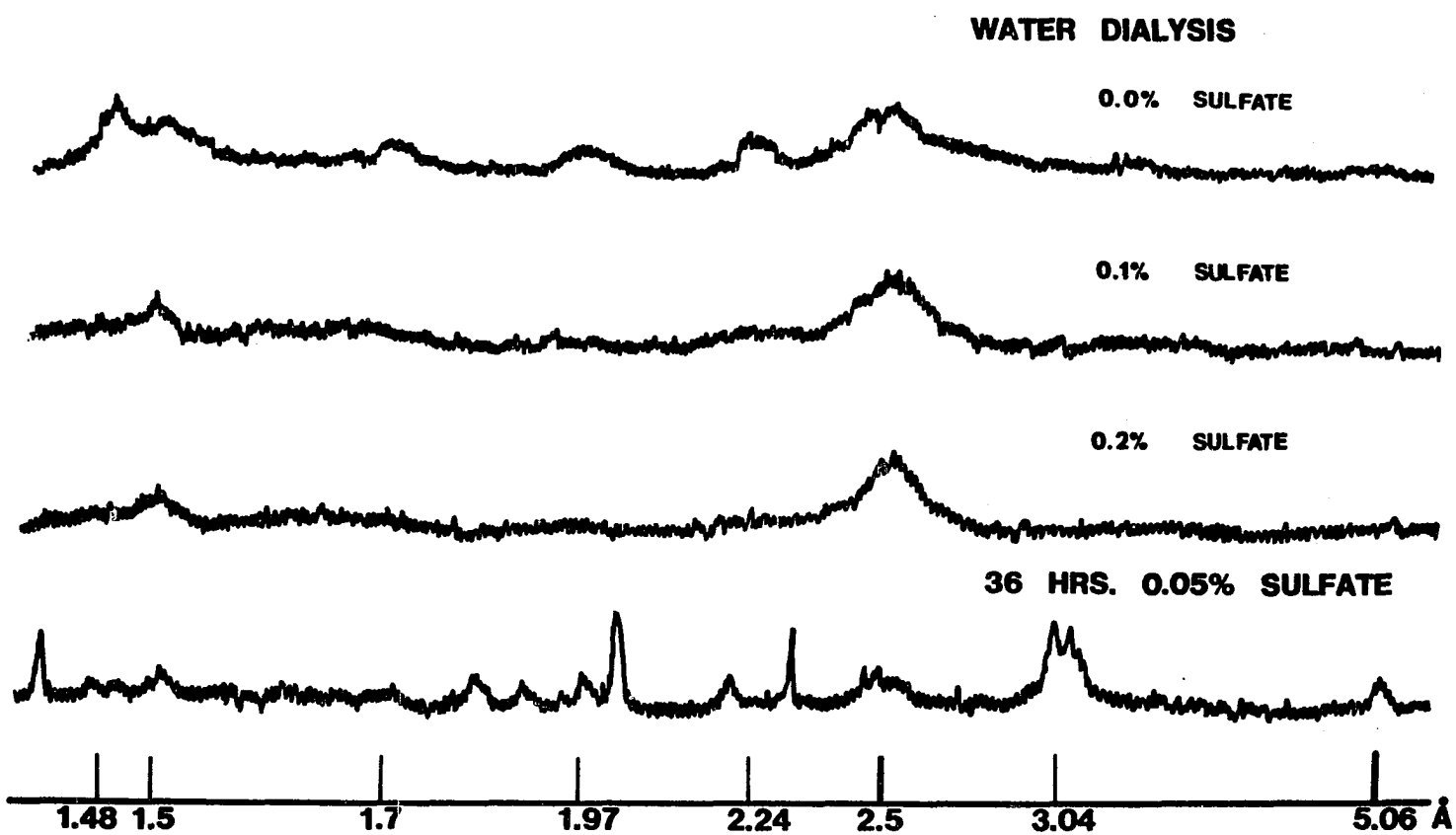

Figure 3.2 XRD spectra of selected water dialyzed laboratory synthates and a 36 hr sample containing sodium jarosite.

Å (110 line of goethite). However, as sulfate is further increased, the goethite line disappears and the crystallinity of the ferrihydrite decreases until only two broad lines become evident at the highest sulfate levels. This trend is in keeping with laboratory observations made at the time of $Fe(NO_3)_3 \cdot 9H_2O$ hydrolysis. The formation of yellowish precipitates was almost immediate when 0.1% or more sulfate was added, but precipitate formation took two to three weeks for the treatments with no sulfate. Fast precipitation is synonymous in this case with less ordered structures.

A comparison of XRD spectra indicates that the synthates most like the natural ferrihydrite (exclusive of quartz) are those hydrolyzed in the presence of 0.1 to 0.15% sulfate, which approximate the levels of dissolved sulfate generally encountered in Black Fork Creek.

Included in Figure 3.2 is a spectrum from a short-term, 36 hr precipitate removed from the 0.05% sulfate treatment during dialysis against distilled water. In addition to some poorly crystallized ferrihydrite, this pattern shows sharp peaks at 5.06, 3.12, 3.04, 2.22, 2.02, 1.97, and 1.83 Å which are indicative of Na-jarosite. Na-jarosite also occurred in the 36-hr precipitates from other treatments but, surprisingly, was not evident at the higher sulfate levels. It also was not present in any of the aged precipitates which had been dialyzed for one month.

The short-term nature of the jarosite in the synthesis study is consistent with its infrequent occurrence in the field. Jarosite was found only once as a surface encrustation during a low rainfall period. It was never observed as a precipitate in the stream environment. This is also consistent with observations made by Miller (1979) in a study on leaching of spoil materials where an accumulation of soluble Na^+, $SO_4^=$, H^+ and Fe^{+3} from pyrite oxidation resulted

in jarosite formation. With subsequent leaching of these materials, jarosite was solubilized and the dissolved iron rapidly hydrolyzed to produce a "ferric hydroxide".

3.4.3 Selective Dissolution, Total Sulfur, and Color

The natural ferrihydrite yields 1.7, 29.6 and 29.9% Fe with Na-pyrophosphate, ammonium oxalate, and CBD extraction, respectively (Table 3.2). The high ratio of ammonium oxalate extractable to CBD extractable Fe further confirms the poorly crystallized nature of the precipitate. The Fe_o/Fe_d ratios obtained from the laboratory synthates are considerably lower than that for the natural precipitate which indictes greater overall crystallinity and/or the presence of crystalline impurities, such as goethite. This effect may be due to the fact that the synthates were initially hydrolyzed at 60° C rather than at temperatures found in the natural environment. Additional support for a thermal effect is provided by data from two precipitates formed under identical conditions (0.0% sulfate, water dialysis) except for temperature of hydrolysis (60° C vs 80° C). The precipitate formed at 80° C yields a substantially lower Fe_o/Fe_d ratio.

Selective dissolution data for the synthesized precipitates also show a distinct effect due to sulfate. Fe_d values are reduced by almost 10% when sulfate is present at the time of initial hydrolysis, which may indicate that sulfate and/or additional water is incorporated into the ferrihydrite structure. The water dialyzed materials also show a general increase in poorly crystallized (ammonium oxalate extractable) components with increase in sulfate concentration. In the sulfate-dialyzed precipitates, no trend is evident, but all Fe_o/Fe_d ratios are higher than when sulfate is absent. Even the 0.0% sulfate treatment with 0.1% SO_4 in the dialysis water had more ammonium oxalate extractable Fe than did that dialyzed with distilled water alone.

Table 3.2 Selective Dissolution Characteristics of the Natural and Synthetic Ferrihydrites

Hyrdolysis Treatment % Sulfate	Fe_o	Fe_d	Fe_o/Fe_d
	—— % ——		
	Water Dialysis		
0.0 (60° C)	39.4	55.6	0.71
0.0 (80° C)	32.1	57.6	0.56
0.025	36.7	47.7	0.77
0.05	34.3	47.2	0.72
0.1	38.8	44.9	0.86
0.15	40.2	46.4	0.87
0.2	42.0	46.1	0.91
	Sulfate Dialysis		
0.00*	44.5	54.8	0.81
0.025	36.0	46.3	0.78
0.05	40.3	46.2	0.87
0.1	38.5	46.3	0.83
0.15	38.5	46.3	0.83
0.2	38.4	46.2	0.83
	Natural Ferrihydrite**		
---	29.6	29.9	0.99

*Dialyzed against 0.1% SO_4 following initial hydrolysis.
**Na-Pyrophosphate-extractable iron (Fe_p) = 1.7%

Total sulfur contents of the laboratory snythates are given in Table 3.3. Substantial quantities of sulfate are apparently adsorbed and/or incorporated into the ferrihydrite structure when sulfate is present in either the hydrolysis or the wash solutions. Even though the sulfate dialysis procedure produced slightly higher total sulfur contents for all initial sulfate levels, the amount incorporated appears to be rather insensitive to the concentration of added sulfate or to the total contact time. This suggests that ferrihydrite can accomodate only a certain critical level of sulfate (3-4%) in its structure. The sulfur content of the natural precipitate is 2.96%, and is comparable to that of the precipitate obtained with the 0.15% sulfate, water dialysis treatment.

The amount of sulfate in the initial hydrolysis solution also influences the color of the resulting precipitate (Table 3.4). Precipitates obtained with no sulfate in the hydrolyzate are very red (10R 3/4). With additions of sulfate, the precipitates generally become yellower. The natural precipitate is slightly lighter in color than the precipitates produced in the 0.15% sulfate treatments. There is no consistent difference in the colors of precipitates with respect to dialysis treatment.

3.4.4 Infrared Analyses

The infrared characteristics of ferrihydrite are still being explored by various researchers. At present, a range in characteristic vibration frequencies have been reported for this mineral and are dependent, to some degree, on whether the material examined was naturally-occurring or synthetic. A composite of the vibration frequencies previously observed for ferrihydrite is given in Table 3.5. As none of the studies indicate influences due to the sulfate ion, information concerning OH and SO_4 vibration frequencies are given for selected sulfate compounds in Table 3.6. The amorphous $Fe(OH)SO_4$ material

Table 3.3 Total Sulfur Contents of Laboratory Synthates*

Hydrolysis Treatment % Sulfate	Water Dialysis	Sulfate Dialysis
	%	
0.0(60°C)	0.03	1.96**
0.0(80°C)	0.06	--
0.025	2.70	3.42
0.05	2.53	3.72
0.1	2.74	3.33
0.15	3.04	4.09
0.2	2.71	3.97

*Natural Ferrihydrite: 2.96% S
**Dialyzed against 0.1% SO_4 following initial hydrolysis

Table 3.4 Effect of Sulfate on the Color of Synthetic Ferrihydrites*

Treatment % Sulfate	Munsell Notation	Color
	Water Dialysis	
0.00	10R 3/4	Dusky red
0.025	2.5YR 2.5/4	Dark reddish brown
0.05	5YR 3/4	Dark reddish brown
0.10	2.5YR 3/6	Dark red
0.15	7.5YR 5/8	Strong brown
0.20	7YR 5/8	Strong brown
	Sulfate Dialysis	
0.00**	7.5YR 6/8	Reddish yellow
0.025	2.5YR 2/4	Dark reddish brown
0.05	5YR 3/4	Dark reddish brown
0.10	5YR 4/6	Yellowish red
0.15	7.5YR 5/8	Strong brown
0.20	5YR 5/8	Yellowish red

*Natural ferrihydrite is 7.5YR 6/8 (Reddish yellow).
**Dialyzed against 0.1% SO_4 following initial hydrolysis.

Table 3.5 IR Vibration Frequencies for Ferrihydrite

Vibration	Material	Frequency	Source
		(cm^{-1})	
OH stretching	Synthetic	3400	A
Carboxyl groups	Natural	1550; 1400	B
Si-O stretching	Natural	985-945	C
	Synthetic	930	C
δ OH bending	Synthetic	800	A
Fe-O	Natural	690	B

A) Russell (1979)
B) Schwertmann and Fischer (1973)
C) Carlson and Schwertmann (1981).

Table 3.6 IR Vibration Frequencies for Some Sulfate Compounds

Vibration	$KFe(SO_4)_2(OH)_6$	$NaFe(SO_4)_2(OH)_6$	Amorphous $Fe(OH)SO_4$	Adsorbed SO_4*
	cm^{-1}			
OH stretching	3385 A; 3383 B	3354 B	3458 A	
HOH deformation	1635 A		1632 A	
v_3 motion of SO_4	1181; 1080 A 1180; 1083 B	1184; 1094 B	1172; 1112; 1138; A	1215 or 1170; C 1050 or 1040
δ OH bending	1003 A; 1012 B	1025 B	1025; 1020 A	
v_1 motion of SO_4	1020 A 1003 B	1008 B	1058 A 1060 B	970 C
v_4 motion of SO_4	650; 626 A 628 B	629 B	650; 638 A	
$[Fe\text{-}O_6]$ oct	550; 505; A 469; 441		585; 538; 505; A 468; 410	
translational OH	509; 474; 252 B	510; 478; 257 B	544; 345 B	
v_2 motion of SO_4	446 B	445 B		
translation of SO_4	336, 320 B	346; 331 B		

A) Powers et al. (1975); B) Shokarev et al. (1972); C) Harrison and Berkheiser (1982).
*Adsorbent was reported to be "amorphous" iron oxide

listed in Table 3.6 is a synthate produced by heating a 20% aqueous solution of $Fe_2(SO_4)_3$ for 6 hr at 180° C in a sealed glass ampoule within a steel bomb (Shokarev et al., 1972). IR spectra for the natural ferrihydrite and water-dialyzed synthates examined in this study are given in Figure 3.3. Spectra from the sulfate-dialyzed synthates are comparable and, hence, are not shown.

The 0.0% sulfate, water dialyzed precipitate shows the simplest IR spectrum. Stretching of structural OH groups is indicated by a broad band near 3400 cm^{-1} that is followed by two small resonance features betwen 2850 and 2950 cm^{-1}. Schwertmann and Fischer (1973) attributed similar bands in natural ferrihydrite to organic compounds (CH groups). In this case, organic compounds are not present and the two lines are unassigned. A very distinct absorption band is observed at 1015 cm^{-1} and is attributed to δ OH bending vibrations. A complex absorption band between 730 and 470 cm^{-1} is probably the result of both translational OH and $[FeO_6]$ octahedral vibrations.

Additions of sulfate alter this spectrum considerably. First, the OH-stretching band becomes broader and more intense and shifts to a slightly lower frequency (3200 cm^{-1}). Vibrational modes for sulfate also become apparent in both the 0.1% and 0.2% sulfate precipitates. A composite band centered at approximately 1150 cm^{-1} probably consists of separate bands at 1210, 1180, and 1110 cm^{-1} that have been assigned for the v_3 motion of SO_4 (Table 3.6) in studies of amorphous $Fe(OH)SO_4$ (Shokarev et al., 1972) and surface adsorbed SO_4 (Harrison and Berkheiser, 1982). The absorption band at 970 cm^{-1} is assigned to δ OH (bending) vibrations, as is the broad band in the region of 800 cm^{-1}. Absorption bands at 640 and 610 cm^{-1} may correspond to v_4 motion of SO_4. Absorption bands at 490, 470 and 410 cm^{-1} correspond best with $[FeO_6]$ octahedral vibrations reported by Shokarev et al. (1972).

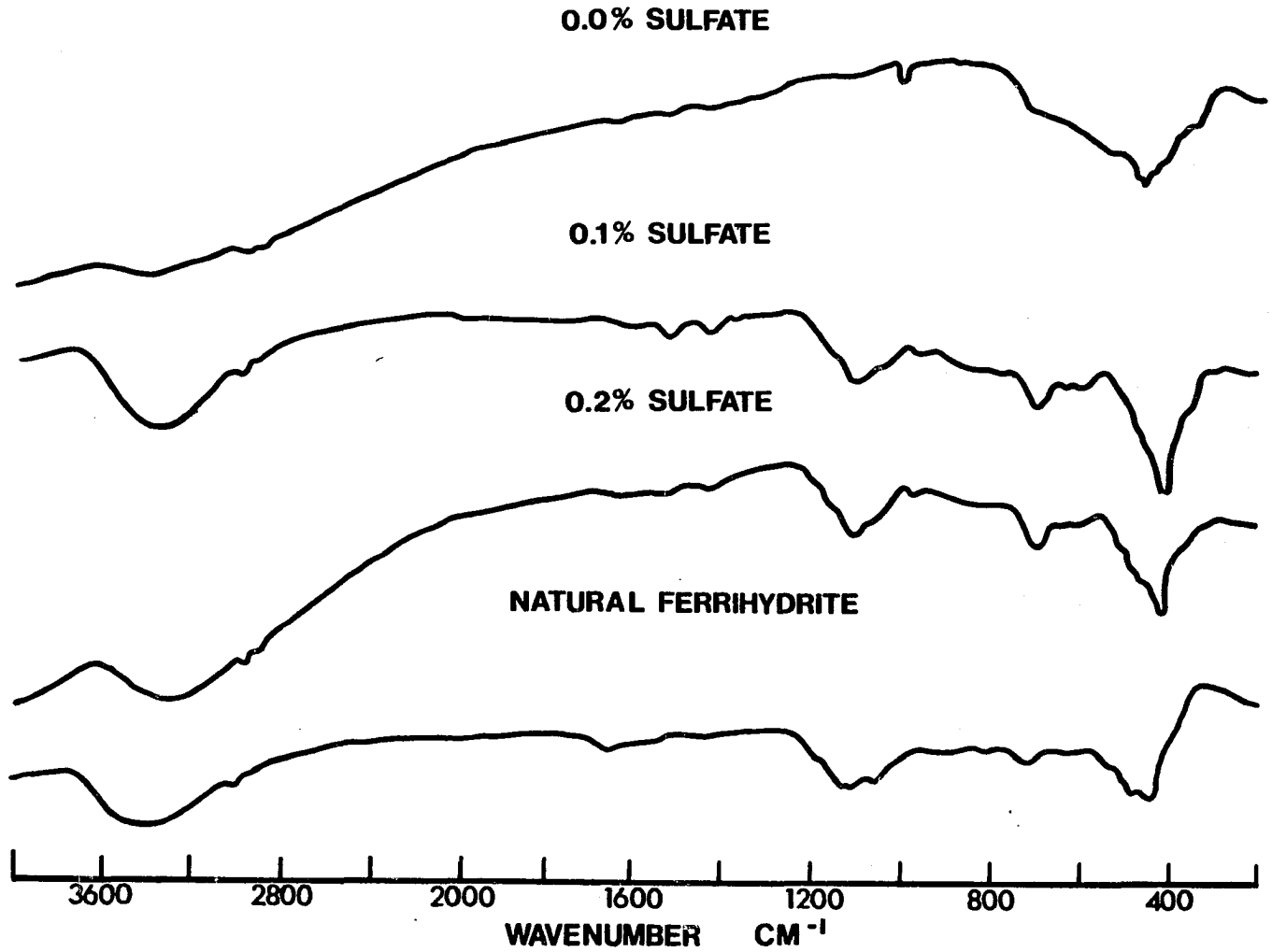

Figure 3.3 IR spectra of selected water dialyzed laboratory synthates and natural ferrihydrite.

One of the more noticeable differences between the ferrihydrite with no sulfate, and those synthesized and/or dialyzed in the presence of sulfate is an apparent shift in the [FeO_6] octahedral absorption bands to slightly lower wavenumbers. This shift indicates that sulfate may interfere with Fe-O bonding and is consistent with data given in Table 3.2 which shows an increase in oxalate extractable Fe and, hence, a decrease in the crystallinity of water-dialyzed samples with increases in sulfate content.

Another absorbance band shift, as yet unassigned, occurs at 730 cm^{-1}. The spectrum from the 0.0% sulfate ferrihydrite shows weak absorption at 730 cm^{-1} which appears as a shoulder on the 470 cm^{-1} absorption band maximum. Upon addition of sulfate, the 730 cm^{-1} band becomes more pronounced and migrates to 700 cm^{-1}. This lower energy of vibration may also be associated with decreases in the crystallinity of ferrihydrite. Infrared vibration frequencies observed in this study for synthetic ferrihydrites are summarized in Table 3.7.

The IR spectrum for natural ferrihydrite is quite similar to those obtained from the sulfate-enriched synthates. A structural OH component is indicated by a pronounced band at 3400 cm^{-1}, and OH deformation of water is suggested by a weak band at 1635 cm^{-1}. There are also weak absorption bands at 1515 and 1425 cm^{-1}, which may be due to organic components. Some δOH bending is indicated by absorption at $\sim$800 cm^{-1}. The v_3 motions of SO_4 are assigned to absorption bands at 1210, 1130 and 1040 cm^{-1}. This assignment is based on the location of v_3 vibrations of SO_4 in other compounds, including the laboratory synthates (Tables 3.6 and 3.7). In the same manner, v_1 motion of SO_4 is assigned to the 1020 cm^{-1} adsorption band. This spectrum also shows a weak adsorption band at 985 cm^{-1} which is most likely due to Si-O stretching. A weak band is noted at 970 cm^{-1}, and may be due to OH bending. A pronounced, unassigned absorption

Table 3.7 Observed IR Vibration Frequencies for Synthetic Ferrihydrites

Vibration	Pure synthate	Sulfate Treated Synthates
	cm^{-1}	
OH stretching	3400	3400-3200
HOH deformation	1630	1630
v_3 motion of SO_4		1210 1180 1110
δ OH bending	970, 800	970, 800
v_1 motion of $SO_4^{=}$		640, 610
$[FeO_6]$ oct	470	490, 470, 410

band is again seen at 720 cm^{-1}. As noted previously, this band varied in placement with respect to sulfate content of the synthates. Other absorption bands in the 400 to 450 cm^{-1} region are considered to be vibrations within $[FeO_6]$ octahedra.

3.4.5 Thermal Analyses

Results from the DSC analyses are given in Figures 3.4, 3.5, and 3.6. The thermograms for natural ferrihydrite obtained under O_2, air, and nitrogen atmospheres (Figure 3.4) show only a broadened, endothermic peak centered at 150° C that is due to water loss. Pronounced shoulders at 100° C and 250° C suggest that water exists at varying levels of organization within the natural ferrihydrite structure. There is no indication of the sharp exothermic peak between 300 and 350° C that normally marks the thermal conversion of ferrihydrite to hematite (Carlson and Scwertmann, 1981).

The 300-350° C exothermic peak is quite evident in thermograms from the water-dialyzed synthetic materials analyzed under O_2 atmosphere (Figure 3.5); however, it occurs at a lower temperature ($\sim$ 250° C) than that normally reported in the literature. It is also followed by a series of three less intense exotherms that suggest a step-wise reorganization of the ferrihydrite structure. Thermograms from the same samples in air are similar, and are not shown here.

Under N_2 (Figure 3.6) the exothermic peak occurs at its normal position of 350° C in the pure (0.0% sulfate) synthate. However, in the sulfate-enriched samples, the peak is completely suppressed. Furthermore, the low temperature endotherm due to adsorbed and structural water is resolved into three distinct components.

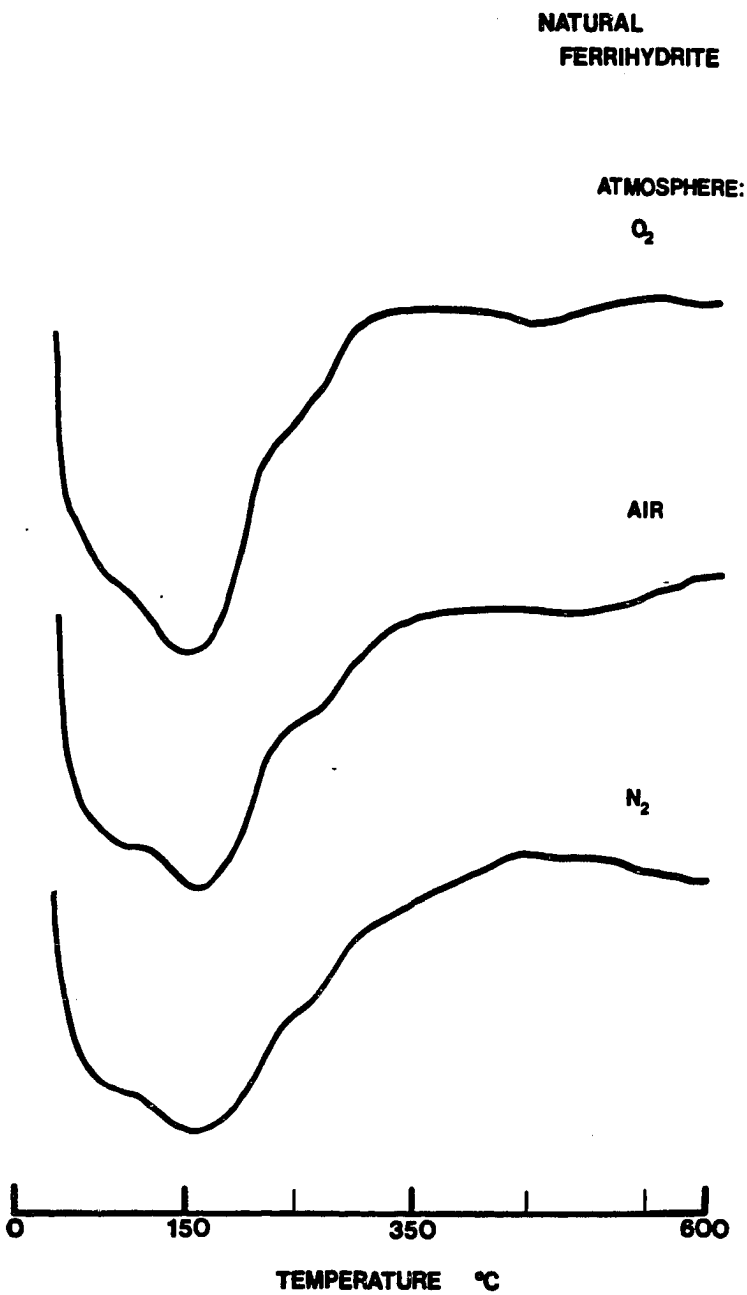

Figure 3.4 DSC spectra of natural ferrihydrite in O_2, air, and N_2 atmospheres.

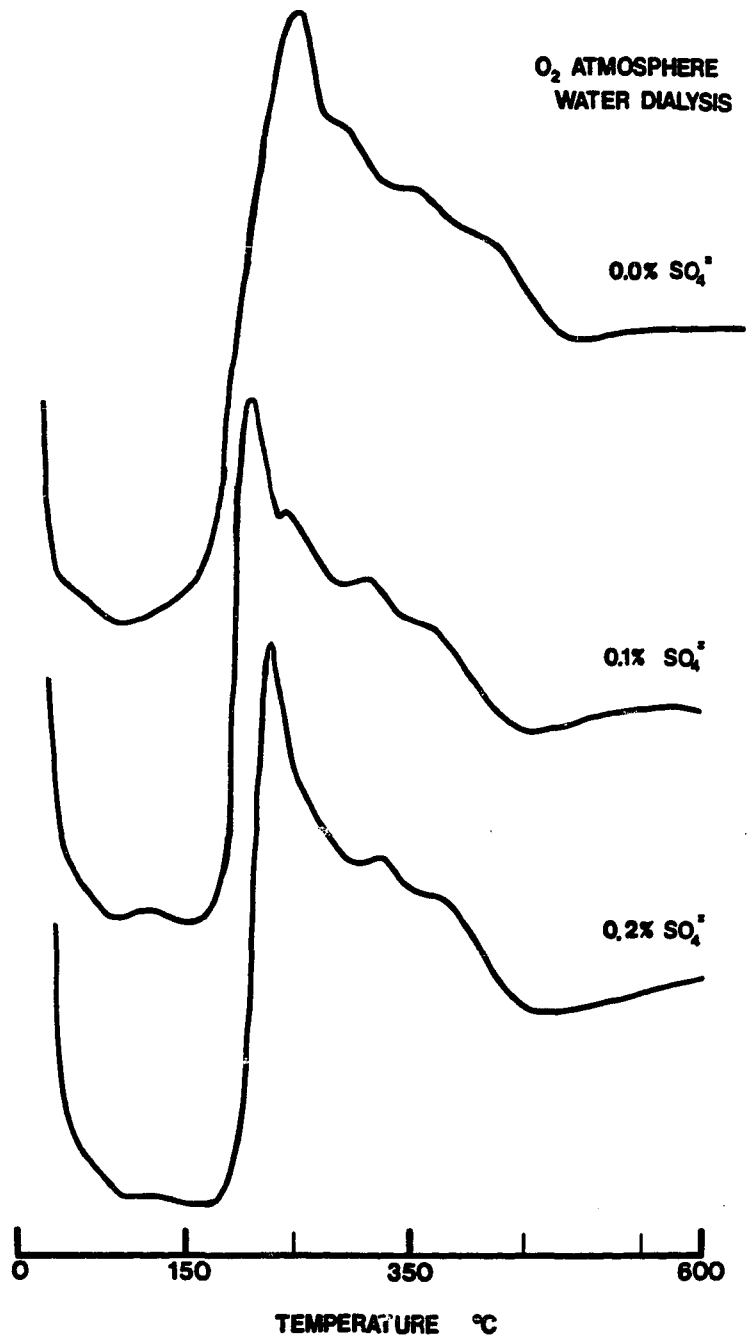

Figure 3.5 DSC spectra of selected water dialyzed laboratory synthates in O_2 atmosphere.

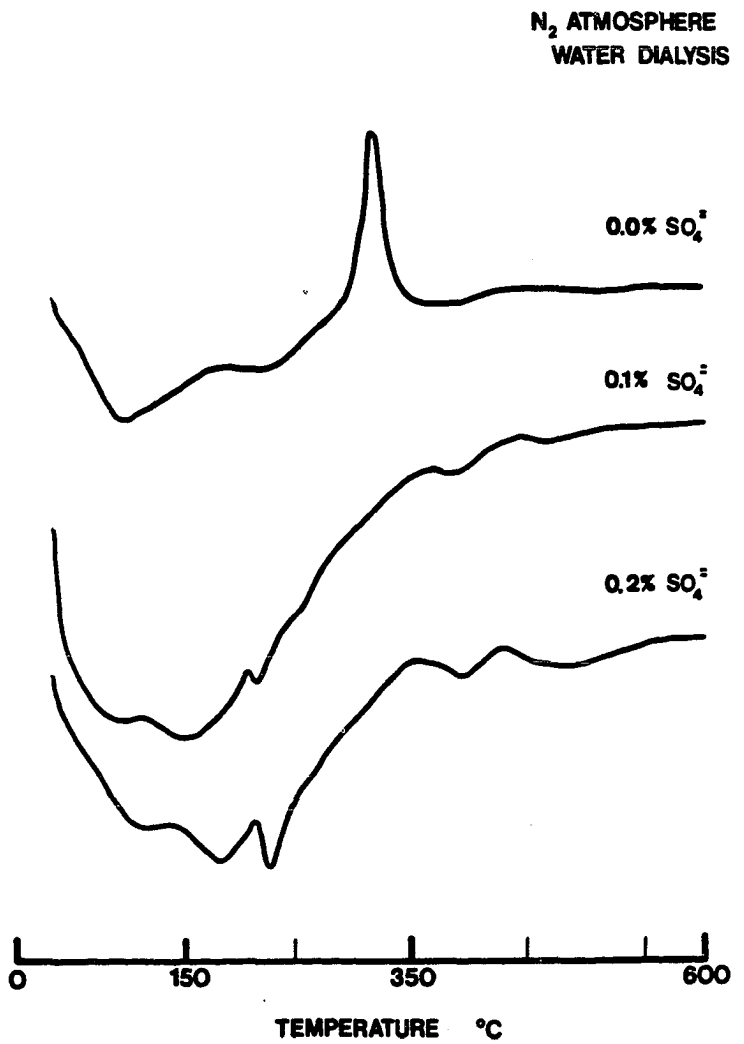

Figure 3.6 DSC spectra of selected water dialyzed laboratory synthates in N_2 atmosphere.

3.4.6 Surface Area Measurements

Results of surface area measurements by N_2 adsorption (BET) are given in Table 3.8 and Figure 3.7. For all treatments, the sulfate dialyzed precipitates have the highest surface areas, ranging from 81 to 310 m^2/g.

The surface areas of both sets of precipitates rise with sulfate treatment to the 0.1% level, and then decrease indicating, perhaps, a greater degree of particle contact and aggregation at the higher sulfate levels. The surface area of the natural ferrihydrite is 97 m^2/g and is similar to that achieved with the 0.15%, water-dialyzed synthate. Assuming a density of 2.8 g/cm^3 (Schwertmann and Fischer, 1973) surface areas shown in Table 3.8 indicate a mean particle diameter of 2-6 nm.

3.4.7 TEM Investigation

The morphology of the synthetic ferrihydrite appears to be dependent upon quantity of sulfate added to the solution at the time of hydrolysis. Figures 3.8-3.15 illustrate the range in morphology observed. The 0.0, 0.025, and 0.05% sulfate treatments produced extremely small particles of iron oxide that aggregate with drying; filaments of aggregated material (Figure 3.8) in some cases give way to more rounded and denser aggregates (Figures 3.12 and 3.13). Further hydrolysis of the ferrihydrite at an elevated temperature (80° C) does not appear to affect the morphological habit (Figure 3.14).

The 0.1% sulfate treatment (Figure 3.9) yielded samples with a mixed morphology which includes particles with a needle-like shape interspersed with the rounded aggregates. The dominant form of ferrihydrite produced in the 0.15 and 0.2% sulfate treatments (Figures 3.10 and 3.15) consists of larger, more electron dense aggregates with striking needle-like surface projections. The morphology of the natural ferrihydrite (Figure 3.11) is intermediate to that

Table 3.8 Surface Area Measurements of Natural and Synthetic Ferrihydrites

Treatment % Sulfate	Water Dialyzed	Sulfate Dialyzed
	m^2/g	
0.00	119	215*
0.025	159	217
0.05	183	228
0.10	232	310
0.15	99	172
0.20	49	82

Natural Ferrihydrite: 97 m^2/g

*Dialyzed against 0.1% sulfate following initial hydrolysis.

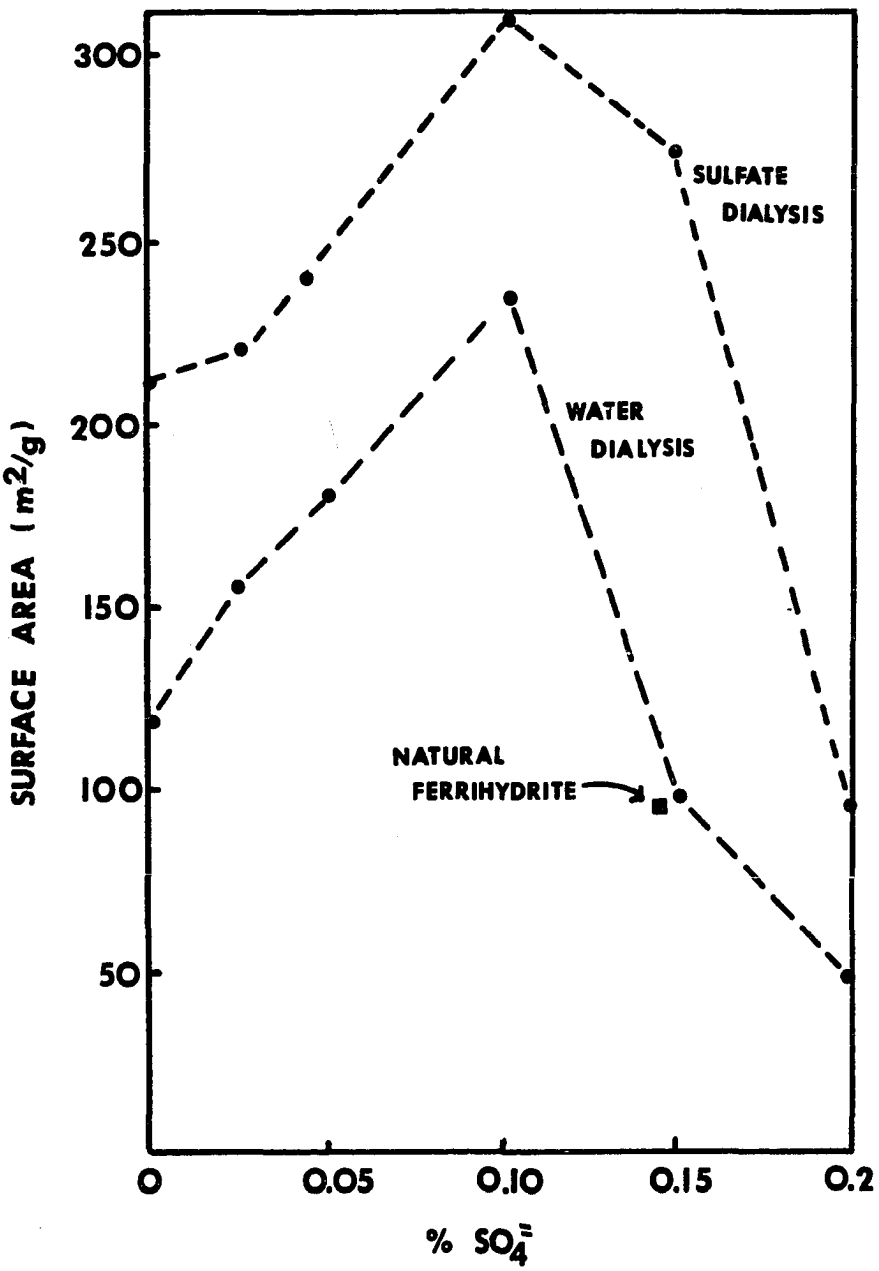

Figure 3.7 Surface areas of natural and synthetic ferrihydrites.

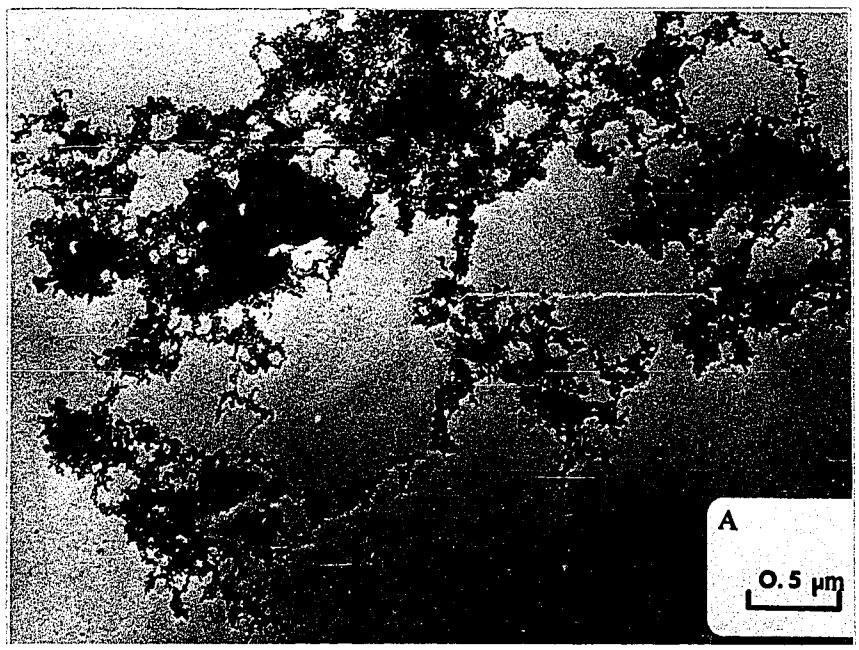

Figure 3.8 TEM micrograph of synthetic ferrihydrite: 0.0% sulfate treatment, water dialyzed.

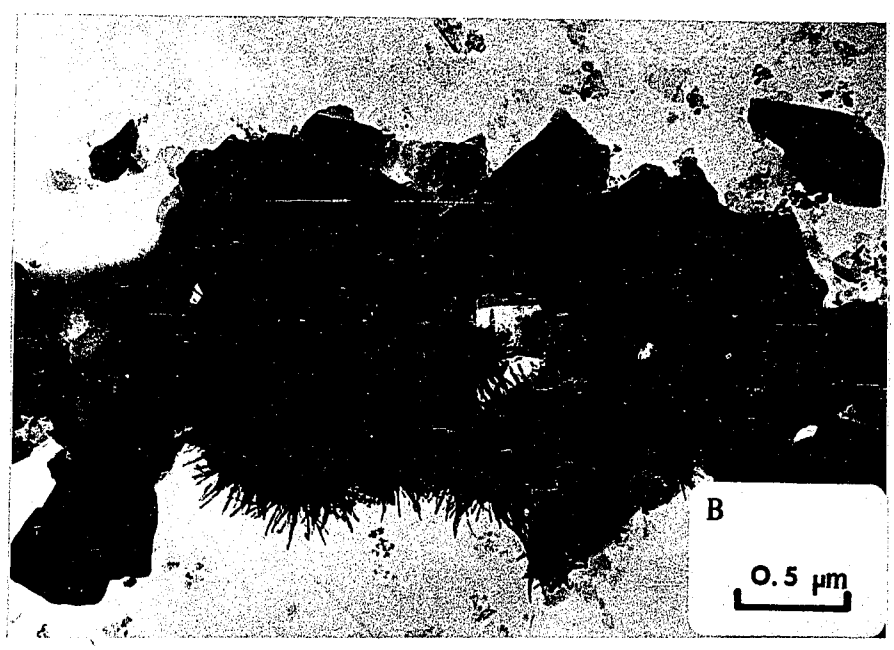

Figure 3.9 TEM micrograph of synthetic ferrihydrite: 0.1% sulfate treatment, water dialyzed.

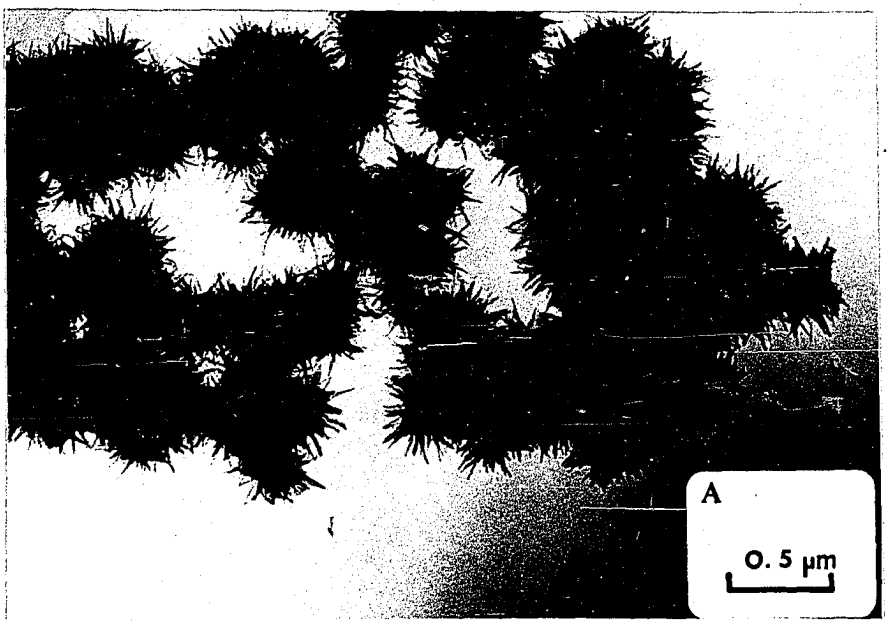

Figure 3.10 TEM micrograph of synthetic ferrihydrite: 0.2% sulfate treatment, water dialyzed.

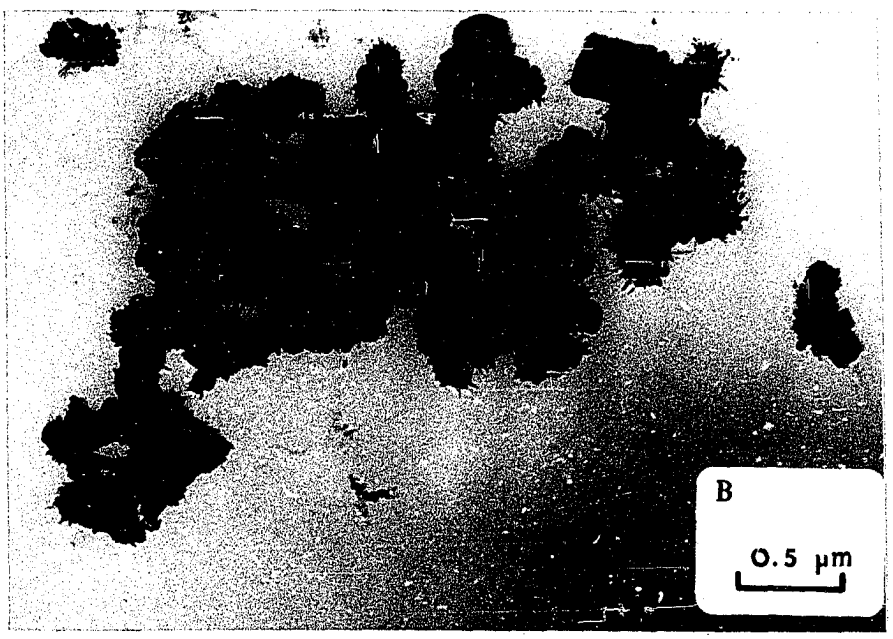

Figure 3.11 TEM micrograph of natural ferrihydrite.

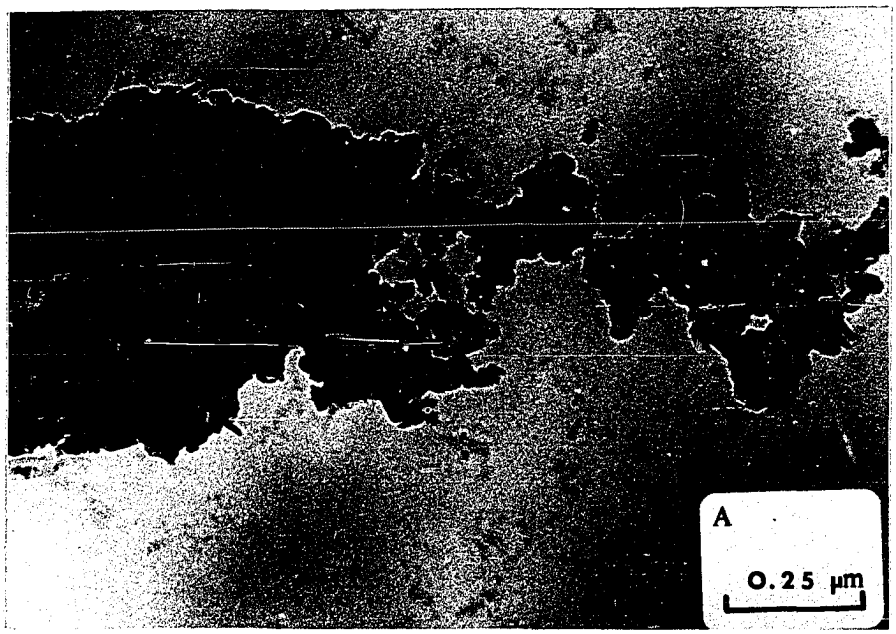

Figure 3.12 TEM micrograph of synthetic ferrihydrite showing globular aggregate nature of materials produced by 0.0% sulfate treatment.

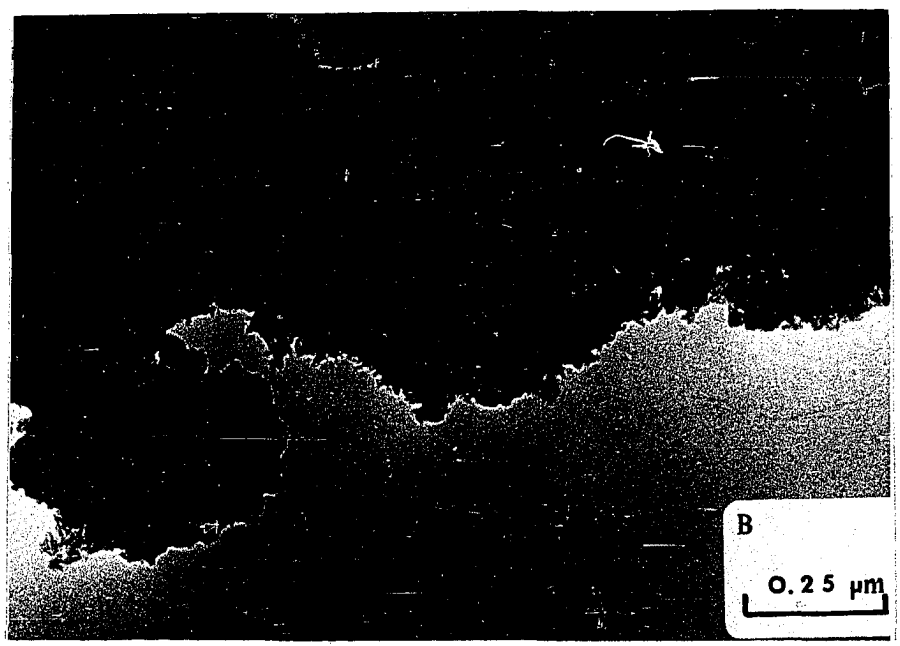

Figure 3.13 TEM micrograph of synthetic ferrihydrite showing the most dense aggregate nature materials produced by 0.0% sulfate treatment.

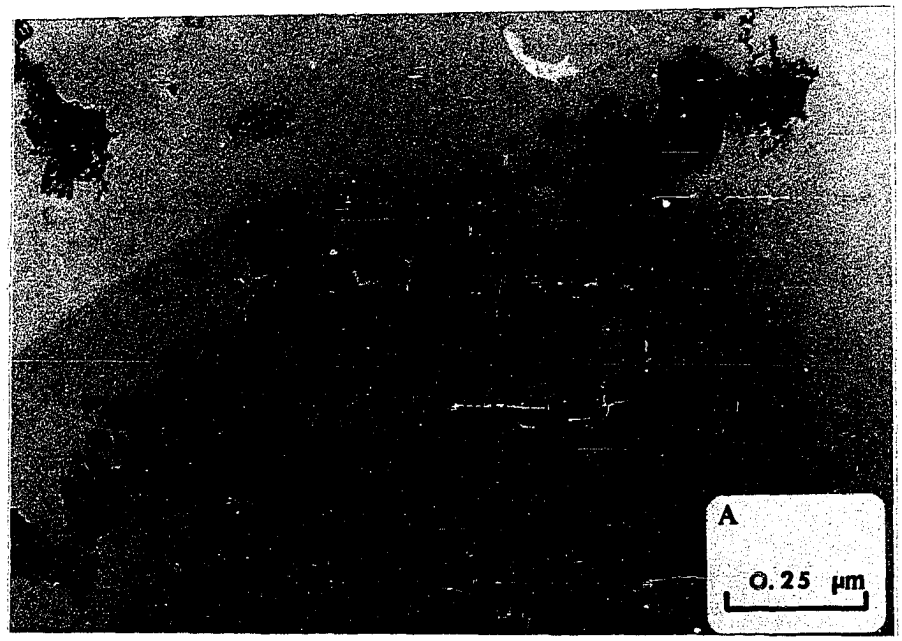

Figure 3.14 TEM micrograph of synthetic ferrihydrite: 0.0% sulfate, 80° C, water dialyzed sample showing filamentatious aggregation.

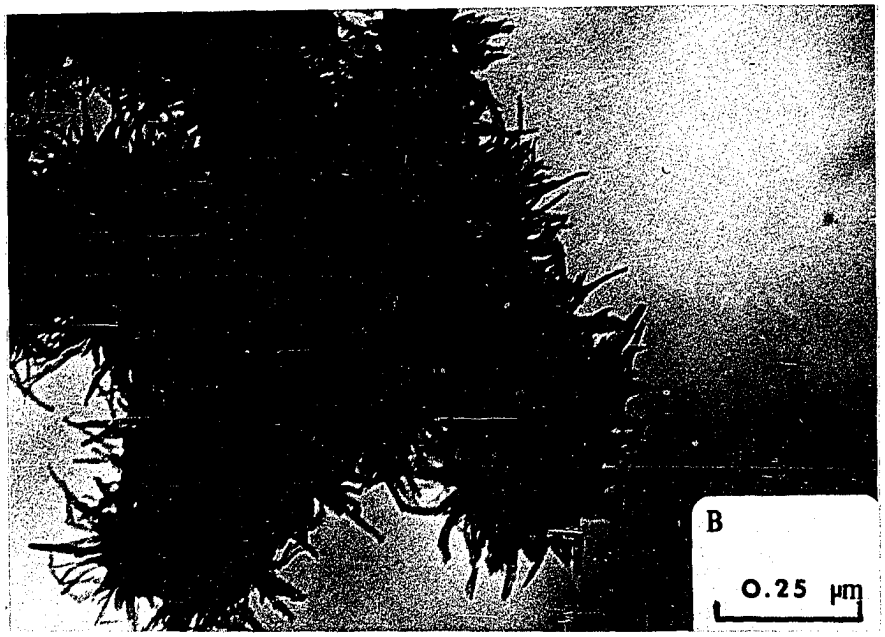

Figure 3.15 TEM micrograph of synthetic ferrihydrite: detail of finger-like projections from 0.2% sulfate treatment, water dialyzed.

produced in the 0.1 and 0.2% sulfate treatments. The natural precipitate consists of a mixture of globular and electron-dense aggregates with finger-like surface features. The electron-dense, finger-like features are less frequent in the natural ferrihydrite sample than in the 0.2% sulfate treatment.

3.4.8 Phosphate Adsorption Characteristics of the Natural Ferrihydrite

A phosphate adsorption isotherm was developed for the natural stream precipitate and is shown in Figure 3.8 in relation to isotherms obtained for bottom sediment clays from Black Fork Creek (Sec. 2.4.2). The concentrated precipitate is clearly the most highly adsorptive material of those studied in the watershed. Figure 3.8 shows how similar bottom sediment materials at site 6 are to the natural precipitate. This similarity supports previous findings (Chapter 2, section 2.4.2) that part of the colloidal precipitate can and does become incorporated into the bottom sediments, thereby increasing ammonium oxalate-soluble components and the overall surface reactivity of the sediments.

3.5 Summary and Conclusions

A comparison of the naturally occurring ferrihydrite resulting from precipitation in streams affected by acid coal mine drainage and synthetically prepared ferrihydrites precipitated in the presence of sulfate suggests many similarities with respect to crystallinity, color, surface area, and morphology. Based on increased rates of precipitation with increases in sulfate at the time of hydrolysis, it appears that this anion acts to neutralize positive surface charge and, thereby, increase aggregate stability. Sulfate clearly has a high affinity for the ferrihydrite surface. Once adsorbed, it tends to suppress ordering of the ferrihydrite, but it also inhibits transformations to more stable iron oxides, such as goethite and hematite.

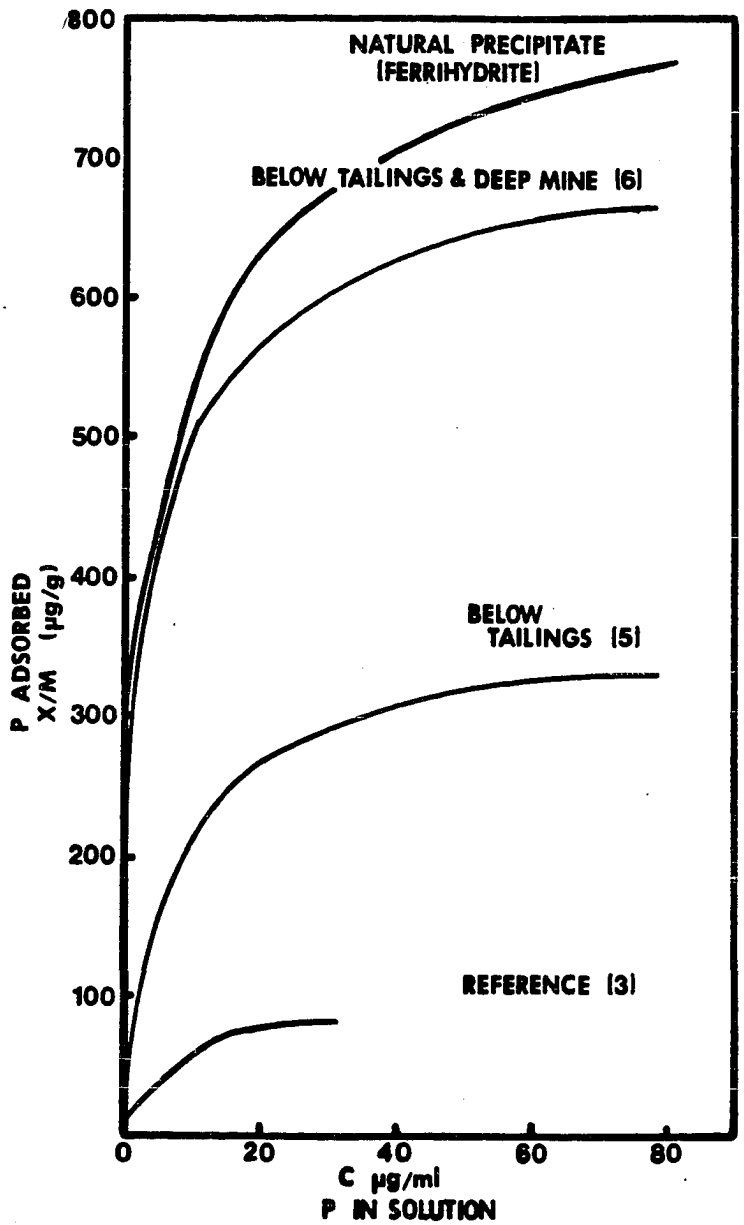

Figure 3.16 Phosphate adsorbtion isotherms obtained with the natural stream precipitate and associated bottom sediment clays from Black Fork Creek.

CHAPTER 4

IRON SPECIATION IN WATERS AFFECTED BY ACID COAL MINE DRAINAGE

4.1 Introduction

It was demonstrated in Chapter 3 that a poorly-crystallized iron oxide (ferrihydrite) had formed in surface waters affected by acid coal mine drainage and that dissolved sulfate influenced the precipitation rate and, perhaps, the stability of the hydrolysis product. The formation of iron oxides under ambient conditions implies the presence of elemental constituents in sufficient relative concentrations to favor both precipitation and crystal growth; however, questions remain concerning the solution chemistry of iron species encountered in acid mine waters and the mechanism(s) by which ferrihydrite is formed under prevailing pH and redox conditions. Consequently, the objectives of this study were: 1) to identify and quantify, insofar as possible, the dissolved iron species present in both acid discharge and the waters of receiving streams in the Black Fork Creek watershed; 2) to establish Eh-pH conditions for these same waters; 3) to determine the effect of sulfate on Fe solution chemistry; and 4) to evaluate possible mechanisms of ferrihydrite formation.

4.2 Literature Review

4.2.1 The Dissolved Species of Iron

The aqueous solution chemistry of iron is complex because it frequently exists in two different oxidation states and forms a variety of hydroxyl complexes in different pH regions. Concentrations of Fe(II) in natural waters can be conveniently determined by any of several colorimetric procedures

involving α, α' bipyridyl, 1, 10 phenanthroline, or related compounds (Heaney and Davison, 1977; APHA et al., 1980; Stucki and Anderson, 1981; and Shapiro, 1066). Further hydrolysis of Fe(II) to form $Fe(OH)^{+}$ and $Fe(OH)_2$ is not of great concern to this discussion because both $Fe(OH)^{+}$ and $Fe(OH)_2$ are favored in environments of high pH and low Eh.

On the other hand, Fe(III) and its hydrolysis to Fe-hydroxyl complexes in aqueous solution need to be considered in detail as the most favorable environment for precipitation of Fe(III) compounds. Hydrolysis of the Fe(III) ion in aqueous solution has been studied by many researchers. Much of the work has centered on the identification and quantitative determination of Fe(III) and its mono and divalent hydroxy cations, and on the measurement of hydrolysis constants.

The hydrolysis of Fe(III) at low to moderate pH's is generally described by the following step-wise reactions:

(4.1) $Fe^{+3} + (H_2O)_6 \longrightarrow [Fe(H_2O)_5OH]^{+2} + H^{+}$ (K_{H1})

(4.2) $[Fe(H_2O)_5OH]^{+2} + H_2O \longrightarrow [Fe(H_2O)_4(OH)_2]^{+} + H^{+}$ (K_{H2})

(4.3) $[Fe(H_2O)_4(OH)_2]^{+} + H_2O \longrightarrow [Fe(H_2O)_3(OH)_3] + H^{+}$ (K_{H3})

The existence of a dimer has also been confirmed at high ionic strengths where total Fe(III) concentrations are in excess of 10^{-3} molar (Milburn and Vosburgh, 1955). Thus, the reaction:

(4.4) $2[Fe(H_2O)_5OH]^{+2} \longrightarrow [Fe_2(H_2O)_{10}(OH)_2]^{+4}$ (K_{H11})

Although the hydrolysis species are aquo-coordinated, as indicated in equations 4.1-4.4, the coordination of the Fe(III)-species with water is not indicated in later discussions for the sake of simplicity.

An activity diagram for aqueous Fe(II) species is given in Figure 4.1. This diagram allows for the estimation of the dominant Fe(III) species in solution as a function of Fe(III) concentration and pH. Activity diagrams such as this are common in the chemistry, geochemistry, and soil science literature (Lindsay, 1979; Garrels and Christ, 1965).

Until recently, individual concentrations of Fe^{+3}, $Fe(OH)^{+2}$ and $Fe(OH)_2^+$ in a system could only be estimated through calculations based on equilibrium constants, measured pH, and known base additions for a known initial Fe^{+3} concentration. This approach assumed the presence of these species in solution. However, as a result of hydrolysis studies by such researchers as Siddall and Vosburgh (1951), Millburn and Vosburgh (1955), and Millburn (1957), the existence of these species has been confirmed. Further studies have employed UV-spectroscopic analyses for the detection of particular Fe(III)-species, often in hetrogeneous solutions. Knight and Silva (1975), for example, have assigned UV-band maxima for Fe^{+3}, $Fe(OH)^{+2}$, $Fe(OH)_2^+$, and the dimer $Fe_2(OH)_2^{+4}$ in their laboratory study of hydrolysis constants. Brown and Kester (1980) reported slightly different band maxima than Knight and Silva (1975) for Fe^{+3} in a rigidly controlled experiment which produced Fe^{+3} as the predominant ion present. Johnson et al. (1979), identified band maxima for $Fe(OH)^{+2}$, $Fe(SO_4)^+$, and $Fe(SO_4)_2^-$ in their study of monomers in solutions resulting from acid mine drainage. Recognized UV-band maxima for both Fe(III)-hydroxy and Fe(III)-sulfate complexes are summarized in Table 4.1. An obvious problem arises in that some band maxima are very similar in wavelength.

Conventional colorimetric determinations of total dissolved Fe(III) probably include all the soluble hydrolysis products and are generally obtained by difference from measurements of total Fe and dissolved Fe(II) (APHA et al.,

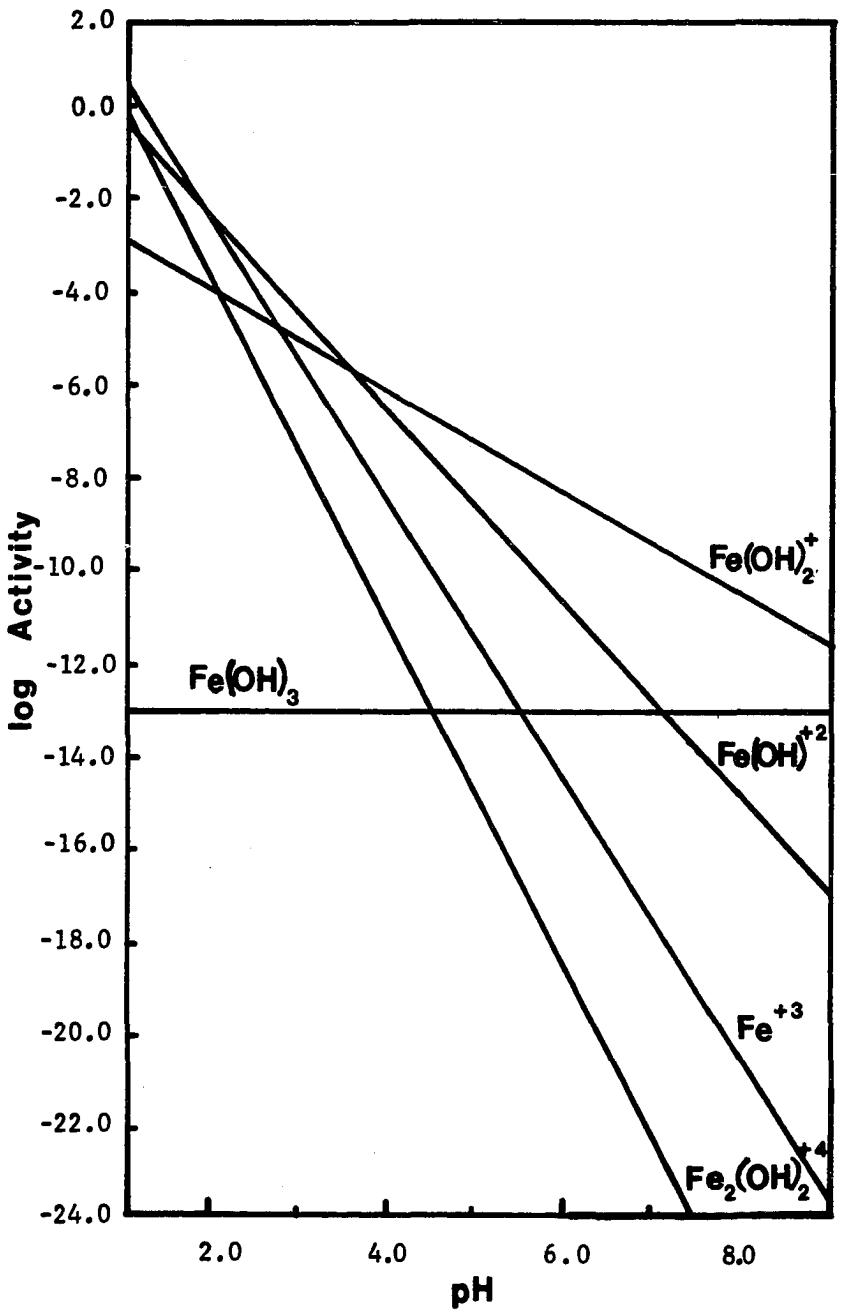

Figure 4.1 The hydrolysis of monomeric Fe(III)-species. After Lindsay (1979).

Table 4.1 Characteristic UV-Band Maxima for Fe(III)-hydroxy and Fe(III)-sulfate Complexes in Water

Species	Maxima (nm)	Source *
Fe^{+3}	240; 195 and 245	A; B
$Fe(OH)^{+2}$	205 and 297; 212 and 300	A; C
$Fe(OH)_2^{+}$	300	A
$Fe_2(OH)_2^{+4}$	240, 335	A
$Fe(SO_4)^{+}$	225, 300	C
$Fe(SO_4)^{-}$	225, 300	C

* A) Knight and Silva (1975); B) Brown and Kester (1980); and C) Johnson et al. (1979)

1980; Stucki, 1981; Stucki and Anderson, 1981). In addition, there is a concern that total Fe(III) concentrations determined colorimetrically may also include polymers of slightly higher molecular weight. A study by Hsu and Ragone (1972) has shown that colloids can interfere with the complexation of Fe^{+3} by SCN, but instant color development of a solution when complexed with SCN indicates the absence of colloidal species. They further recommend the calculation of the Fe^{+3} species concentration from total Fe(III) based on a model proposed by Lamb and Jacques (1938):

$$(4.5)\quad [\text{Fe(III) total}] = [Fe^{+3}] + \frac{k_1[Fe^{+3}]}{[H^+]} + \frac{k_1k_2[Fe^{+3}]}{[H^+]^2} + \frac{k_1k_2k_3[Fe^{+3}]}{[H^+]^3}$$

where k_1, k_2 and k_3 are hydrolysis constants for step-wise hydrolysis.

4.2.2 Eh-pH Stability Diagrams of the Fe(II) and Fe(III) Systems

The chemistry of iron in aqueous systems is not merely a function of pH and the concentration of iron present. It is further complicated by oxidation-reduction.

In considering the Eh-pH interactions encountered in natural, aqueous environments, the most fundamental relation of interest is the stability of water. Strong oxidizing agents may oxidize water to O_2, and strong reducing agents may reduce it to H_2. Figure 4.2, taken from Baas-Becking et al. (1960), shows the Eh-pH region in which water is thermodynamically stable compared to O_2 (g) and H_2 (g). This diagram indicates that Eh values for systems in equilibrium with water and the atmosphere must be within a finite range (Eh = -0.85 to +1.25 v). Baas-Becking et al. (1960) also conducted a thorough survey of the Eh and pH in

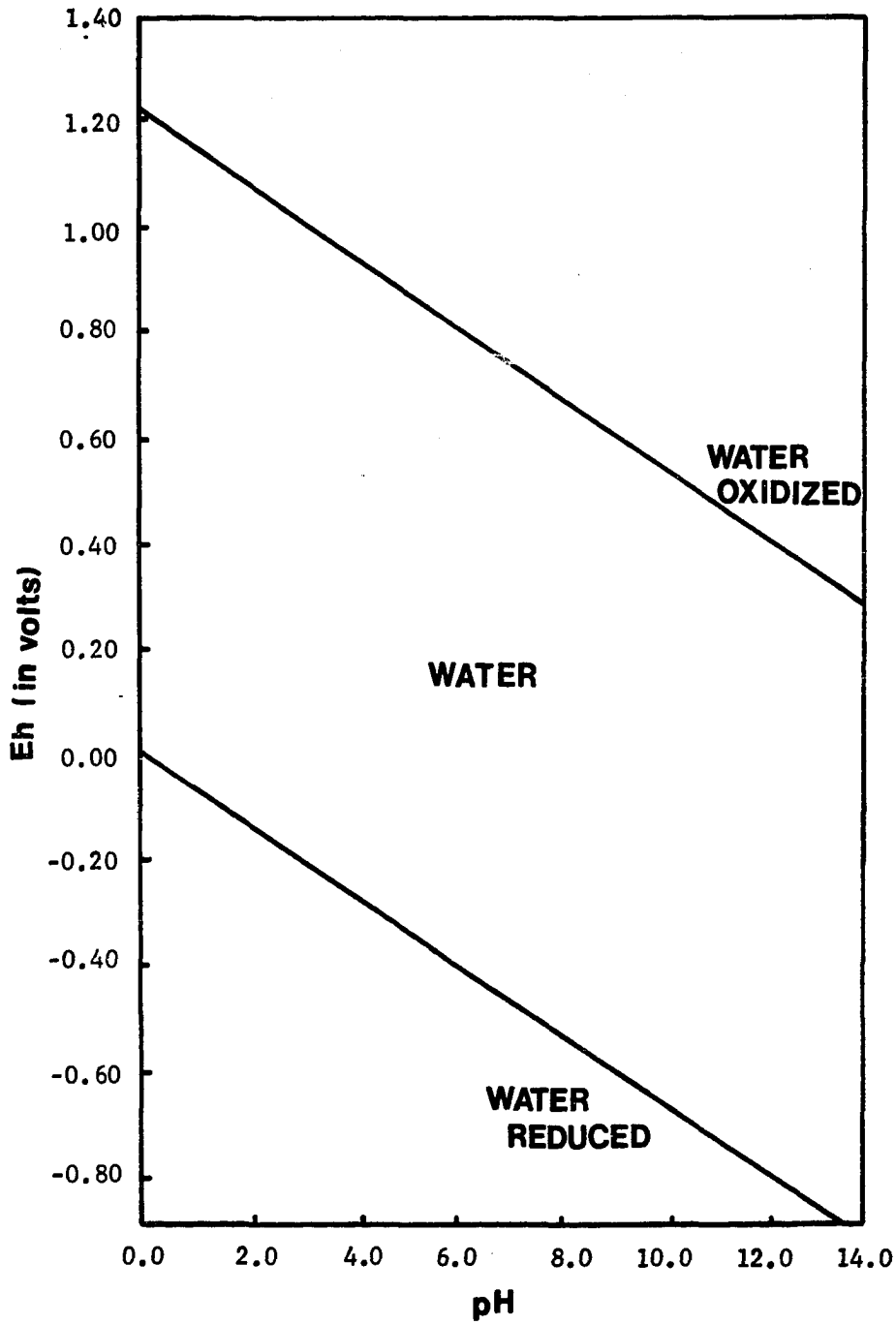

Figure 4.2 Stability field diagram for water. After Baas-Becking et al. (1960).

many natural environments, and found that the majority of these environments, including acid mine water, actually fall within the more restricted boundaries shown in Figure 4.3.

The theoretical Eh-pH limits of Fe(II) and Fe(III) species in aqueous systems are shown in Figure 4.4. This diagram, as with that of water, is a plot of pH against Eh in which regions are delineated by thermodynamic computations to show the conditions under which certain ionic species of Fe will be predominant. The fundamental relationship which determines the line dividing oxidized and reduced species is the Nernst oxidation-reduction equation. The diagram is taken from Hem and Cropper (1959), and is very similar to that given in Garrels and Christ (1965).

Although the initial Eh and pH values for groundwaters could easily fall within the Fe(II) stability field, the reduced system would not ordinarily be stable under subaerial conditions. Hem and Cropper (1959) state that water exposed to air should normally have an Eh of about +0.5 volts. Consequently, oxidized iron species should be favored at neutral to mildly alkaline pH's. In acid mine drainage, Fe(II) would seemingly be favored except under highly oxidizing conditons; however, bacteria such as T. ferrooxidans can obtain energy from the oxidation of ferrous iron, and it is possible that the Fe(II)→ Fe(III) reaction would be much faster under these conditions (Lundgren et al., 1972).

The rate of oxidation is not the only factor influencing the dissolved iron system in acid mine drainage. High concentrations of sulfate (4,500-16,500 µg/ml are reported in extreme cases (Johnson et al., 1979) associated with acid mine drainage, and the sulfate ion could further alter Eh-pH stability relationships of the iron system.

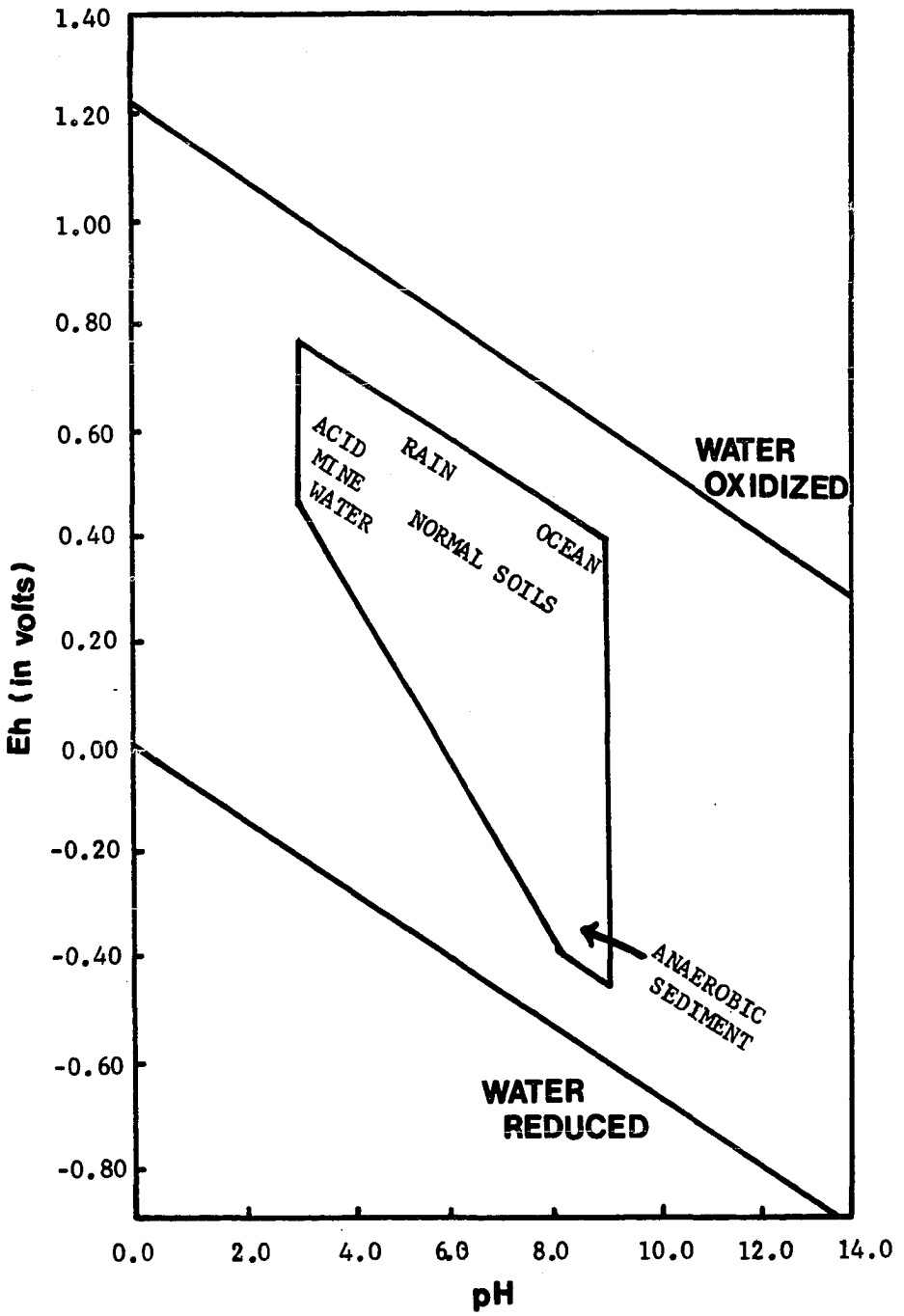

Figure 4.3 Theoretical limits of the Eh-pH relationship found in the natural environment. After Baas-Becking et al. (1960) and Barnum (1982).

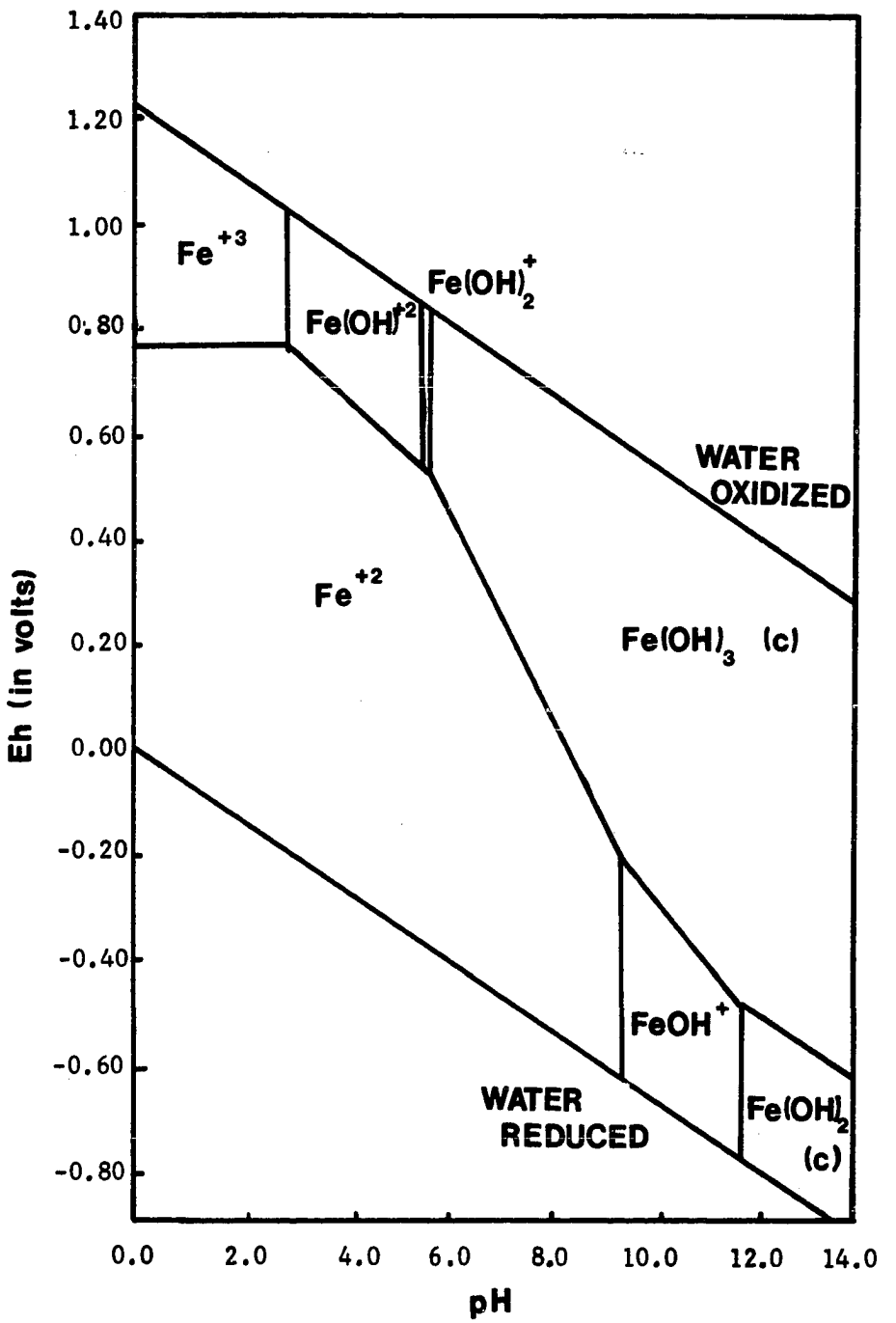

Figure 4.4 Stability field diagram for the aqueous Fe(II) and Fe(III) system. After Garrels and Christ (1965).

4.2.3 The Influence of Sulfur on Eh-pH Relationships of the Aqueous Fe System

The use of Eh-pH diagrams to evaluate reactions involving sulfur has been criticized because oxidation or reduction of sulfur through chemical agents alone is very slow. However, as stated in the previous section, evidence for the microbiological catalysis of oxidation-reduction reactions in the sulfur system is great. Any of five principal forms of sulfur may occur in natural waters (Hem, 1960). These include undissociated H_2S at low Eh and low to neutral pH; HSO_4^- at low pH (<2) and high Eh; and HS^- at neutral to high pH and low Eh (Figure 4.5). By far the most prevalent sulfur species in the usual pH ranges of natural water, including that reported for acid mine drainage, is $SO_4^=$. Free sulfur is also thermodynamically possible as a stable intermediary product. However its existence is hypothetical, and it is questionable whether S° can or will exist in the presence of other sulfur species due to microbial action. The zone occupied by S° on the Eh-pH diagram more likely can be accepted as a zone of instability for other sulfur species.

A relationship between dissolved sulfur, dissolved iron, and solid phase iron sulfides/hydroxides present in a system can also be described by an Eh-pH diagram. Figure 4.6, taken from Hem (1960), is representative of these relationships under the following limitations: the activity of dissolved iron was assigned at 0.01 µg/ml, or 10^{-7} molal, which is the lower limit of detection by routine analysis. Total sulfur activity was also limited, in this case to 0.3 µg/ml or 10^{-5} molal, near the limit of detection for H_2S. The implications of these concentrations are important when applying the diagram to the situation of acid mine drainage. For example, increases in total iron or sulfate concentrations will increase the stability fields for solid phase $Fe(OH)_3$ or $Fe(OH)_2$ and limit the

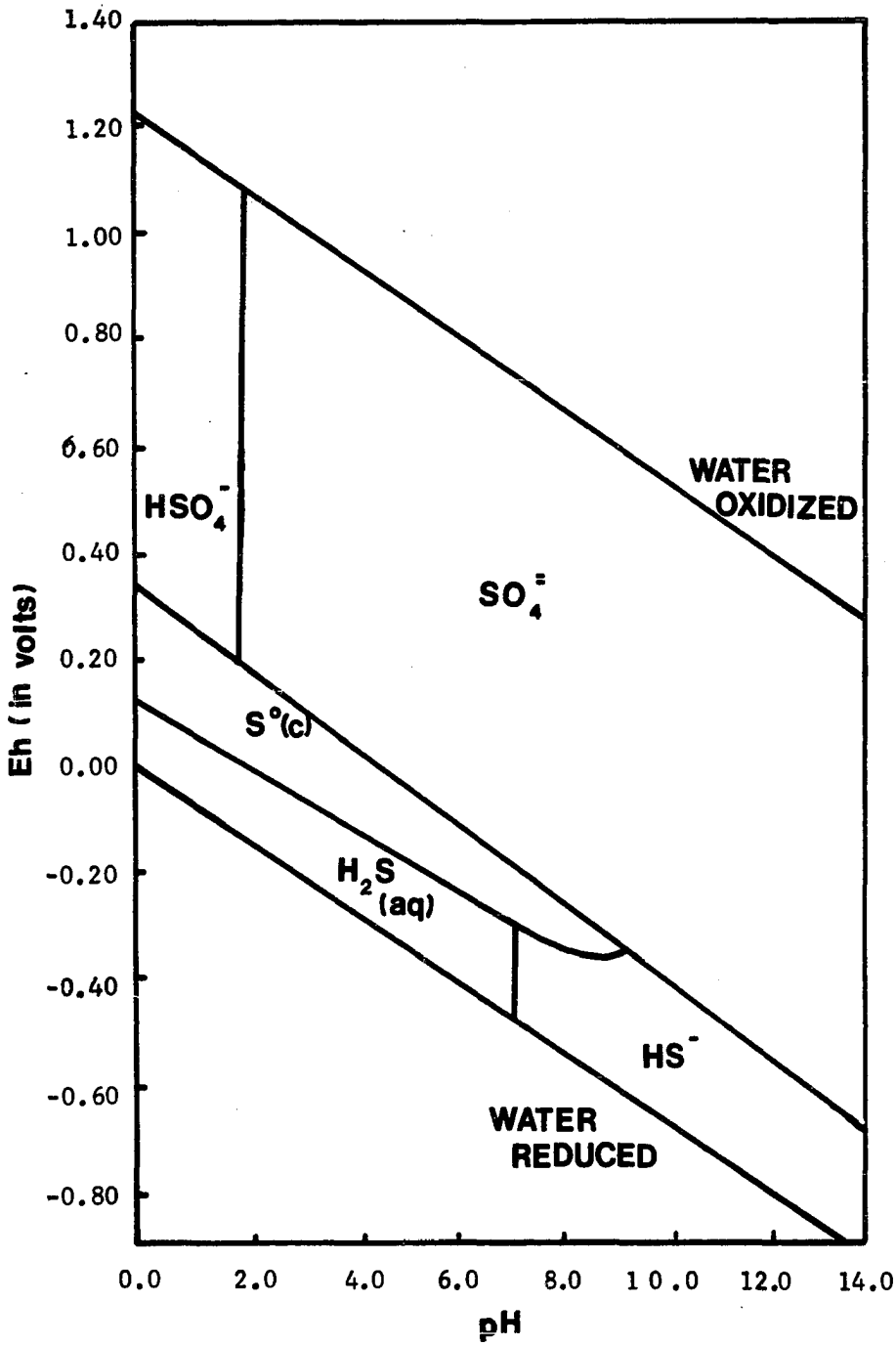

Figure 4.5 Stability fields of sulfur species. After Garrels and Christ (1965).

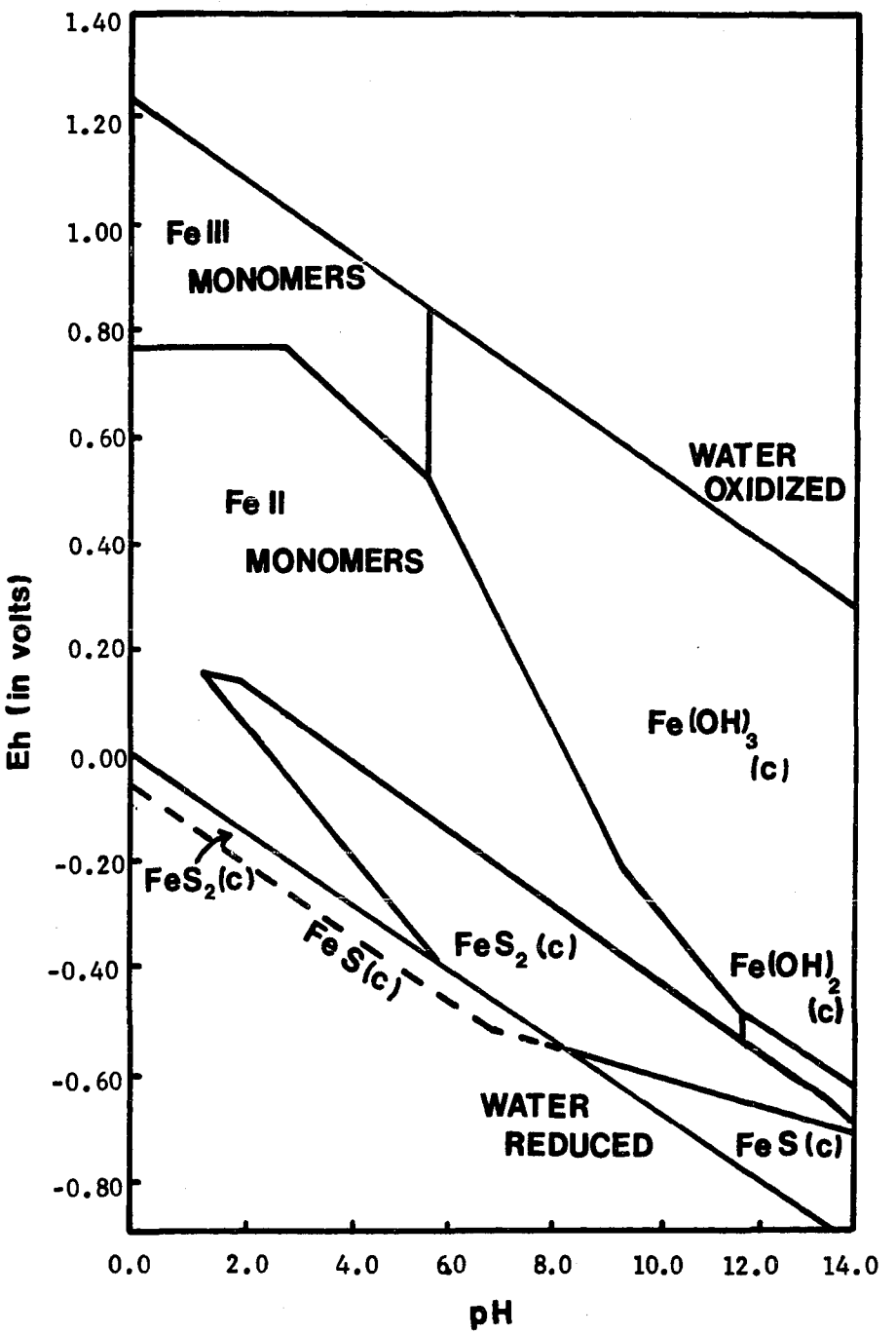

Figure 4.6 Stability fields for iron in the presence of sulfur. After Hem (1960).

activity of Fe(II) or Fe(III) ionic species. Figure 4.7, also taken from Hem (1960), demonstrates the increased stability field of solid phase iron compounds when activity of iron is increased from 0.01 μg/ml to 100 μg/ml, under the influence of 100 μg/ml sulfur.

Stability diagrams such as these can be used to predict the presence of ion species based on measured Eh and pH for a particular system. It can also be used to confirm the tendency for precipitation within a system. However, while the Eh-pH relationship can predict precipitation, it does not help to describe a mechanism for that precipitation, and it frequently does not account for environmental conditions or kinetic factors that ultimately determine the formation of various solid-phase compounds.

4.2.4 Precipitation, Polymer Growth, and Crystallization

Excluding solution pathways and OH/Fe ratios which do not yield ferric hydroxide species, synthesis studies show that, upon aging $Fe(OH)_3$ (assumed to be ferrihydrite) at low pH and with slow dehydration, a number of compounds may be produced depending on solution conditions. For example, Arden (1951) found that αFeOOH (goethite) was produced in sulfate systems. However, another synthesis study indicated that hematite (α Fe_2O_3) was the resulting end product in the presence of sulfate (Dousma et al., 1979). Other studies in chloride and nitrate systems suggest that the resulting precipitate is goethite (Dousma et al., 1979). Likewise, a study by Matijevic and Scheiner (1978) indicates that different Fe-oxide minerals were produced from acid solutions containing nitrate, perchlorate, or chloride ions. The solutions with chloride produced either akaganeite (β-FeOOH) or hematite depending on the concentration of Fe and/or Cl ions. The solutions containing nitrate or perchlorate ions consistently yielded hematite. Knight and Silva (1974) found

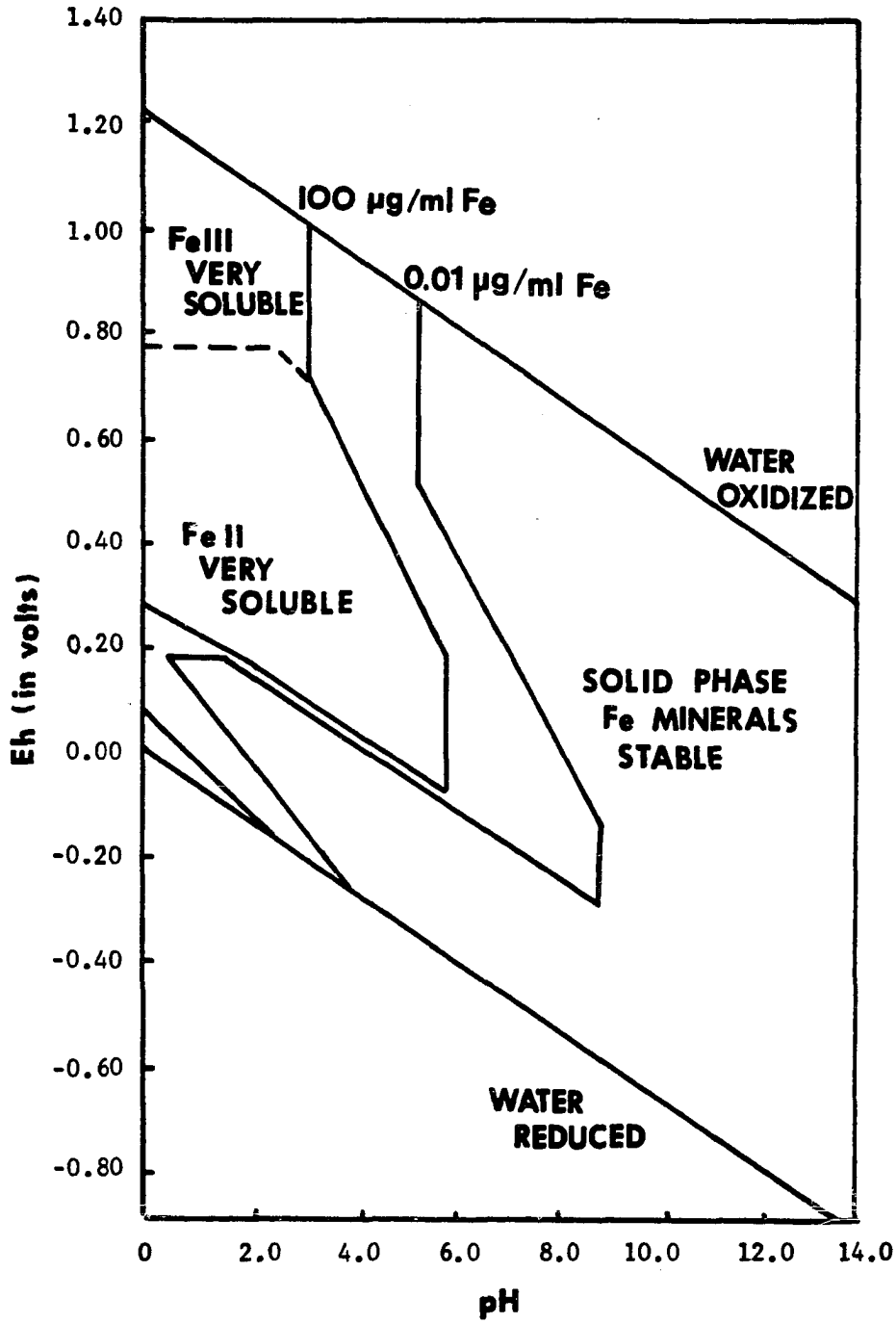

Figure 4.7 Activity of dissolved iron related to Eh and pH in the presence of dissolved sulfur species. After Hem (1960).

that the type of precipitate resulting from perchlorate solutions also depends greatly on the amount of base added. Low amounts of base added resulted in lepidocrocite and akaganeite. At high base additions, the perchlorate solutions resulted in goethite.

Most of these studies were conducted at elevated temperatures and were primarily concerned with identifying an end product of crystallization. The Na-jarosite and ferrihydrite observed in this acid mine drainage study (Chapter 3) are probably not end products. The synthesis study discussed in Chapter 3 indicates that Na-jarosite is a precursor to ferrihydrite, and that ferrihydrite is itself, though persistent in acid mine drainage, probably an intermediate product which ultimately will alter to goethite or hematite even at temperatures approximating those found in natural environments.

Most laboratory synthesis studies also do not investigate relationships between the hydrolysis products in solution and the mechanism by which solid phases are produced. Lamb and Jacques (1938) suggest a mechanism of continuing $Fe(OH)_3$ monomeric aggregation. They indicate that, while initial hydrolysis of Fe^{+3} produces monomeric $Fe(OH)^{+2}$, $Fe(OH)_2^{+}$ and $Fe(OH)_3$, continued hydrolysis produces precipitate growth by condensation of $Fe(OH)_3$ on initial $Fe(OH)_3$ nuclei. As long as $Fe(OH)_3$ continues to condense on $Fe(OH)_3$ nuclei, the monomeric species continue to form, lowering pH. Upon aging, the $Fe(OH)_3$ dehydrates to form FeOOH species.

Hsu and Ragone (1972) favor this mechanism, but claim that the initial number of nuclei relative to the concentration of monomeric species is a key factor in understanding the process. They suggest that at low concentations $Fe(OH)_3$ has difficulty reaching optimal size for condensation, but once nuclei are present, they grow rapidly. In the case of a large concentration of Fe^{+3}, the

conversion is fast, and a large number of nuclei form, resulting in an $Fe(OH)_3$ colloidal product of decreased size. Also, Hsu and Ragone made a case for the preferential condensation of $Fe(OH)_3$ over other monomeric species based on the charge of the $Fe(OH)_3$ acting as nuclei. At a pH below the isoelectric point, edge OH ions would attract H^+ causing the surface to become positively charged. Consequently, conditions are more favorable for the condensation of neutral $Fe(OH)_3$ units on nuclei rather than for incorporation of the positively charged Fe^{+3}, $Fe(OH)^{2+}$, or $Fe(OH)_2^+$ species.

An alternative viewpoint has been suggested by Knight and Silva (1974). Basically, the initial steps involve the hydrolysis of Fe^{+3} to form $Fe(OH)^{+2}$, $Fe(OH)_2^+$ and the dimer, $Fe_2(OH)_2^{+4}$. The following pathways have been suggested:

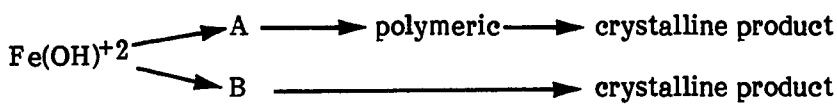

The pathway leading to "A" involves the formation of the dimer and then polycation growth. Pathway "B" involves the formation of $Fe(OH)_2^+$ and is favored because $Fe(OH)_2^+$ is a more likely precursor for direct crystalline phases since the addition of a mononuclear entity at a crystal face would be facilitated by the comparative ease, relative to a dimer or higher molecular weight species, of rearranging coordinated hydroxyl or oxyhydroxyl groups along with water to the geometry required for incorporation at the crystal face. Unfortunately, the weakest point in the argument is that no mechanism for the production of initial crystal nuclei is provided.

Other studies have investigated the hypothesis of polymer growth through dimerization, a process similar to the "A" pathway suggested above. Dousma and de Bruyn (1976) suggest that the hydrolysis of iron takes place in two parts.

First, hydrolysis to monomers and dimers occurs, and then further hydrolysis yields larger polymers. A continuation of their study (Dousma and de Bruyn, 1978) resulted in the proposal of two pathways for the growth of the larger polymers. Both result in sedimentation and precipitation, and both begin with secondary particles which are clusters (maximum size $\sim$ 500 Å) formed by slow aggregation of smaller, primary particles. One pathway involves the formation of a precipitate through the attachment of new particles at the ends of the flocculated material, and generally occurs at low ionic strengths. At higher ionic strengths, ($\sim$ 0.4 M), flocculation of the primary particles becomes rapid, and produces what is referred to as a "polydisperse suspension". Below is an illustration of the reaction scheme of Dousma and de Bruyn (1978):

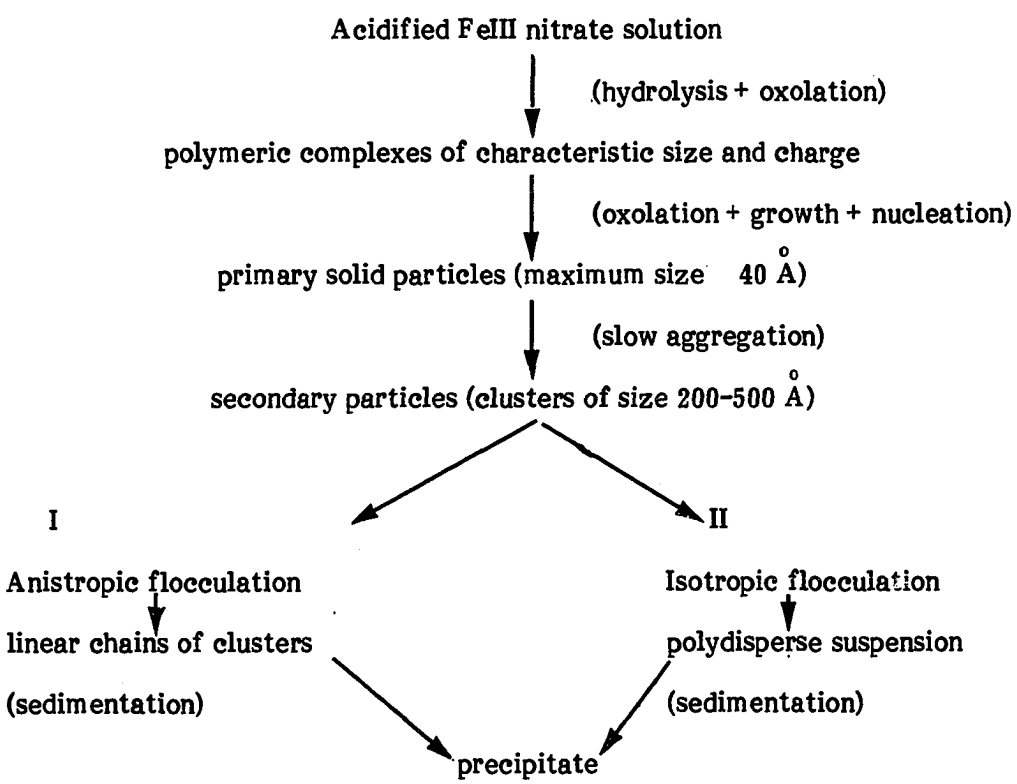

The resulting precipitate is most likely amorphous or poorly crystallized iron hydrous oxide. Although there is no discussion to this effect by Dousma and de Bruyn (1978), a conceptual analog may well be ferrihydrite. If this is the case, other more crystallized compounds such as hematite are then produced by either dehydration and/or molecular rearrangement. On the other hand, since it is known that goethite can be produced from slow hydrolysis, and without ferrihydrite as a precursor, the resulting precipitate postulated by Dousma and de Bruyn (1978) may be α FeOOH under favorable conditions.

4.3 Materials and Analytical Procedures

4.3.1 Selection of Field Sites

Field sites for this study were located within the Black Fork Creek watershed, and were selected based on field and laboratory observations from an earlier bottom sediment and water quality study (See Chapter 2). The locations are given in Figure 4.8; a total of six sites were chosen (Sites A-F). The first site (A) was along Ogg Creek, and was a reference site outside the zone of pollution. Site B was located at the point of discharge of acid waters from tailings and, possibly, an abandoned mine shaft on the west side of Bennett Run. The third site (C) was located on Bennett Run below the point of entry of acid mine drainage from the tailings. The fourth site (D) was located below the confluence of Ogg Creek and polluted waters from Bennett Run. Site E was about 1 km below the fourth. It was selected to examine changes in iron speciation with distance from the initial sources of pollution and mixing. The sixth and final site (F) was a breached air vent from another abandoned mine in the area (No. 52 Mine, see Figure 2.1). Selection of these sites allowed for comparisons of unpolluted waters with acid drainage water and also with stream water which had been affected by acid effluents.

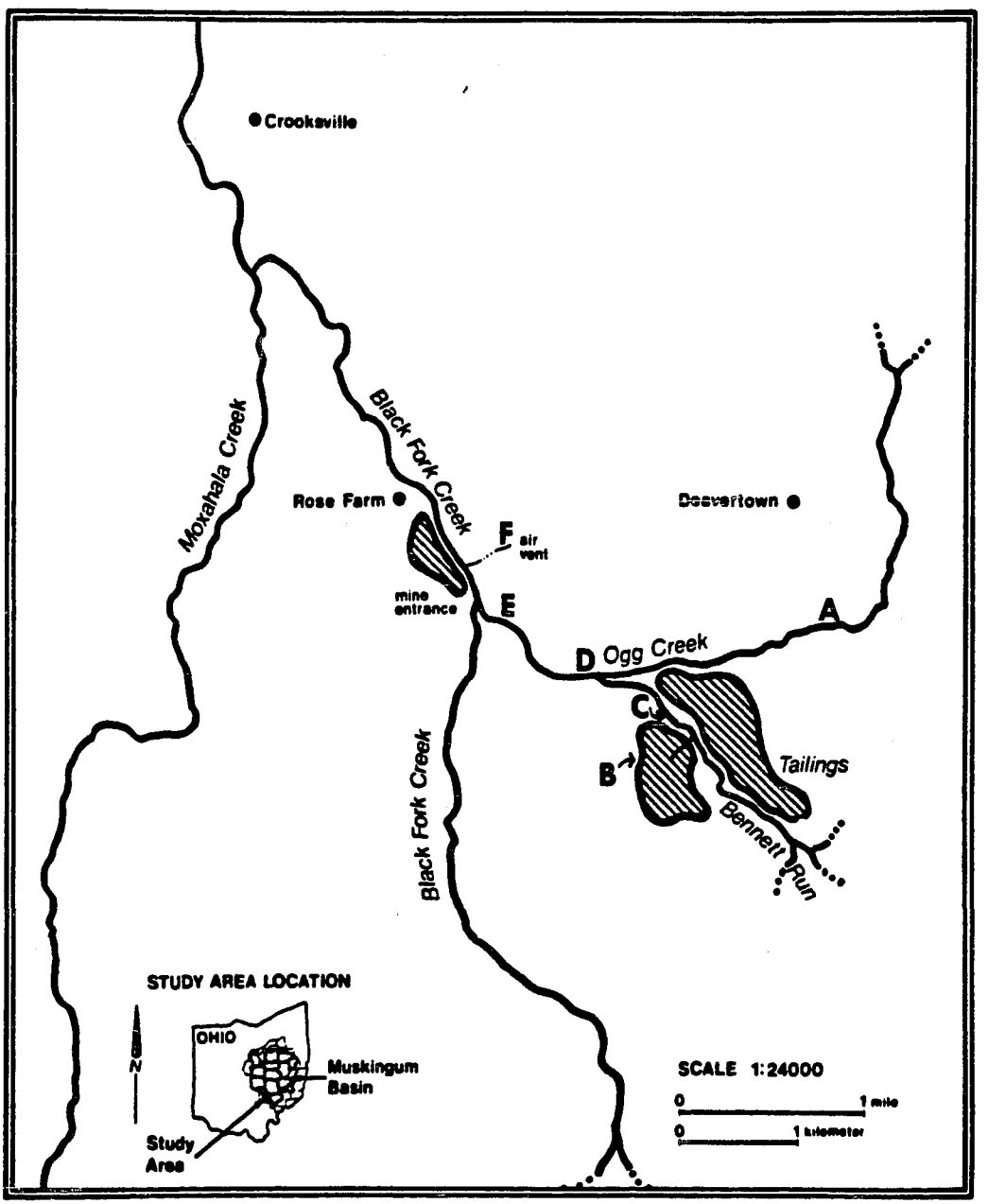

Figure 4.8 Location of field sites for study of dissolved iron species in waters affected by acid mine drainage.

4.3.2 Sample Collection and Routine Laboratory Analyses

From each site, three 500-ml samples of solution were collected using new polyurethane bottles washed in 5N HCl and wrapped with aluminum foil. The acid wash insured against iron contamination, and the aluminum foil inhibited the photolytic reduction of Fe(III) to Fe(II). All bottles were completely filled during collection and were purged with two to three full volumes of water in an effort to exclude as much oxygen as possible. The samples were transported to the laboratory in an ice chest; total transport time was approximately 3 hr. This collection procedure was modified from that recommended by Heaney and Davison (1977) for the collection and transport of lake waters.

Immediately upon returning to the laboratory, dissolved H_2S, electrical conductivity, dissolved oxygen, pH, and Eh were determined. Only the volume of sample required for these tests was brought to room temperature; the rest was kept refrigerated. The determination of H_2S was made on 25 ml of sample using a Hatch Model HS-7 test kit. Electrical conductivity was measured using a YSI Model 31 conductivity bridge with a 0.1 cell constant. Dissolved oxygen was determined using a YSI Model 57 oxygen meter with a temperature-altitude correction factor of 0.98. The pH of the water samples was measured using a Beckman SS-2 pH meter with Corning Ag/AgCl internal pH and calomel electrodes. Redox potential was measured using an Orion Research Ionalyzer Model 407A with a combination Pt-calomel electrode. These redox values were converted to Eh(mV) by adding the potential generated by the calomel electrode, as adjusted to room temperature (Wood, 1976). The conversion used was:

(4.5) $Eh_{mV} = \text{Redox (mV)} + 1000\,[0.244 - 0.0066\,(T^{\circ}C - 25^{\circ}C]$

These laboratory analyses provided general characteristics of the water samples, and enabled evaluations with respect to geochemical stability. In

addition, water samples from each site were sent to the Ohio Agricultural Research and Development Center at Wooster, Ohio for SO_4 and metal analyses. All dissolved ion measurements were made on filtrates passed through 0.4 μm Nucleopore membrane filters. Sulfate was analyzed by a turbidimetric method (APHA et al., 1980), and metals (Ca, Mg, Na, Al, Mn, Sr, Cd, Cu, Pb, Ni, and Zn) were analyzed by plasma emission spectroscopy (ICAP) using a Jarrell-Ash Model 975 Plasma Autocomp Spectrometer.

4.3.3 Sequential Ultrafiltration

A schematic of the plan of analysis is given in Figure 4.9. Before ultrafiltration was begun, an aliquot of original unfiltered sample was removed and colorimetrically analyzed for dissolved Fe(II) and total Fe. Then, 125 ml of each sample was sequentially filtered through 1, 0.4, 0.2 and 0.1 μm filters. Aliquots of the filtrates were removed after each filtration and were analyzed for total Fe content to provide estimates of colloidal iron distribution. All samples were vacuum filtered in partial darkness. In addition, the samples were filtered into and poured from new foil-wrapped 125-ml polyurethane bottles which had been washed with 5N HCl. This precaution was necessary to inhibit the photolytic reduction of Fe(III) during the filtration process.

4.3.4 Dissolved Fe(II), Total Fe, and Fe(III)

Orthophenanthroline (1,10 phenanthroline) hereafter referred to as "phen", was used as the complexing agent in all colorimetric Fe determinations. Two types of analyses were conducted: Fe(II) by phen; and total iron, also by phen, following reduction of Fe(III) by addition of hydroxylamine hydrochloride in the presence of light. Fe(III) was then determined by subtraction of Fe(II) from total Fe. As described in the flow chart (Figure 4.9), total Fe was determined on all samples: unfiltered, as well as those which had been sequentially filtered,

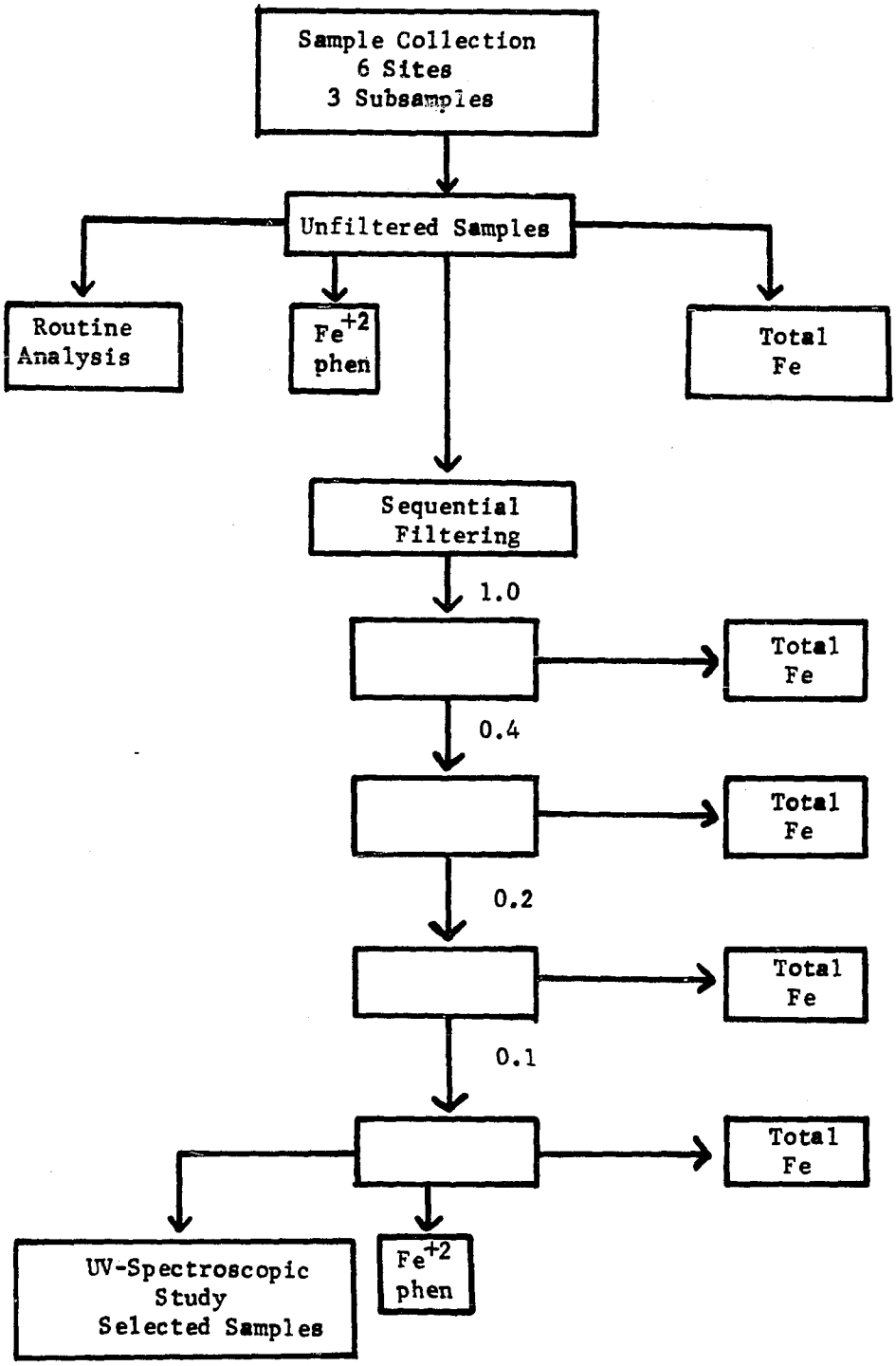

Figure 4.9 Flow chart for iron analysis.

with aliquots removed after each filter treatment. Dissolved Fe(II) was determined on both unfiltered samples and those passing through the 0.1 μm filters.

4.3.4.1 Dissolved Fe(II). Dissolved Fe(II) was analyzed by placing an appropriate amount of sample in a 50-ml volumetric flask and adding the following reagents in the exact sequence listed: 2 ml 1N H_2SO_4, 1 ml 10% phen in 95% ethanol, and 2 ml of 10% sodium citrate. Samples were compared immediately to standards ranging from 0-10 μg/ml in Fe(II); the stock solution for Fe(II) was a 500 μg/ml solution of ferrous ammonium sulfate. Analyses were conducted using a Beckman Model 24 Spectrophotometer with a visible light source at 510 nm.

4.3.4.2 Total Fe. Analysis for total iron was a modified procedure of that discussed above. A 2-ml aliquot of 10% hydroxylamine hydrochloride was added to the iron sample prior to addition of H_2SO_4, phen, and sodium citrate. The samples were then brought to volume in 50-ml volumetric flasks, transferred to 50-ml erlenmeyers, stoppered, and allowed to reduce in the presence of flourescent light (Stucki, 1981) by placing the erlenmeyer beakers on a light table for no less than 36 hr. Analyses were conducted using a Beckman Model 24 Spectrophotometer with a visible light source at 510 nm.

4.3.4.3 Dissolved Fe(III) and Colloidal Fe. Dissolved Fe(III) was estimated by subtraction of dissolved Fe(II) from total Fe measured in the 0.1 μm filtrates. Estimates of colloidal Fe were obtained by subtraction of total Fe in the 0.1 μm filtrates from total Fe detected in the unfiltered samples.

4.3.5 UV-Spectroscopic Analysis

An attempt was made to identify various dissolved Fe(III) species by conducting a spectroscopic absorption scan over the UV-range. Standard

solutions were prepared and analyzed prior to analysis of the field samples. Two Fe(II) standards, 10 μg/ml $FeCl_2$, and 10 μg/ml $Fe(NH_4)_2(SO_4)_2 \cdot 6H_2O$ were examined to check for possible spectral interferences from Fe(II). Ultra violet spectra of two Fe(III) standards were also obtained. The first Fe(III) standard was a mixture of 1 μg/ml each of $FeCl_3$ and H_2SO_4. The second was a 10 μg/ml solution of ferric ammonium sulfate [$Fe(NH_4)(SO_4)_2 \cdot 12H_2O$]. The UV analysis was performed at room temperature with a Beckman Model 24 Spectrophotometer using a 1 cm quartz cell with air as a reference. Absorbance was recorded manually at 2.5 nm intervals over a wavelength range of 190 to 380 nm. Samples were always scanned from large to small wavelengths, in accordance with the manufacturer's suggestion.

Four field samples were selected for study. In all cases, only the 0.1 μm filtrates were examined in order to reduce spectral interference from colloidal materials. Filtrates from site A (reference), site B (tailings), site D (downstream from the tailings) and site F (breached air vent) were analyzed in the mannner described above, except that the samples were kept in foil-wrapped containers until analysis to avoid photochemical reduction of Fe(III) while the samples warmed to room temperature.

4.4 Results and Discussion

4.4.1 ICAP and EC Data

Table 4.2 shows EC and concentrations of some of the more significant metals (Ca, Mg, Na, Al) found in the waters from Black Fork Creek watershed. (Complete analyses are given in Appendix B). Electrical conductivity is highest in waters from the two sites draining the abandoned mines (tailings and air vent), and decreases downstream from the site of pollution from the tailings. This tendency corresponds with trends in dissolved Mg and Al in the same samples.

Table 4.2 EC and Major Metals Detected by ICAP Analysis of Water from Black Fork Creek Watershed

Site	EC	Ca	Mg	Na	Al
	mmhos/cm		µg/ml		
A-Reference	0.3	43.4	9.9	18.1	---*
B-Tailings	4.8	79.9	45.9	18.8	343.3
C-Stream	2.6	80.2	36.7	31.2	154.0
D-Stream	1.6	76.1	26.3	24.2	83.2
E-Stream	1.6	83.2	26.6	22.2	74.2
F-Air Vent	3.8	224.7	145.0	207.7	14.6

* Non-detectable. Detection limits for ICAP in µg/ml: Ba, Mn = 0.001; Sr = 0.002; Cd, Cu, Zn = 0.003; Ni = 0.008; P = 0.02.

Magnesium decreases to 58% of that detected at the tailings and Al to 22% of that added by pollution from the tailings. Calcium and Na do not show such distinct decreases at downstream sites. This is most likely due to higher levels of these two metals in the waters of Ogg Creek immediately above the zone of pollution.

Comparison of Ca, Mg, Na, and Al concentrations in drainage waters from the tailings with those from the air vent indicate the diversity in concentrations of these metals in local acid mine effluents. The air vent concentrations are approximately three times that of waters from the tailings for Ca and Mg, and 11 times the Na concentration at the tailings site. However, the tailings water has an Al concentration 24 times that found in drainage waters from the air vent. Irrespective of the range in concentration of these different metals, increased amounts detected in the mine drainage waters are associated with increased electrical conductivity (EC) within the basin.

4.4.2 Eh, pH, Dissolved Oxygen and Sulfur Data

Results from routine laboratory analyses are given in Table 4.3 along with sulfate concentrations for the six sites. Dissolved oxygen is highest in areas affected by acid mine drainage, the lowest value being the reference site. This may not be unusual. The high acidity in acid mine drainage greatly limits the type of organisms found in that environment, thus keeping biological oxygen demand (BOD) at a minimum. Also, water in the stream at the reference site is not protected by shade. Dissolved oxygen at a site that is unprotected from sunlight can actually be lower than one would normally expect due to temporary but significant diurnal fluctuations in BOD caused by increased microbial activity.

Table 4.3 Sulfate, Dissolved Oxygen, Eh and pH of Water Samples from Black Fork Creek Watershed

Site	DO	Eh	pH	Sulfate
	µg/ml	volts		µg/ml
A-Reference	4.5	0.314	7.3	310
B-Tailings	5.0	0.584	2.9	4543
C-Stream	5.1	0.646	2.9	2000
D-Stream	5.1	0.659	3.1	1020
E-Stream	4.8	0.711	3.2	920
F-Air Vent	4.9	0.414	4.7	2523

Eh varies in the same way that dissolved oxygen does, and serves to indicate that the principal agent active in the system for oxidation and reduction is most likely oxygen. However, the importance of Thiobacillus species oxidizing sulfur and iron should not be discounted.

As might be expected, the pH of the waters sampled for this study is highest at the reference site. The pH drops as a result of pollution from the tailings, and begins to rise downstream at sites D and E, most likely due to dilution by the discharge of small surface drainageways.

There were no measurable quantities of H_2S at any of the sites. However, sulfate concentrations are quite high in effluents from the tailings and air vent. Also, the sulfate data seem to reflect downstream dilution effects better than do the other parameters listed in Table 4.3. The dissolved sulfate is highest in waters flowing from the tailings, and decreases by half in the stream at site C. Additional decreases occur downstream at sites D and E due to further dilution by fresh water from Ogg Creek. Levels of sulfate can be correlated with Eh-pH relationships which exist at each site. Figure 4.10 is taken from Hem (1960) and indicates established stability fields for sulfur species based on Eh and pH. The field sites are placed in this diagram with respect to measured Eh and pH. Note that all points occur within the SO_4 activity field. This supports the presence of measurable quantities of sulfate and explains why laboratory tests revealed no detectable H_2S.

4.4.3 Sequential Ultrafiltration Data for Iron

Results from sequential ultrafiltration procedures are found in Table 4.4. Total iron in the system is given by the unfiltered values. Iron is very low in the reference area and greatly increases as a result of drainage from the tailings. The two sites with the greatest amount of iron are the tailings and the air vent,

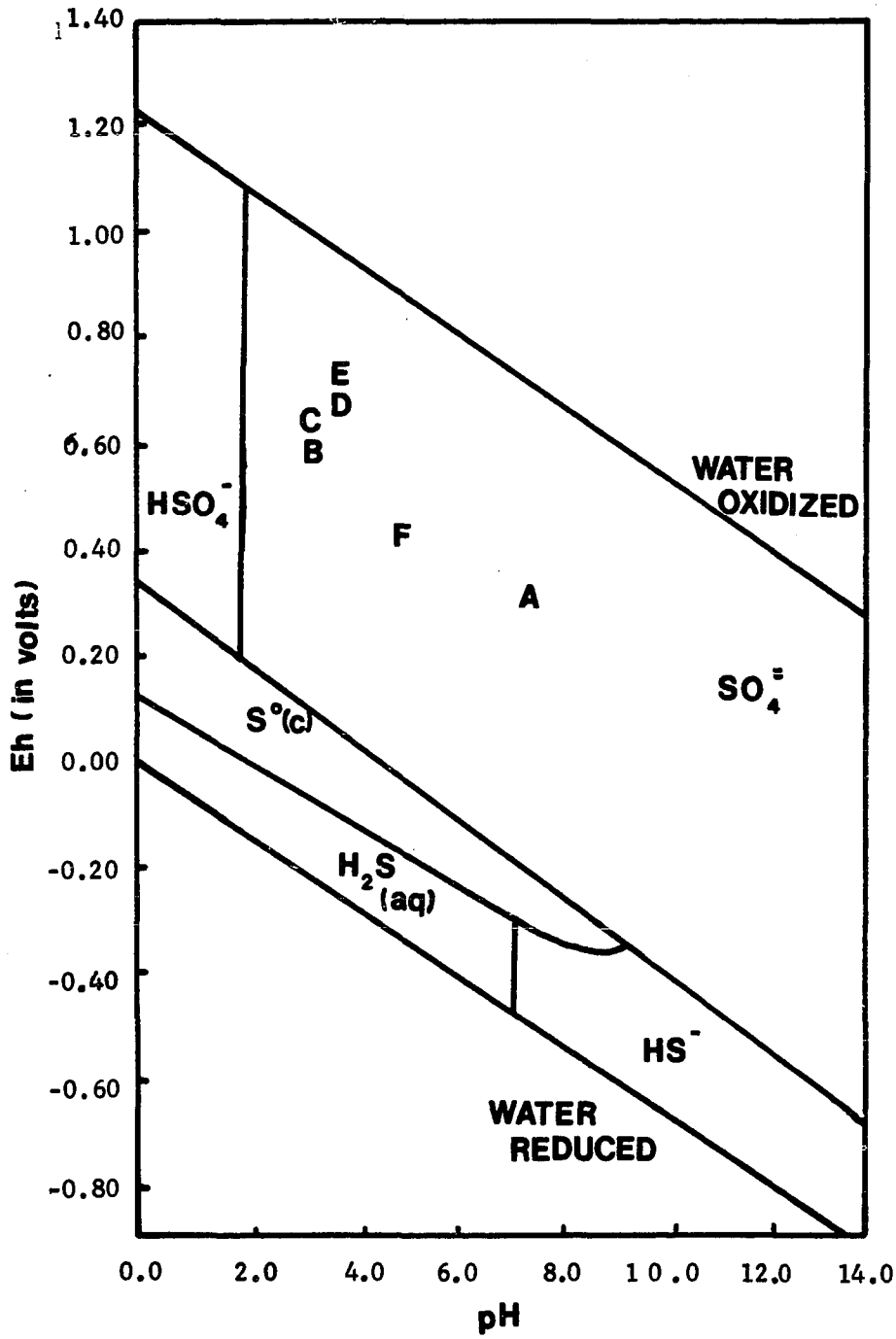

Figure 4.10 Field sites with respect to sulfur stability field.

Table 4.4 Iron Detected Following Sequential Ultrafiltration of Water Samples from Black Fork Creek Watershed

Site	Total Fe					Colloidal* Fe
	unfiltered	1 μm	0.4 μm	0.2 μm	0.1 μm	
		μg/ml				%
A-Reference	0.25**	0.14	0.06	0.04	0.03	88
B-Tailings	1245	1228	1197	1173	1172	6
C-Stream	113	104	99	94	94	17
D-Stream	271	149	143	139	138	49
E-Stream	117	97	92	91	88	25
F-Air Vent	594	520	500	500	487	18

* Colloidal Fe = $\frac{\text{Total Fe (unfiltered)} - \text{Total Fe (0.1 μm filtered)}}{\text{Total Fe (unfiltered)}} \times 100$

** Detection limit is 0.001 μg/ml. Difference in significant figures reflect differences in size of aliquots.

and there is a 10-fold decrease in total iron at the sites downstream from the tailings. This decrease is much greater than can be accounted for by simple dilution and must be largely due to precipitation as suggested by field observations.

The amount of colloidal iron detected by ultrafiltration also supports the conclusion that iron is removed from the water by precipitation. Colloidal Fe is arbitrarily defined as the difference between the total Fe in unfiltered water samples and total Fe in the 0.1 μm filtrates. Note that the % colloidal material increases downstream from the site of pollution at the tailings.

Evidence of precipitation is further supported by Eh-pH relationships. Figure 4.11 (after Hem, 1960) places the data within the iron stability field for both 0.01 and 100 μg/ml Fe. At low concentrations (0.01 μg/ml Fe) precipitation of iron would occur only at the reference site (A). However, with increased amounts of dissolved iron in the system, precipitation will be more likely to occur at lower pH and under more oxidizing conditions. At 100 μg/ml, nearly all the sites should show evidence of precipitation. The exception is the water flowing from the tailings, and no evidence for precipitation was seen at that site in the field. However, extensive precipitaion did occur over a period of 2 weeks when samples from that site were taken to the laboratory and left in the refrigerator.

An attempt to compare the results from sequential ultrafiltration with the KSCN method used by Hsu (1967) and Hsu and Ragone (1972) was made to see if dissolved Fe(III) and Fe(III) colloidal material could be determined separately. This KSCN procedure did not prove successful as the KSCN apparently oxidized dissolved Fe(II) and yielded greater Fe(III) results. Also, KSCN did not seem as stable a colorimetric procedure as phen. The absorption curve from the standard

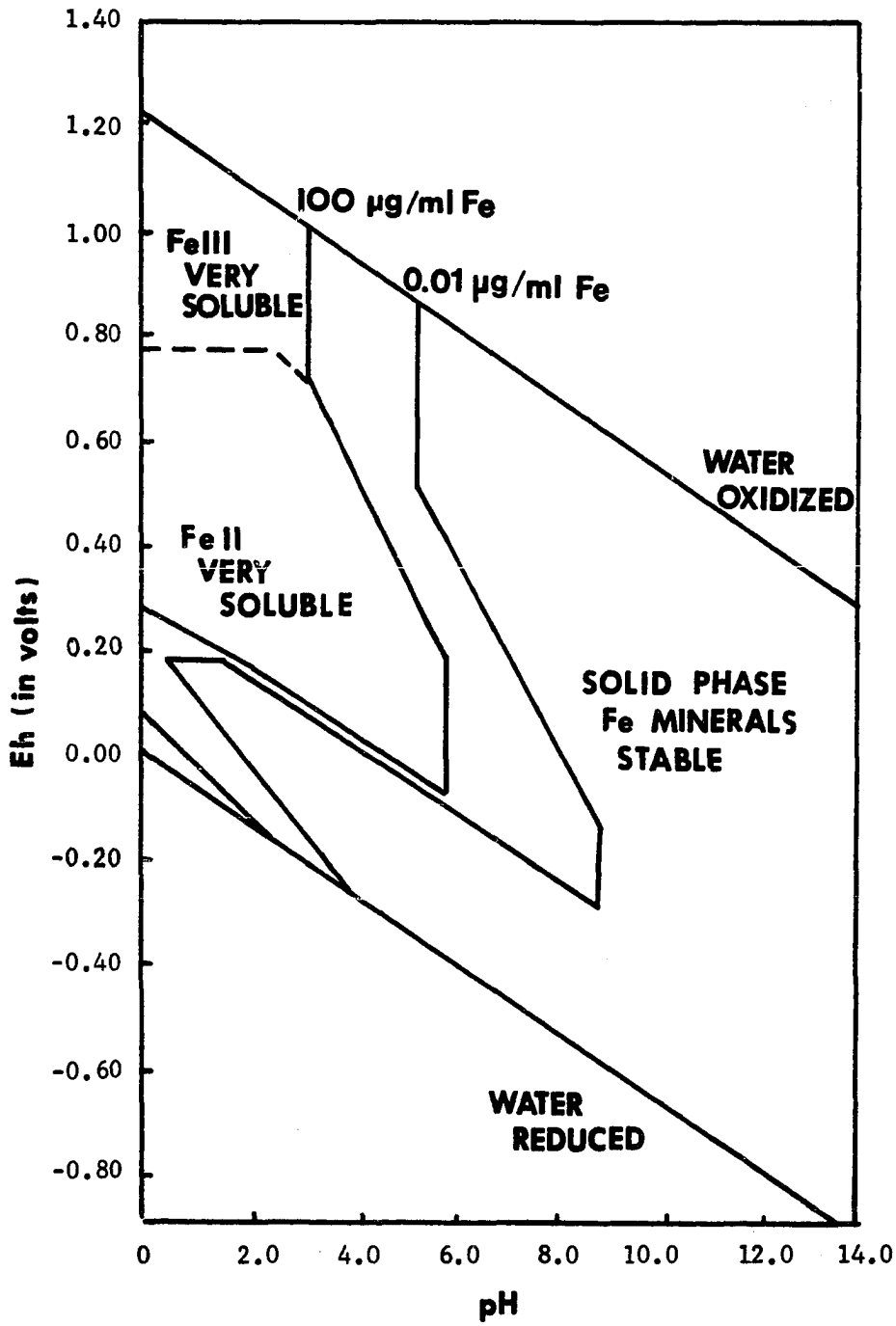

Figure 4.11 Field sites with respect to iron stability field. After Hem (1960). Iron stability in the presence of 100 µg/ml sulfur.

solutions would drift considerably over a 24-hr period. However, this could be corrected by adding 1 drop of 30% H_2O_2 to the standards before reading absorption.

4.4.4 Speciation of Dissolved Iron

For the purposes of this discussion, all iron detected in the 0.1 µm filtrates is considered to be dissolved iron. While it is very likely that the Fe(III) component does have a solid phase constituent (considered a polymer since it is < 0.1 µm in diameter), separation of the dissolved Fe(III) component from the Fe(III) polymer was not attempted because sequential ultrafiltration data (Table 4.4) indicate that solid phase Fe(III) materials are concentrated in the larger size fractions (0.1 and 0.4 µm).

4.4.4.1 Oxidation State of Iron in Solution. The study indicates that the oxidation state of iron in solution can vary greatly in waters affected by acid mine drainage (Table 4.5). Fe(II) accounts for over 90% of the total dissolved iron at the tailings and air vent sites. Dissolved Fe(II) subsequently decreases downstream from the tailings, while % dissolved Fe(III) increases.

Of major concern is the large quantity of Fe(II) present in the acid discharge waters (sites B and F, especially) when both dissolved oxygen and Eh measurements indicate that the waters are well oxidized. This result is most likely related to the production of Fe(II) as discussed in Chapter 2, section 2.2.1. Singer and Stumm (1970) proposed an initiator reaction and propagating cycle which produce high quantities of Fe(II) in waters affected by acid mine drainage:

A. Initiator reaction, producing Fe(II):

(4.6) $FeS_2 + 1/2O_2 + 2H^+ \longrightarrow Fe^{+2} + 2S^\circ + H_2O$

B. Propagating cycle in which Fe(III) is utilized in pyrite oxidation, producing Fe(II):

Table 4.5 Fe(II) and Fe(III) in 0.1 μm Filtrates of Water Samples from Black Fork Creek Watershed

Site	TDI*	Fe(II)	Fe(II)/TDI	Fe(III)	Fe(III)/TDI
	μg/ml		%	μg/ml	%
A-Reference	0.03	0	0	0.03	100
B-Tailings	1172	1118	95	54	5
C-Stream	94	69	73	25	27
D-Stream	138	82	59	56	41
E-Stream	88	9	10	79	90
F-Air Vent	487	478	98	9	2

*Total Dissolved Iron (TDI) = total iron passing a 0.1 μm filter

(4.7) $4Fe^{+2} + O_2 + 4H^+ \longrightarrow 4Fe^{+3} + 2H_2O$

(4.8) $2Fe^{+3} + FeS_2 \longrightarrow 2S^\circ + 3Fe^{+2}$

Such a cycle placing Fe(II) in solution helps explain the large quantities of Fe(II) detected in the waters sampled at sites B and F.

4.4.4.2 Iron Speciation as Predicted from Eh-pH and Activity Diagrams. Given the production cycle of Fe(II) described by Singer and Stumm (1970), and known Eh-pH measurements for the samples, it is possible to use the Eh-pH diagram to establish an environmental explanation for the occurrence of Fe(II) and Fe(III) in a particular sample. In this case, Figure 4.11 can be used to predict the oxidation state of Fe in the samples. In this context, site B can be expected to have the highest percentage of Fe(II), and sites A, D, and E the highest percentages of Fe(III). Waters from both sites C and F are very close to the solid phase boundaries and could be expected to contain significant amounts of Fe(II). This trend is supported by phen analyses (Table 4.5) which show higher levels of Fe(II) in solution for sites B, C and F (95, 73, and 98%, respectively) compared to the other sites.

The Eh-pH relationships shown in Figure 4.11 can be used to predict precipitation and also the predominant oxidation state of Fe species in solution. However, except under very well oxidized conditions, Eh-pH relationships do not aid significantly in the identification of the Fe(III) monomeric species, especially those resulting from Fe(III) hydrolysis. Information concerning the presence of these species is necessary for a complete understanding of Fe(III) precipitation; however, identification of the separate monomeric species is difficult. One method, though indirect, is to use the Fe(III) activity-pH diagram to predict which monomeric forms may be present in the samples. Figure 4.12 places the water samples with respect to stability fields for monomeric Fe(III) species.

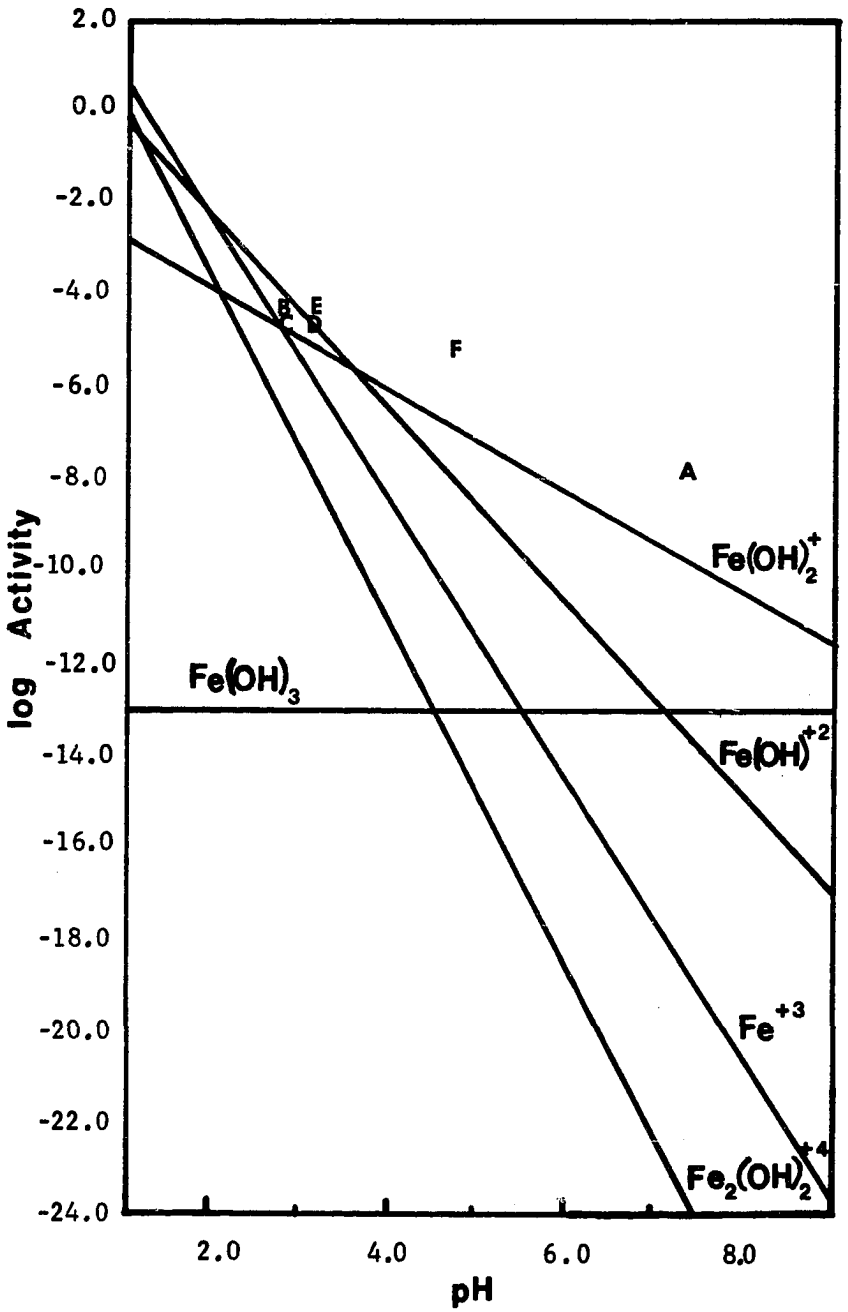

Figure 4.12 Field sites with respect to Fe(III) stability field. After Lindsay (1979).

This diagram indicates that $Fe(OH)_2^+$ is most likely to be in abundance in the reference (A) and air vent waters (F). Site C will most likely have a mixture of Fe^{+3} and $Fe(OH)_2^+$, while the tailings site (B) and the downstream sites D and E will have $Fe(OH)^{+2}$ as the predominent Fe(III) monomeric species.

4.4.4.3 UV-Analysis of Iron Species in Solution. Although UV-spectral analysis is not useful for measuring concentrations of the monomeric species of Fe(III), it is a useful tool in the direct identification of the monomers present. UV-spectra differ greatly depending on the types of ions present. Figures 4.13 through 4.17 represent spectra of known inorganic reagent-grade materials which serve as standards for comparison of the spectra from the field samples. Interpretation of band maxima is based on UV-maxima reported in the literature and summarized in Table 4.1.

Ultraviolet spectra for two Fe(II) standards, 10 µg/ml $FeCl_2$, and 10 µg/ml $Fe(NH_4)_2(SO_4)_2 \cdot 6H_2O$, are given in Figures 4.13 and 4.14. Both have absorption band maxima at about 197 nm, suggesting a characteristic maximum for Fe(II). A second maximum at 260 nm exists in the spectrum of ferrous ammonium sulfate, and is probably due to a $Fe(SO_4)$ complex. Ultraviolet spectra for Fe(III) standards are shown in Figures 4.15 and 4.16. Figure 4.15 is a spectrum of a mixture of $FeCl_3$ and H_2SO_4, while 4.16 is a solution of ferric ammonium sulfate. Both show band maxima at or near 210 nm. This corresponds to a maximum identified by Johnson et al. (1979) for $Fe(OH)^{+2}$ at 212 nm. Other maxima common to both are found in the 250 nm and 300 nm range. The ferric ion has been shown to have a primary band maximum at 240 nm (Knight and Silva, 1975) with secondary absorption at 195 nm (Brown and Kester, 1980). Enhanced absorption in the 240 nm region of the ferric ammonium sulfate spectrum is probably related to the presence of $Fe(SO_4)$ species. Subdued band

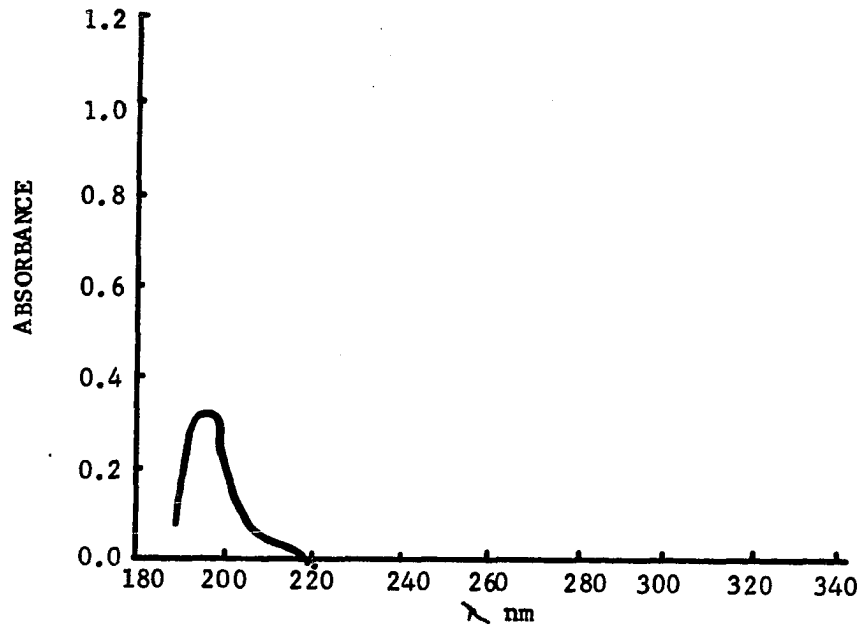

Figure 4.13 UV-spectra of Fe(II) standard solution: 10 µg/ml $FeCl_2$.

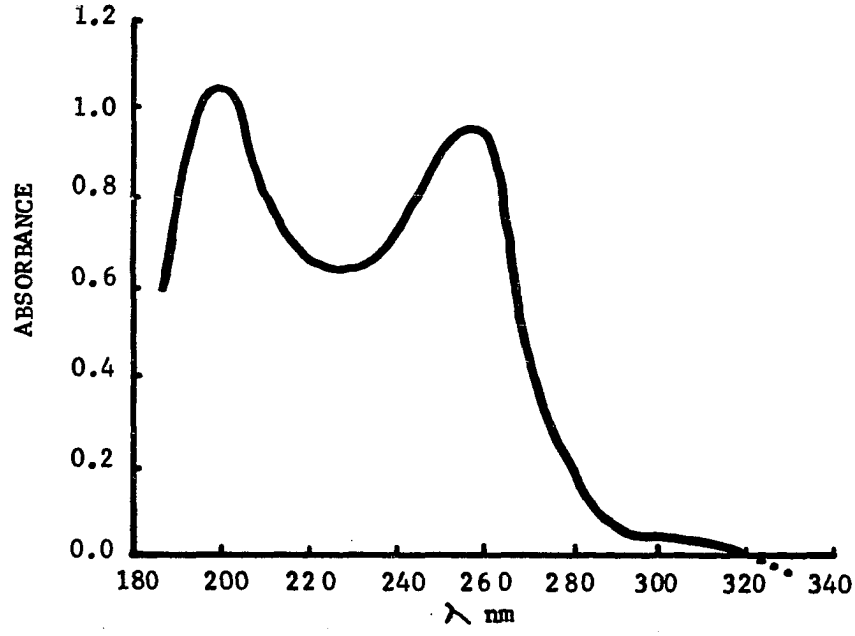

Figure 4.14 UV-spectra of Fe(II) standard solution: 10 µg/ml ferrous ammonium sulfate. $[Fe(NH_4)_2(SO_4)_2 \cdot 6\ H_2O]$.

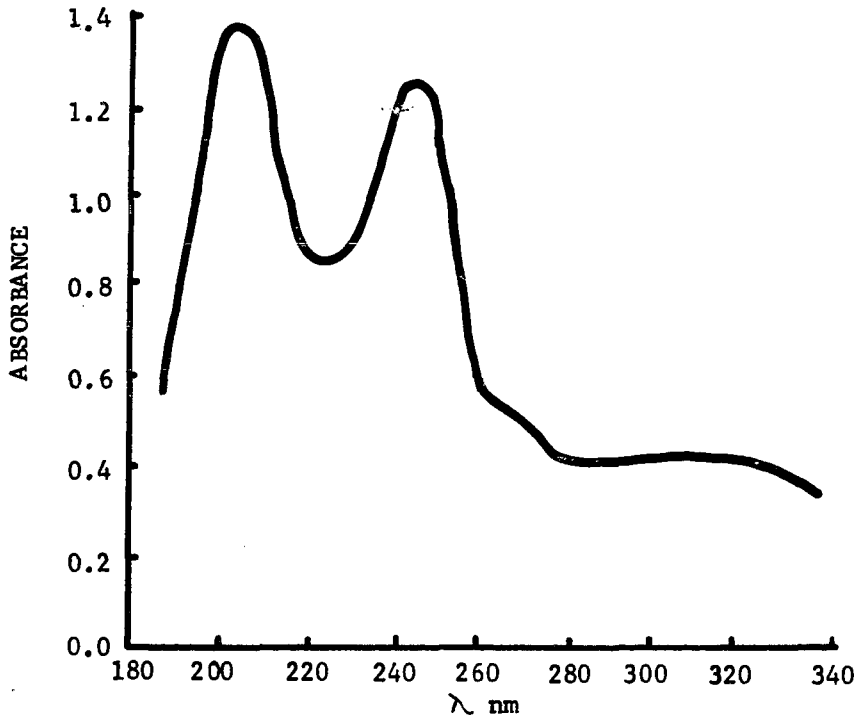

Figure 4.15 UV-spectra of Fe(III) standard solution: mixture of 1 µg/ml each, $FeCl_3$ and H_2SO_4.

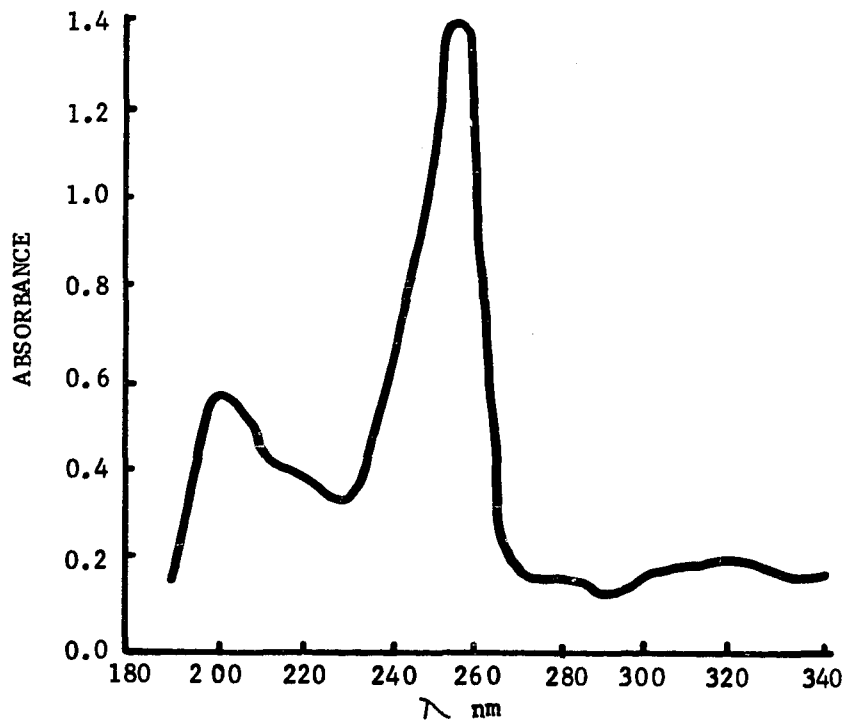

Figure 4.16 UV-spectra of Fe(III) standard solution: 10 µg/ml ferric ammonium sulfate [$Fe(NH)_4 (SO_4)_2 \cdot 12 H_2O$].

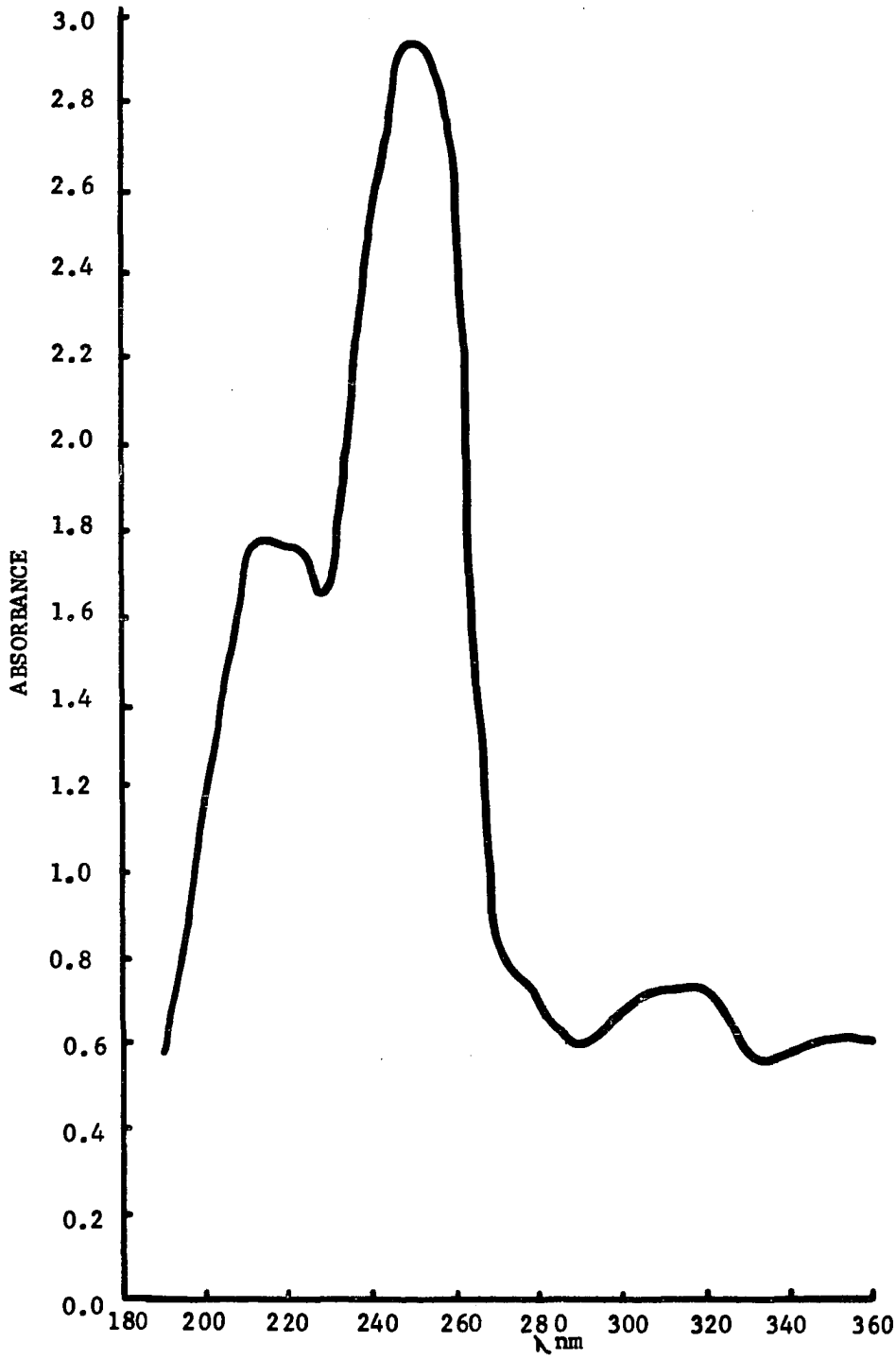

Figure 4.17 UV-spectra of Fe(III) standard solution: 1 μg/ml $FeCl_3$.

maxima in the 300 nm region of Figures 4.15 and 4.16 are related to $Fe(SO_4)$ species (Johnson et al., 1979), $Fe(OH)^{+}_{2}$, or the dimer $Fe_2(OH)_2^{+4}$ (Knight and Silva, 1975). As Knight and Silva (1975) have stated, it is not possible to identify $Fe_2(OH)_2^{+4}$ (maxima at 240 and 335 nm) in the presence of Fe^{+3} (maximum at 240 nm) and $Fe(OH)_2^{+}$ (maximum at 300 nm). A standard spectrum which excludes SO_4 is shown in Figure 4.17. This spectrum is of a 1 µg/ml solution of $FeCl_3$. Maxima occur at 212, 225, 245-250, and 300-335 nm and support the presence of Fe^{+3}, $Fe(OH)^{+2}$ and possibly $Fe(OH)_2^{+}$.

Based on the UV-absorption spectra of the standard solutions, comparisons of the UV-spectra from four field sites were made. Figures 4.18-4.21 show spectra from the field sites. The reference (site A) and the air vent (site F) yield similar spectra (Figures 4.18 and 4.19). Rather broad bimodal absorption maxima occur in the 200-215 nm range, and it is possible to postulate the presence of $Fe(OH)^{+2}$ and $Fe(OH)_2^{+}$. The similarity of the two spectrum is significant because Fe(II) species would be expected in the case of the air vent site. However, Figure 4.13 indicates that the absorption spectrum for Fe(II) may be extremely limited, and Fe(II) could be hidden by the larger Fe(III) species band maximum at 205-212 nm. Ultraviolet spectra of water from the tailings and stream water below the tailings (sites B and D) are very different compared to the reference and air vent sites, but similar when compared with each other. Most distinct are the maxima at 245 and 300 nm. However, a case for a maximum in the region of 215 nm can also be made for the water from the tailings. These spectra indicate the presence of Fe(III), $Fe(OH)^{+2}$, and possibly $Fe(OH)_2^{+}$ and/or $Fe(SO_4)$ species.

This study suggests the types of Fe(III) monomers which are found in these acid mine waters. At the air vent site, $Fe(OH)^{+2}$ and $Fe(OH)_2^{+}$ were in

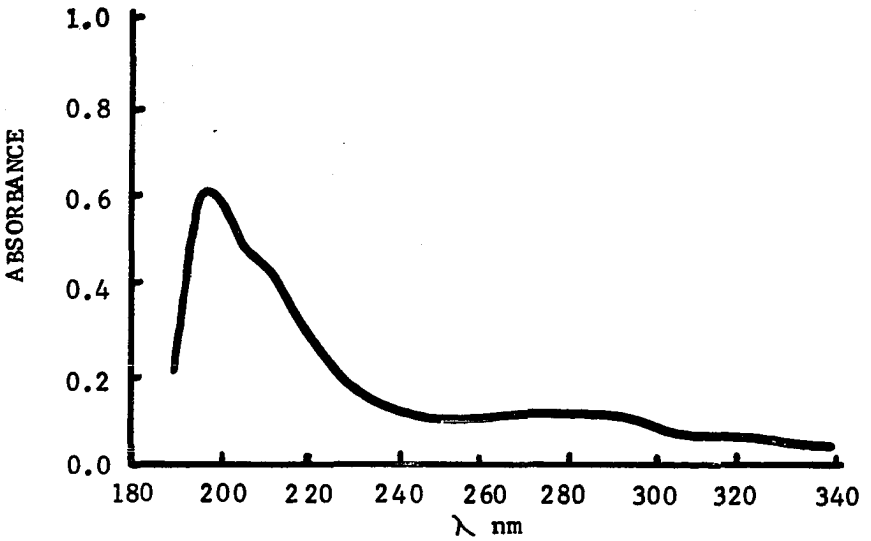

Figure 4.18 UV-spectra of waters from the reference site (A).

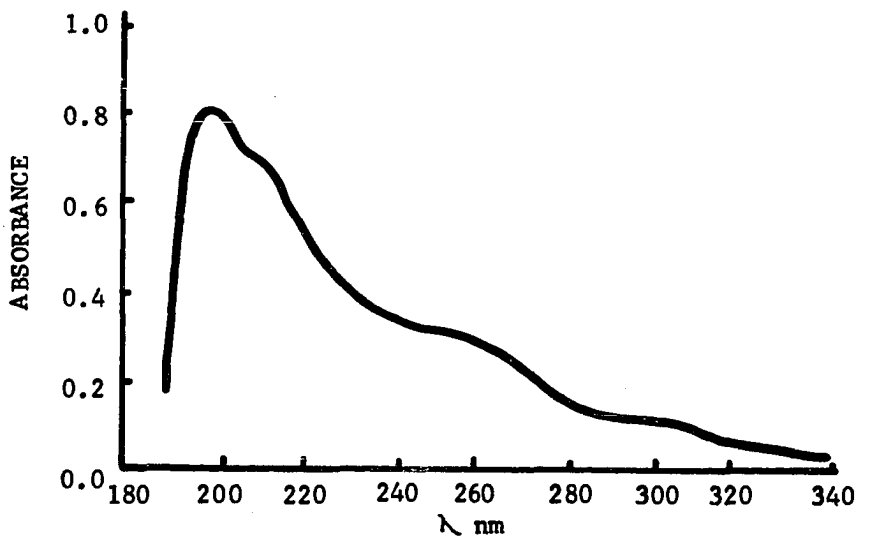

Figure 4.19 UV-spectra of drainage waters from the breached air vent site (F).

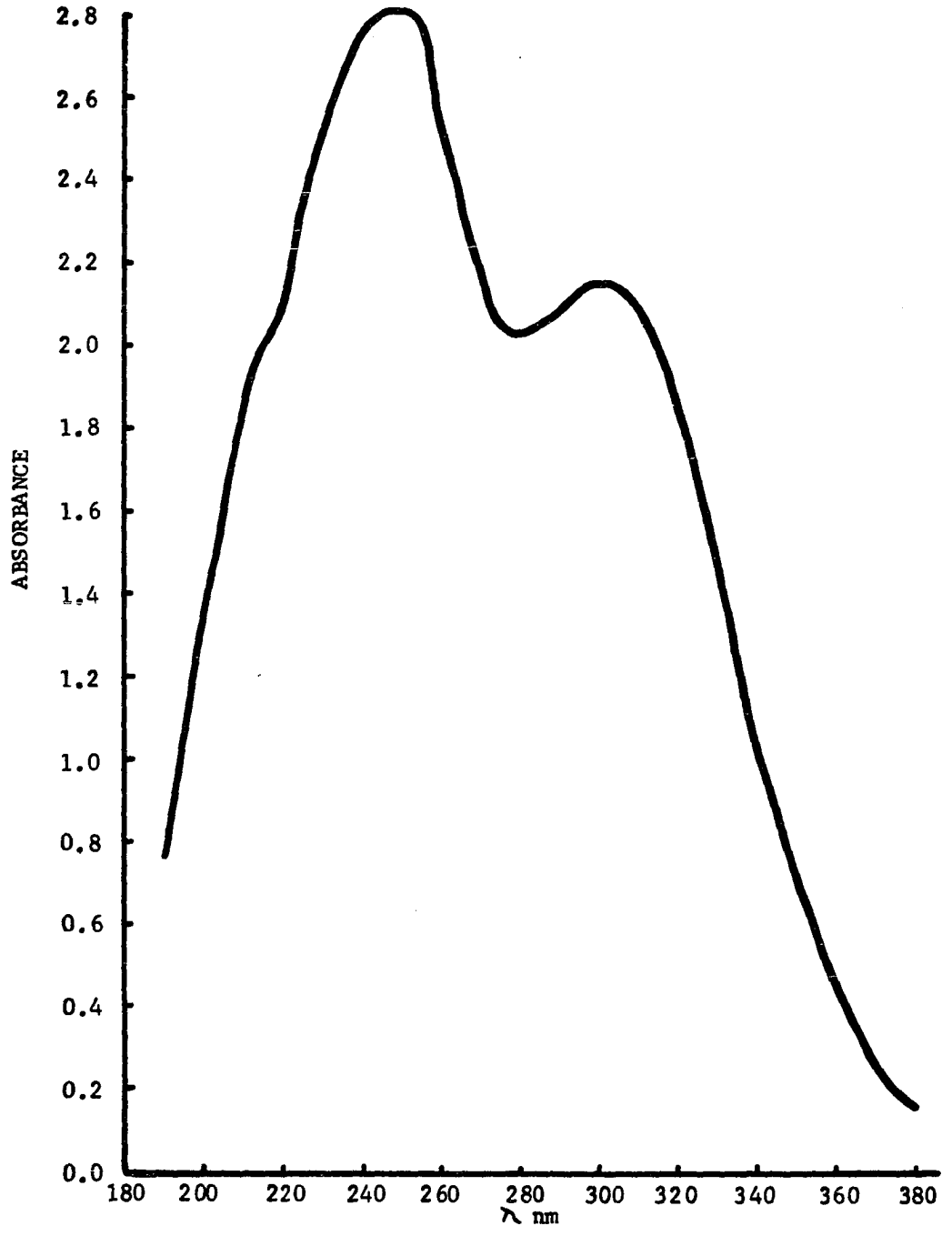

Figure 4.20 UV-spectra of drainage waters from the tailings site (B).

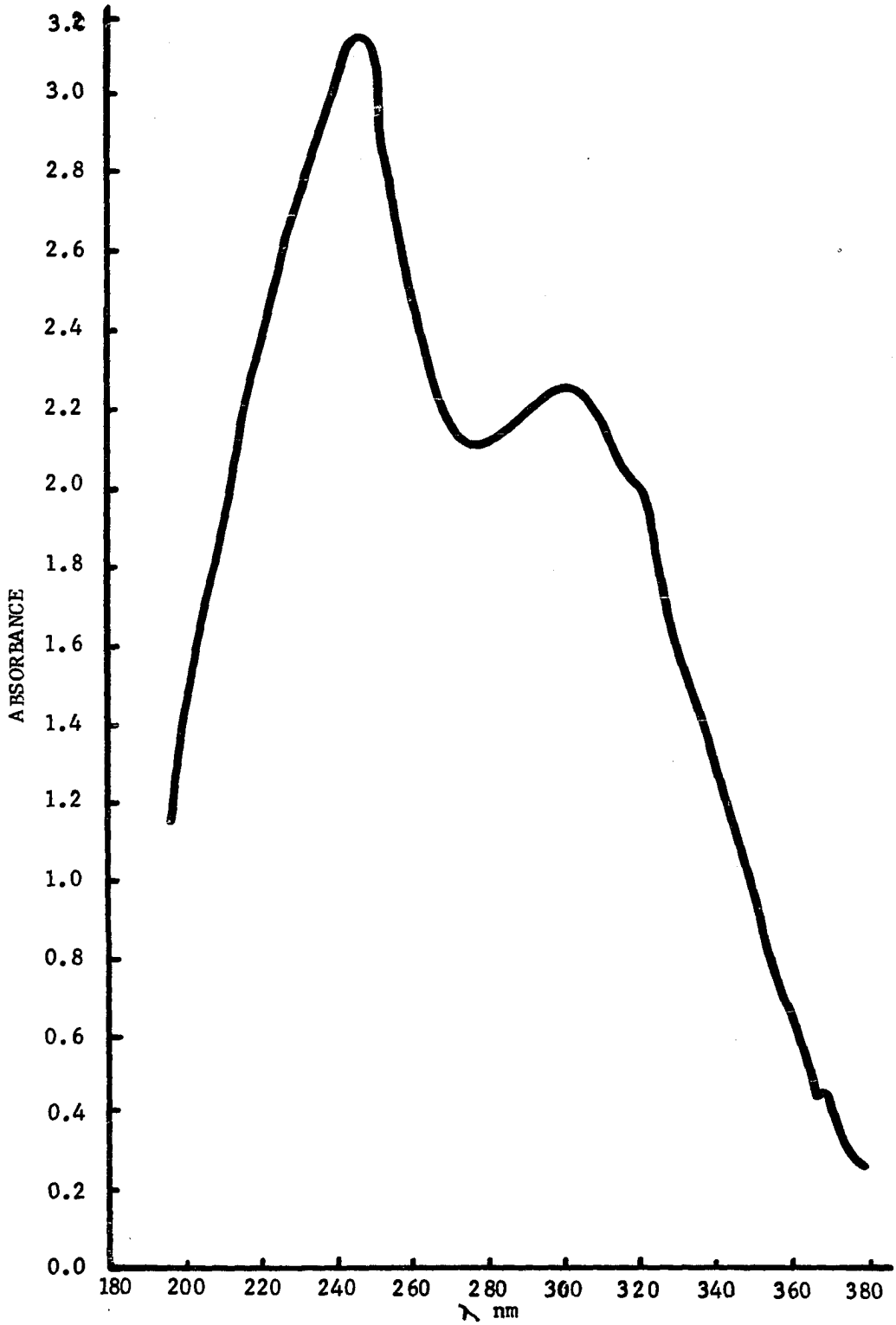

Figure 4.21 UV-spectra of stream water below the tailings site (D).

evidence. In waters from the tailings and downstream sites, Fe^{+3}, $Fe(OH)^{+2}$, and $Fe(OH)_2^+$ were in evidence. Presence of the dimer could not be established because its UV-spectrum is so similar to that of other Fe(III) species.

4.4.5 Polymerization and Precipitation of Fe from Acid Mine Drainage

During the course of field work in the Black Fork Creek watershed, observations suggested two separate modes of iron precipitation that were spatially separated. The first is the formation of voluminous yellowish ferrihydrite found in the stream channel. This material seems to form and accumulate rapidly. The second type of precipitation is associated with acid mine waters from the air vent. These waters are not channelized, and flow over the landscape in sheet-fashion. This brings the waters into intimate contact with both soil and organic materials. The resulting precipitate is a slowly accumulating travertine-like deposit composed primarily of goethite and some ferrihydrite.

Fe(III) speciation studies with UV-spectra and the Fe(III) activity-pH diagram reported in the two previous sections indicate that these two areas may also differ in the types of dissolved Fe(III) species present. These studies indicate that there is a mixture of Fe(III) species in the stream environment. UV-spectra allowed for identification of Fe^{+3}, $Fe(OH)^{+2}$ and $Fe(OH)_2^+$, and predictions of the Fe(III) species in solution from solubility relationships (Figure 4.12) indicated that the dominant monomer, particularly in downstream sites D and E, should be $Fe(OH)^{+2}$. UV-spectra of waters from the air vent established the presence of $Fe(OH)^{+2}$ and $Fe(OH)_2^+$, while the solubility diagram indicated that the predominant monomer under those concentrations of iron and pH should be $Fe(OH)_2^+$.

4.4.5.1 Polymerization and Precipitation in the Stream Environment.

Presence of the $Fe(OH)^{+2}$ monomer as the predominant ion species in the stream

sites is significant, as this monomer forms the dimer, $Fe_2(OH)_2^{+4}$. As discussed by Knight and Silva (1974) and also Dousma and de Bruyn (1976), the dimer acts as the precursor of polymer growth which ultimately leads to the formation of a crystalline product. While laboratory data give no direct evidence of the existence of polymers in the system, the poorly crystallized product, ferrihydrite does result.

Schwertmann and Taylor (1977) discuss the formation of ferrihydrite by fast hydrolysis. Field and laboratory observations (see Chapter 3) support the rapid formation of ferrihydrite, particularly in the presence of sulfate. The fast precipitation and levels of dissolved sulfate in downstream sites indicate that sulfate may act as a catalyst during ferrihydrite formation. Laboratory observation indicated that sulfate was intimately associated with a flocculated colloidal phase almost immediately after precipitation. It is possible that it aids in nucleation and polymer aggregation by lowering surface charge and introducing irregularities in double layer thickness, especially in larger polynuclear iron species (Dousma et al., 1979). Association of the sulfate ion with the colloidal precipitates may also be indicated by data from Table 4.3. Sulfate was very high where a minimum of precipitation occurred (sites B and F) but was much lower in the stream sites. However, it is also recognized that dilution in the stream may be a factor in sulfate decreases as well.

With time, ferrihydrite should alter to form other more crystallized products. Schwertmann and Taylor (1977) indicate that hematite can be formed with dehydration, and that under conditions conducive to structural alteration and oxolation, goethite can form. However, in the case of ferrihydrite formed from acid mine drainage waters, further alteration to a respective end product is

unlikely to occur in the stream for two reasons: residence time and sulfate surface adsorption. The ferrihydrite forming in the stream during low flow periods is easily entrained, and is quickly flushed downstream upon the succeeding storm cycle. Even with longer residence time the formation of hematite or, especially, goethite at ambient temperatures may well be inhibited by high sulfate adsorption. Ferrihydrite has a structure similar to that of hematite and, for alteration to goethite to occur, dissolution and structural rearrangement is necessary. It is likely that this alteration is impeded by the sulfate ion. This may be the reason why at ambient temperatures Dousma et al., (1979) report aging of FeIII oxide to form hematite in the presence of sulfate, but formation of goethite with Cl^- or NO_3^-.

4.4.5.2 Precipitation of Iron Oxides from Waters at the Air Vent. The second pathway for the formation of crystalline material suggested by Knight and Silva (1974) requires production of $Fe(OH)_2^+$. This is the same monomeric species expected to be dominant in waters from the air vent. This second pathway postulates direct precipitation of the $Fe(OH)_2^+$ ion on crystal nuclei. As indicated previously, associated with water from the breached air vent as it flows across the soil surface toward the stream is a travertine-like deposit composed primarily of goethite, but containing some ferrihydrite. Predominance of goethite may result from two factors. The first is slow hydrolysis and the other is that goethite formation does not necessarily require ferrihydrite as a precursor (Schwertmann and Taylor, 1977). Formation of goethite by direct precipitation of the $Fe(OH)_2^+$ monomer does require oxolation and dehydration. This process is more likely to occur in the travertine-like deposits which are occasionally subject to drying.

However, no mechanism for the initial formation of crystalline nuclei was suggested by Knight and Silva (1974) in their proposal of the pathway of crystallization by contact precipitation. Examination of this pathway in the laboratory may be difficult because of this, but under the environmental conditions encountered in the field, it is possible that soil, in particular inorganic and organic colloids at the surface of the landscape over which air vent waters are flowing, may play an active role in crystalline growth by contact aggregation.

4.5 Summary and Conclusions

It appears that both the color and rate of ferrihydrite formation is influenced by the presence of sulfate in the stream waters. Although sulfate enhances the formation of ferrihydrite by lowering surface charge and aiding aggregation, it most likely hinders the alteration of ferrihydrite to more crystalline species.

Further, iron precipitation resulting from acid mine drainage may well be occurring along two distinctly separate pathways in the Black Fork Creek watershed: in the stream, polymer growth resulting initially in ferrihydrite; from waters in contact with soil surfaces, contact precipitation of goethite and/or ferrihydrite.

LIST OF REFERENCES

1. Arden, T. V. 1950. The solubility products of ferrous and ferrosic hydroxides. J. Chem. Soc. (London) p. 882-885.

2. Arden, T. V. 1951. The hydrolysis of ferric iron in sulphate solution. J. Chem. Soc. (London) p. 350-363.

3. Arkesteyn, G. J. M. W. 1979. Pyrite oxidation by Thiobacillus ferrooxidans with special reference to the sulfur moiety of the mineral. Antonie van Leeuwenhoek J. Microbiol. Serol. 45:423-435.

4. APHA, AWWA, and WPCF. 1980. Standard methods for the examination of water and wastewater. 15th ed. 1134 p.

5. Baas-Becking, L. G. M., I. R. Kaplan, and D. Moore. 1960. Limits of the natural environment in terms of pH and oxidation-reduction potential. J. Geol. 68:243-286.

6. Bacon, J. R. and R. P. Maas. 1979. Contamination of Great Smokey Mountains trout streams by exposed anakeesta formations. J. Environ. Qual. 8:538-543.

7. Barnhisel, R. I. and H. F. Massey. 1969. Chemical, mineralogical and physical properties of eastern Kentucky acid-forming coal mine spoils. Soil Sci. 108:367-372.

8. Barnum, D. W. 1982. Potential-pH diagrams. J. Chem. Education. 59:809-812.

9. Bascomb, C. L. 1968. Distribution of pyrophosphate-extractable iron and organic carbon in soils of various groups. J. Soil Sci. 19:251-268.

10. Berg, W. H. and W. M. Vogel. 1969. Toxicity of acid coal-mine spoils to plants. p. 57-68. In Ecology and reclamation of devastated land. Gordon and Breach. New York.

11. Bernas, B. 1968. A new method for decomposition and comprehensive analysis of silicates by atomic absorption spectrometry. Anal. Chem. 40:1682-1686.

12. Berner, R. A. 1971. Principles of chemical sedimentology. McGraw-Hill. New York. 240 p.

13. Berry, R. W., G. P. Brophy, and A. Naqash. 1970. Mineralogy of the suspended sediment in the Tigris, Euphrates, and Schatt-Al-Arab Rivers of Iraq, and the recent history of the Mesopotamean Plain. J. Sed. Petrol. 40:131-139.

14. Black, C. A. 1968. Soil-plant relationships. John Wiley and Sons, New York. 792 p.

15. Blanchard, R. 1968. Interpretation of leached outcrops. Nevada Bur. of Mines Bull. 26. 196 p.

16. Board on Unreclaimed Strip Mined Lands. 1974. Land reborn. State of Ohio. 91 p.

17. Brown, J. B. 1971. Jarosite-goethite stabilities at 25° C, 1 ATM. Mineral. Deposita. 6:245-252.

18. Brown, M. F. and D. R. Kester. 1980. Ultraviolet spectroscopic study of ferric iron solutions. Appl. Spectrosc. 34:377-380.

19. Brunauer, J., P. H. Emmett, and E. Teller. 1938. Adsorption of gases in multimolecular layers. J. Amer. Chem. Soc. 60:309-319.

20. Bureau of Mines, USDI. 1977. Research on the hydrology and water quality of watersheds subjected to surface mining; second semi-annual technical report. 105 p.

21. Carlson, L., A. Vuorinen, P. Lahermo, and O. H. Tuovinen. 1980. Mineralogical, geochemical and microbiological aspects of iron deposition from groundwater. p. 355-364. In Biogeochemistry of ancient and modern environments. Springer-Verlag. New York.

22. Carlson, L. and U. Schwertmann. 1981. Natural ferrihydrites in surface deposits from Finland and their association with silica. Geochim. Cosmochim. Acta. 45:421-429.

23. Chadwick, M. J. 1969. Methods of assessment of acid, colliery spoil as a medium for plant growth. p. 81-91. In Ecology and Reclamation of Devasted Land. Gordon and Breach. New York.

24. Chao, T. T. and P. K. Theobald, Jr. 1976. The significance of secondary iron and manganese oxides in geochemical exploration. Econ. Geol. 71:1560-1569.

25. Chukhrov, F. V., B. B. Zvyagin, A. I. Gorshkov, K. P. Ermilova, and V. V. Balashova. 1973. Ferrihydrite. Isvest. Akad. Nauk. S.S.S.R. 1973. p. 23-33.

26. Cronce, R. C., L. T. Kardox, E. J. Ciolkosz. 1980. The effect of soil on the renovation of acid coal mine drainage water. J. Environ. Qual. 9:621-626.

27. Cummings, D. G., W. T. Plass, and G. E. Gentry. 1965. Chemical and Physical properties of spoil banks in the eastern Kentucky coal fields. U.S. Forest Serv. Res. Paper. CS-17. 94 p.

28. Curtis, W. R. 1972. Chemical changes in stream flow following surface mining in eastern Kentucky. Proc. 4th Symp. on Coal Mine Drainage Research. Mellon Institute, Pittsburgh, Penn. 344 p.

29. Dousma, J. and P. L. deBruyn. 1976. Hydrolysis-precipitation studies of iron solutions. I. Model for hydrolysis and precipitation from FeIII nitrate solutions. J. Coll. Interface Sci. 56:527-539.

30. Dousma, J. and P. L. deBruyn. 1978. Hydrolysis-preciptation studies of iron solutions. II. Aging studies and the model for precipitation from FeIII nitrate solutions. J. Coll. Interface Sci. 64:154-170.

31. Dousma, J., D. den Ottelander and P. L. deBruyn. 1979. The influence of sulfate ions in the formation of iron III oxides. J. Inorg. Nucl. Chem. 41:1565-1568.

32. Dugan, P. R. 1975. Biochemical ecology of water pollution. Plenum Press, New York. 159 p.

33. Dugan, P. R. and C. I. Randles. 1968. The microbial flora of acid mine water and its relationship to formation and removal of acid. Water Resources Center. The Ohio State University. 124 p.

34. Ehlman, A. J. 1968. Clay mineralogy of weathered products and of river sediments. Puerto Rico. J. Sed. Petrol. 38:885-894.

35. Elder, L. W. 1930. A comparison of certain hydrogen ion indicator electrodes in the presence of ferric iron. Trans. Amer. Electrochem. Soc. 57:383-393.

36. EPA. 1976. Evaluation of surface mine reclamation techniques, Campbell's Run Watershed, Pennsylvania. EPA Technological Series. EPA-60012-76-111. 51 p.

37. EPA. 1971. Inorganic sulfur oxidation by iron oxidizing bacteria. Water Quality Office, Report #14010 DAY. 149 p.

38. EPA. 1974. Methods for Chemical Analysis of Water and Wastes. EPA-62516-74003a. 298 p.

39. EPA. 1977. Catawissa Creek mine drainage abatement project. Interagency energy-environment research and development program report. EPA-60017-77-124. 165 p.

40. Freitknecht W., R. Giovanoli, W. Michaelis, and M. Muller. 1973. Uber die Hydrolyse von Eisen (III) Salzlodungen. I. Die Hydrolyse der Losungen von Eisen (III) chlorid. Helv. Chim. Acta 56:2847-2856.

41. Garrels, R. M. and Christ, C. L. 1965. Solutions, minerals and equilibria. Harper and Row, New York. 450 p.

42. Green, D. B., T. J. Logan, and N. E. Smeck. 1978. Phosphate adsorption-desorption characteristics of suspended sediments in the Maumee River Basin of Ohio. J. Environ. Qual. 7:208-212.

43. Gorbunov, N. I., G. S. Dzyadevich, B. M. Tunik. 1961. Methods of determining non-silicate amorphous and crystalline sesquioxides in soils and clay. Soviet Soil Sci. 11:1252-1259.

44. Harmesen, G. W., A. Quispel, and D. Otzen. 1954. Observations on the formation and oxidation of pyrite in the soil. Plant Soil. 5:324-347.

45. Harrison, J. B. and V. E. Berkheiser. 1982. Anion interactions with freshly prepared hydrous iron oxides. Clays Clay Miner. 30:97-102.

46. Heaney, S. I. and W. Davison. 1977. The determination of ferrous iron in natural waters with 2,2'bipyridl. Limn. Oceanogr. 22:753-760.

47. Hem, J. D. 1960. Some chemical relationships among sulfur species and dissolved ferrous iron. p. 57-73. In Chemistry of iron in natural water. Geological Survey Water Supply Paper 1459-C.

48. Hem, J. D. and W. H. Cropper. 1959. Survey of ferrous-ferric chemical equilibria and redox potentials. p. 1-30. In Chemistry of iron in natural water. Geological Survey Water Supply Paper 1459-A.

49. Hooper, F. F. 1969. Eutrophication indices and their relation to other indices of ecosystem change. p. 225-253. In Eutrophication: Causes, consequences, correctives. Natural Acad. Sci., Washington, D. C.

50. Hsu, P. H. 1967. Determination of iron with thiocyanate. Soil Sci. Soc. Am. Proc. 31:353-355.

51. Hsu, P. H. and S. E. Ragone. 1972. Aging of hydrolyzed iron III solutions. J. Soil Sci. 23:17-31.

52. Imeson, A. C. and J. M. Verstraten. 1981. Suspended solid concentrations and river water chemistry. Earth Surf. Proc. Landforms. 6:251-263.

53. Jackson, M. L. 1975. Soil chemical analysis—advanced course. 2nd ed. Published by the author, Dept. of Soil Science, University of Wisconsin, Madison. 895 p.

54. Jackson, T. A. and W. D. Keller. 1970. A comparative study of the role of lichens and "inorganic" processes in the chemical weathering of recent Hawaii lava flows. Am. J. Sci. 296:446-460.

55. Jenne, E. A. 1975. Trace element sorption by sediment and soils--sites and processes. Vol. 2. p. 424-554. In Molybdenum in the Environment. Marcel Dekker. New York.

56. John, M. K. 1970. Colorimetric determination of phosphorus in soil plant materials with ascorbic acid. Soil Sci. 109:214-220.

57. Johnson, A. H., D. R. Bouldin, E. A. Goyette, and A. M. Hedges. 1976. Phosphorus losses by stream transport from a rural watershed: Quantities, processes, sources. J. Environ. Qual. 5:148-147.

58. Johnson, D. B., W. I. Kelso, and D. A. Jenkins. 1979. Bacterial streamer growth in a disused pyrite mine. Environ. Pollut. 18:107-118.

59. Jones, L. A., N. E. Smeck, and L. P. Wilding. 1977. Quality of water discharged from three small agronomic watersheds in the Maumee River Basin. J. Environ. Qual. 6:296-302.

60. Kelly, D. P. 1967. Problems of the autotrophic microorganisms. Sci. Progr. 55:35-51.

61. Kelly, D. P., P. R. Norris, and C. L. Brierley. 1979. Microbial methods for the extraction and recovery of metals. In Microbial Technology. Soc. Gen. Microbiol. p. 263-308.

62. Kelly, W. C., and E. N. Goddard. Telluride ores of Boulder County, Colorado. Geol. Soc. Am. Memoir 109. 237 p.

63. Klages, M. G and Y. P. Hsieh. 1975. Suspended solids carried by the Gallatin River of southwestern Montana. II. Using mineralogy for inferring sources. J. Environ. Qual. 4:68-73.

64. Knebel, H. J., J. C Kelley, and J. T. Whetten. 1968. Clay minerals of the Columbia River: A qualitative, quantitative and statistical evaluation. J. Sed. Petrol. 38:600-611.

65. Knight, R. J. and R. N. Silva. 1974. Precipitation in hydrolysed iron III solutions. J. Inorg. Nucl. Chem. 36:591-597.

66. Knight, R. J. and R. N. Silva. 1975. Spectrophotometric investigation of iron III hydrolysis in light and heavy water at 25° C. J. Inorg. Nucl. Chem. 37:779-783.

67. Kolthoff, I. M., E. C. Sandell, E. J. Meehan, and S. Bruckenstein. 1969. Quantitative chemical analysis. 4th Edition. Macmillan Co. New York. 1199 p.

68. Krauskopf, K. B. 1979. Introduction to geochemistry. 2nd ed. McGraw-Hill, New York. 617 p.

69. Lamb, A. B. and A. G. Jacques. 1938. The slow hydrolysis of ferric chloride in dilute solution. II. The change in hydrogen ion concentration. J. Am. Chem. Soc. 60:1215-1525.

70. Lee, G. F. and W. Stumm. 1960. Determination of ferrous iron in the presence of ferric iron with bathophenanthroline. J. Am. Water Works Assoc. 52:1567-1574.

71. Lindsay, W. L. 1979. Chapter 10: Iron. p. 128-149. In Chemical equilibria in soils. John Wiley and Sons. New York.

72. Locke, A. 1926. Leached outcrops as guides to copper ore. Williams and Wilkins. Baltimore. 175 p.

73. Logan, T. J. 1977. Chemical and mineralogical indices of sediment transformation during fluvial transport. In Proc. 5th Guelph Symposium on Geomorphology, p. 199-208.

74. Logan, T. J. 1979. The Maumee River Basin pilot watershed study. Volume II. Sediment, phosphates, and heavy metal transport. EPA-90019-79-005-B. 133 p.

75. Logan, T. J. and R. C. Stiefel. 1979. Maumee River pilot watershed study: Watershed characteristics and pollutant loadings, Defiance area, Ohio. EPA-90519-79-005-A. 135 p.

76. Lundgren, D. G., J. R. Vestal, and F. R. Tabita. 1972. The microbiology of mini drainage pollution. p. 69-90. In Water pollution microbiology. Wiley Interscience. John Wiley and Sons. New York.

77. Matijevic, E. and P. Scheiner. 1978. Ferric hydrous oxide sols. III. Preparation of uniform particles by hydrolysis of FeIII-chloride, -nitrate and -perchlorate solutions. J. Coll. Interface Sci. 63:509-524.

78. McKeague, J. A., J. E. Brydon, and N. M. Miles. 1971. Differentiation of forms of extractable iron and aluminum in soils. Soil Sci. Soc. Am. Proc. 35:33-38.

79. McKibbon, W. L. 1975. The effect of moisture content, temperature, and leaching on the weathering of pyrite laden rock. M.S. Thesis. Ohio State University. 125 p.

80. Milburn, R. M. 1957. Aspectrophotometric study of the hydrolysis of iron III ion. III. Heats and entropies of formation. J. Am. Chem. Soc. 79:537-540.

81. Milburn, R. M. and W. C. Vosburgh. 1955. A spectrophotometric study of the hydrolysis of iron III ion. H. Polynuclear species. J. Am. Chem. Soc. 77:1352-1355.

82. Miller, S. D. 1979. Chemistry of a pyrite strip-mine spoil. Ph.D. Dissertation. Yale University. 186 p.

83. Minear, R. A. and B. A. Tschantz. 1976. The effect of coal surface mining on the water quality of mountain drainage basin streams. J. Water Poll. Control Fed. 48:2549-2569.

84. Mustoe, G. E. 1981. Bacterial oxidation of manganese and iron in a modern cold spring. Geol. Soc. Am. Bull. 92:147-153.

85. Nightingale, H. I. 1972. Nitrates in soil and groundwater beneath irrigated and fertilized crops. Soil Sci. 114:300-311.

86. Nordstrom, D. K. 1980. Aqueous pyrite oxidation and the consequent formation of secondary iron minerals. In Press.

87. Nordstrom, D. K., E. A. Jenne, and J. W. Ball. 1979. Redox equilibria of iron in acid mine waters. p. 51-79. In Chemical modeling in aqueous systems: speciation, sorption, solubility, and kinetics. Am. Chem. Soc. Symp. Series. No. 93.

88. Nordstrom, D. K. and T. V. Dagenhart. 1978. Hydrated iron sulfate minerals associated with pyrite oxidation: Field relations and thermodynamic properties. Abstract. Geol. Soc. Am. Ann. Mtg., Toronto, Canada.

89. Nuhfer, E. B. 1967. Efflorescent minerals associated with coal. M.S. Thesis. West Virginia University. Morgantown. 74 p.

90. Oades, J. M. 1963. The nature and distribution of iron compounds in soils. Soils Fert. 26:69-80.

91. Ohio Dept. of Natural Resources, Division of Water. 1968. Water inventory of the Muskingum River Basin. Ohio Water Plan Inventory Report No. 21. 199 p.

92. Oloya, T. O. 1979. Chemical aspects of sediment and soil phosphorus. Ph.D. Dissertation. Ohio State University. 286 p.

93. Orchiston, H. D. 1953. Adsorption of water. I. Soils at 25° C. Soil Sci. 453-465.

94. Petersen, J. R. and J. Gschwind. 1972. Leachate quality from acidic spoil fertilized with liquid digested sludge. J. Environ. Qual. 4:410-412.

95. Pinet, P. R. and W. P. Morgan, Jr. 1979. Implications of clay-provenance studies in two Georgia estuaries. Soc. Econ. Paleontol. Mineral. 49:575-580.

96. Post, G. J. 1956. A study of three methods for determination of organic carbon in Ohio soils of sevral great soil groups and the profile distribution of carbon-nitrogen ratios. M.S. Thesis, The Ohio State University. 73 p.

97. Powers, D. A., G. R. Rossman, H. J. Schugar; H. B. Gray. 1975. Magnetic behavior and infrared spectra of jarosite, basic iron sulfate, and their chemical analogs. J. Solid State Chem. 13:1-13.

98. Rhoton, F. E. 1978. Clay mineralogical relationships between watershed soils, runoff and bottom sediments in the Maumee River Basin, Ohio. Ph.D. Dissertation, The Ohio State University. 190 p.

99. Rose, R. R. 1975. Aspects of water quality and their relationships to hydrology in coal mined drainage basins in the Cumberland Mountains. M.S. Thesis. Univ. of Tenn., Knoxville. 193 p.

100. Russell, J. D. 1979. Infrared spectroscopy of ferrihydrite: evidence for the presence of structural hydroxyl groups. Clay Miner. 14:109-114.

101. Rutledge, E. M., L. P. Wilding, and M. Elfield. 1967. Automated particle-size separation by sedimentation. Soil Sci. Soc. Am. Proc. 31:287-288.

102. Sartori, F., R. Riffaldi, and R. Levi-Minzi. 1979. Occurrence of chloritic intergrades in the recent sediments of the Arno River (Italy). Clay Miner. 14:47-65.

103. Schneider, H. I. and E. E. Angino. 1980. Trace element, mineral, and size analysis of suspended flood materials from selected eastern Kansas rivers. J. Sed. Petrol. 50:1271-1278.

104. Schwertmann, U. 1979. Is there amorphous iron oxide in soils. Agronomy Abstracts. Am. Soc. Agron. Madison, Wisc.

105. Schwertmann, U. and W. R. Fischer. 1973. Natural "amorphous" ferric hydroxide. Geoderma. 10:237-247.

106. Schwertmann, U. and R. M. Taylor. 1977. Iron oxides. p. 145-180. In Minerals in soil environments. Soil Sci. Soc. Am. Madison, Wisc.

107. Shapiro, J. 1966. On the measurement of ferrous iron in natural waters. Limn. Oceanogr. 11:293-298.

108. Sharpley, A. N. and J. K. Syers. 1979. Phosphorus inputs into a stream draining an agricultural watershed. Water Air Soil Poll. 11:417-428.

109. Shokarev, M. M., E. V. Margulis, F. I. Vershinina, L. I. Beisekeeva, and L. A. Savechenko. 1972. Infrared spectra of iron(III) hydroxide sulphates and hydroxides. Russian J. Inorg. Chem. 17:1292-1296.

110. Siddall, T. H. and W. C. Vosburgh. 1951. A spectrophotometric study of the hydrolysis of iron III ion. J. Am. Chem. Soc. 73:4270-4272.

111. Singer, P. C. and W. Stumm. 1970. Acid mine drainage: the rate determining step. Sci. 197:1121-1123.

112. Singer, M. J. and R. H. Rust. 1975. Phosphorus in surface runoff from a deciduous forest. J. Environ. Qual. 4:307-311.

113. Soil Survey Staff. 1972. Soil Survey Laboratory Methods and Procedures for Collecting Soil Samples. Soil Survey Investigations Report No. 1. USDA-SCS. U. S. Govt. Printing Office, Washington, D. C. 63 p.

114. Sommers, L. E. and D. W. Nelson. 1972. Determination of total phosphorus in soils: A rapid perchloric acid digestion procedure. Soil Sci. Soc. Am. Proc. 36:902-904.

115. Stewart, K. M. and G. A. Rohlich. 1967. Eutrophication—A Review. State of California. The Resources Agency. State Water Quality Control Board pub. no. 34. 117 p.

116. Stucki, J. W. 1981. The quantitative assay of minerals for Fe^{+2} and Fe^{+3} using 1,10-phenanthroline: II. A photochemical method. Soil Sci. Soc. Am. J. 45:638-641.

117. Stucki, J. W. and W. L. Anderson. 1981. The quantitative assay of minerals for Fe^{+2} and Fe^{+3} using 1,10-phenanthroline: I. Sources of variability. Soil Sci. Soc. Am. J. 45:633-637.

118. Terry, R. V., W. L. Powers, R. V. Olson, L. A. Murphy, and R. M. Rubison. 1981. The effect of beef feedlot runoff on the nitrate-nitrogen content of a shallow aquifer. J. Environ. Qual. 10:22-26.

119. Tisdale, S. L. and W. L. Nelson. 1975. Soil fertility and fertilizers. Macmillan Company. New York. 693 p.

120. Towe, K. M. and W. F. Bradley. 1967. Mineralogical constitution of colloidal "hydrous ferric oxides". J. Coll. Interface Sci. 24:384-392.

121. Tuttle, J. H., P. R. Dugan, and C. I. Randles. 1969. Microbial sulfate reduction and its potential utility as a water pollution abatement procedure. Appl. Microbiol. 17:297-302.

122. U.S. Army Corps of Engineers. 1982. Lake Erie wastewater management study: Final Report. U.S. Army Corps of Engineers District. Buffalo, New York. 223 p.

123. USDA. 1975. Muskingum River Basin. Type IV Survey Report. Columbus, Ohio.

124. U. S. Geological Survey. 1978. Water Resources Data for Ohio, Volume 1. Ohio River Basin. 383 p.

125. Walling, D. E., M. R. Peart, F. Oldfield, R. Thompson. 1979. Suspended sediment sources idenfitied by magnetic measurements. Nature 281:110-113.

126. Watanabe, F. S. and S. R. Olsen. 1965. Test of an ascorbic acid method for determining phosphorus in water and $NaHCO_3$ extracts from soil. Soil Sci. Soc. Am. Proc. 29:677-678.

127. Williams, E. B. 1973. An investigation of chloride contamination in the Tuscarawas and Muskingum River Valleys. M.S. Thesis. Ohio State University. 110 p.

128. Williams, J. D. H., T. P. Murphy, and T. Mayer. 1976. Rates of accumulation of phosphorus forms in Lake Erie sediments. J. Fish Res. Board. Can. 33:430-439.

129. Wiram, V. P. 1976. Pyrite in the Coxville Sandstone Member Linten Formation and its effects in acid mine conditions near Latta, Greene County, Indiana. Dept. Nat. Res. Geol. Survey. Occasional Paper 20. 10 p.

130. Whiteker, R. A. and N. Davidson. 1953. Ion-exchange and spectrophotometric investigation of iron III sulfate complex ions. J. Am. Chem. Soc. 75:3081-3085.

131. Wood, W. W. 1976. Guidelines for collection and field analysis of groundwater samples for selected unstable constitutents. Tech. Water-Resources Investigations, Book 1, Chapter D2, U. S. Geol. Surv. 24 p.

132. Zodrow, E. L., J. Wiltshire, and K. McCandlish. 1979. Hydrated sulfates in the Sydney coalfield of Cape Breton, Nova Scotia. II. Pyrite and its alteration products. Can. Mineral. 17:63-70.

APPENDIX A

EXPANDED TABLES FROM WATER QUALITY STUDIES REPORTED IN CHAPTER 2

Table A.1 Black Fork Creek and Tributaries Water Quality, March, 1981.

Site	Ca	Mg	Na	Fe	Al	Mn	P	Cd	Cu	Pb	Ni	Zn	Sr	SO_4
	µg/ml													
1	27.8	8.3	13.8	0.36	0.14	0.03	0.02	---*	0.01	---	0.01	0.01	0.14	43
2	29.2	8.1	12.9	0.01	0.02	0.09	0.03	---	---	---	0.03	0.01	0.14	35
3	26.4	8.5	11.5	0.01	0.01	0.05	0.02	---	0.01	---	0.01	0.01	0.12	41
4	41.9	14.5	14.2	94.60	37.43	1.16	0.17	---	---	---	0.07	0.23	0.17	589
5	38.7	11.0	13.0	24.55	13.67	0.84	0.06	---	0.02	---	0.05	0.19	0.17	254
6	35.8	10.6	12.8	15.20	1.97	0.48	0.02	---	0.01	---	0.02	0.04	0.15	163
7	37.5	12.00	15.9	19.66	2.91	0.60	0.03	---	0.01	---	0.02	0.46	0.17	193
8	38.7	12.1	16.9	18.97	3.38	0.64	0.04	---	0.01	---	0.03	0.05	0.19	199
9	46.0	14.2	24.2	18.03	3.33	0.79	0.05	---	0.01	---	0.03	0.06	0.33	207

* Non-detectable. Detection limits for ICAP in µg/ml: Mn, Cu = 0.001; Sr, Cd = 0.002; Fe = 0.005; Zn = 0.006; Pb, Ni = 0.008; Al = 0.01; P = 0.02.

Table A.2. Black Fork Creek and Tributaries Water Quality, August, 1981.

Site	Ca	Mg	Na	Fe	Al	Mn	P	Cd	Cu	Pb	Ni	Zn	Sr	Ba	SO_4
	µg/ml														
1	53.1	12.9	35.4	0.82	0.11	0.27	---*	---	0.01	---	---	0.01	0.37	0.07	54
2	41.7	9.9	20.5	0.71	0.04	0.06	---	---	0.01	---	---	0.02	0.25	0.06	31
3	31.4	9.2	12.5	0.09	0.07	0.08	---	---	0.01	---	---	0.02	0.14	0.04	31
4	66.5	29.6	20.8	329.00	94.30	4.37	0.09	---	0.48	0.05	0.15	0.33	0.24	0.02	1630
5	68.3	18.5	18.4	52.60	33.30	2.40	---	---	0.23	---	0.05	0.13	0.25	0.05	570
6	87.7	30.4	25.3	61.13	40.77	3.73	---	---	0.02	0.03	0.08	0.19	0.39	0.04	777
7	108.0	50.1	64.8	132.00	34.27	5.01	---	---	0.03	0.03	0.09	0.24	0.63	0.36	1006
8	114.7	53.6	83.3	123.00	30.33	5.21	---	---	0.03	0.03	0.08	0.24	0.74	0.03	1080
9	147.3	56.5	104.3	70.00	27.67	4.99	0.06	---	0.03	0.04	0.08	0.27	1.53	0.04	962

* Non-detectable. Detection limits for ICAP in µg/ml: Ba, Mn, Cu = 0.001; Sr, Cd = 0.002; Fe = 0.005; Zn = 0.006; Pb, Ni = 0.008; Al = 0.01; P = 0.02.

APPENDIX B

EXPANDED TABLE FROM WATER QUALITY STUDY REPORTED IN CHAPTER 4

Table B.1 Metals in Solution as Detected by ICAP for Iron Speciation Analysis, August, 1982.

Element	Site A	B	C	D	E	F
	µg/ml					
Ca	43.4	79.9	83.8	76.1	83.2	224.7
Mg	9.9	45.9	36.7	26.3	26.6	145.0
Na	18.1	18.8	31.2	24.2	22.2	207.7
Al	---	343.3	154.0	86.6	74.2	14.6
Mn	0.01	3.54	4.56	3.34	3.69	10.93
P	0.03	0.83	0.11	0.04	0.08	0.12
Cd	---*	0.01	---	---	---	---
Cu	---	0.03	0.06	0.03	0.03	0.01
Ni	---	0.34	0.19	0.10	0.11	0.13
Zn	0.05	0.80	0.49	0.24	0.23	0.57
Sr	0.21	0.24	0.34	0.30	0.31	1.70

* Non-detectable. Detection limits for ICAP in µg/ml: Ba, Mn = 0.001; Sr = 0.002; Cd, Cu, Zn = 0.003; Ni = 0.008; P = 0.02.